Non-Markovian barrier-crossing dynamics at equilibrium and non-equilibrium

Dissertation
zur Erlangung des Grades eines
Doktors Naturwissenschaften
(Dr. rer. nat.)

am Fachbereich Physik
der Freien Universität Berlin

vorgelegt von:
Laura Lavacchi

Berlin 2024

Erster Gutachter:	**Prof. Dr. Roland R. Netz** **Freie Universität Berlin**
Zweiter Gutachter:	**Prof. Dr. Benjamin Lindner** **Humboldt University Berlin**
Tag der Disputation:	**13.05.2024**

Declaration of authorship

Name: Lavacchi
First name: Laura

I declare to the Freie Universität Berlin that I have completed the submitted dissertation independently and without the use of sources and aids other than those indicated. The present thesis is free of plagiarism. I have marked as such all statements that are taken literally or in content from other writings. This dissertation has not been submitted in the same or similar form in any previous doctoral procedure.

I agree to have my thesis examined by a plagiarism examination software.

Date: 28.02.2024 Signature: .....

Abstract

Many biological systems can be described by the concept of barrier crossing. Rare events, such as protein folding or chemical reactions, can be modeled as systems that must cross a barrier potential to change their states.These systems do not occur in isolation but, are rather coupled with their environment. Typically we choose a reaction coordinate and project out all the other orthogonal degrees of freedom. If the orthogonal degrees of freedom relax as rapidly as the reaction coordinates, non-Markovian memory effects must be taken into account in order to accurately describe the dynamics.

In this thesis, we study the mean first-passage time τ_{MFP} for various non-Markovian systems using the generalized Langevin equation. We begin by considering a multi-exponential memory kernel exhibiting various memory times and friction coefficients. We then propose a heuristic formula that shows that the τ_{MFP} is dominated by the single memory exponential with short memory time as well as large amplitude.

Following this, we take into consideration a generalized Langevin equation out of equilibrium, thereby deriving three effective parameters that consider the effect of the memory time out of equilibrium. Changing the temperature, the τ_{MFP} demonstrates non-Arrhenius behavior and increases dramatically when the random force relaxation time is longer than the friction relaxation time.

Since many chemical and biological systems exhibit asymmetric free-energy profiles, we next consider an asymmetric potential. From simulation data, we gather evidence that the dynamics in one well is independent of the other. Therefore, we describe the dynamics via the times $\tau_{MFP}^{L,R}$ that are needed to reach the barrier from left and right, respectively.

In the final section, we focus on another important factor that characterizes the process of barrier crossing, the mean transition path time τ_{MTP}. Again, we concentrate on a non-Markovian system, and, with the help of simulations, derive a heuristic formula. In particular, we introduce the memory time, substituting the effective parameters found above into a previous Markovian formula. Contrary to the mean first-passage time τ_{MFP}, the mean transition path time τ_{MTP} reaches its maximum in the Markovian case; for intermediate memory time it decreases, particularly for smaller mass, and settles on a constant value for large memory times.

Kurzfassung

Viele biologische Systeme können mit dem Konzept des Barriereübergangs beschrieben werden. Seltene Ereignisse, wie die Proteinfaltung oder chemische Ereignisse, können als Systeme modelliert werden, die eine Potenzialbarriere überwinden müssen, um ihren Zustand zu ändern. Diese Systeme treten nicht isoliert auf, sondern sind vielmehr mit ihrer Umgebung gekoppelt. Typischerweise wird eine Reaktionskoordinate gewählt, wobei alle anderen orthogonalen Komponenten in der Projektion nicht betrachtet werden. Falls die orthogonalen Freiheitsgrade so schnell wie die Reaktionskoordinaten relaxieren, müssen Memoryeffekte berücksichtigt werden, um die Dynamik genau zu beschreiben.

In dieser Arbeit untersuchen wir die mittlere Reaktionszeit τ_{MFP} für verschiedene nicht-Markovsche Systeme mithilfe der generalisierten Langevin-Gleichung. Zuerst betrachten wir einen multi-exponentiellen Memorykernel, der verschiedene Memoryzeiten und Reibungskoeffizienten aufweist. Wir schlagen dann eine heuristische Formel vor, die zeigt, dass τ_{MFP} von einer einzelnen Exponentialfunktion mit sowohl kurzer Memoryzeit als auch großer Amplitude dominiert wird.

Im Anschluss betrachten wir eine generalisierte Langevin-Gleichung abseits des Gleichgewichts und leiten drei effektive Parameter ab, die den Effekt der Memoryzeit außerhalb des Gleichgewichts berücksichtigen. Ändert man die Temperatur, verhält sich die mittlere Reaktionszeit τ_{MFP} nicht gemäß der Arrhenius-Gleichung und steigt dramatisch an, wenn die Relaxationszeit der Zufallskraft länger ist als die Reibungsrelaxationszeit.

Da viele chemische und biologische Systeme asymmetrische freie-Energie-Profile aufweisen, betrachten wir als Nächstes ein asymmetrisches Potenzial. Aus Simulationsdaten sammeln wir Beweise dafür, dass die Dynamik in einem Tal des Potenzials unabhängig vom Anderen ist. Daher beschreiben wir die Dynamik durch die benötigten Zeiten $\tau_{MFP}^{L,R}$, um die Barriere von links bzw. von rechts zu erreichen.

Im letzten Abschnitt betrachten wir einen weiteren wichtigen Faktor, der den Prozess des Barriereübergangs charakterisiert, die mittlere Übergangspfadzeit τ_{MTP}. Wir betrachten wieder ein nicht-Markovsches System und leiten mithilfe von Simulationen eine heuristische Formel her. Insbesondere führen wir die Memoryzeit ein, indem wir die oben erwähnten effektiven Parameter in eine bereits bekannte Markovsche Formel einsetzen. Im Gegensatz zur mittleren Reaktionszeit τ_{MFP} erreicht die mittlere Übergangspfadzeit τ_{MTP} ihr Maximum im Markovschen Fall; für intermediäre Memoryzeiten nimmt sie ab, insbesondere für kleine Massen, und nimmt für große Memoryzeiten einen konstanten Wert an.

Contents

Chapter 1

Introduction

When we study biophysical objects (biological phenomena studies with a physical model), we come to realize that such objects never occur in isolation, but are rather immersed in a kind of heat bath. In 1827, Scottish botanist Robert Brown observed under a microscope the motion of pollen particles in water, noting that the single pollen particle was moving in a chaotic fashion [1]. This mechanism was later explained as the result of many minor collisions between the pollen particle and the surrounding water molecules. So in order to ascertain the final position of the pollen particle, one must consider a multitude of random variables. This dynamic occurs not only in biophysical systems, but also across a more comprehensive range of systems, for example in the price of an asset [2, 3] or the tracking of a tropical cyclone [4].

The first theoretical explanation of Brownian motion was put forth in 1905 by Albert Einstein [5] and independently discovered one year later by Marian Smoluchowski [6]. Einstein and Smoluchowski described the phenomenon with a diffusion equation without considering inertial effects. Subsequently, in 1908, Paul Langevin took into account the inertial behavior of the particle and introduced a stochastic force [7] as follows:

$$m\ddot{x}(t) = -\gamma\dot{x}(t) - \nabla U\left(x(t)\right) + F_R(t), \tag{1.1}$$

where m and γ denote the particle's mass and its friction coefficient, respectively. The variable x represents the particle's position, and the dots denote the derivative with respect to time. The external potential is $U\left(x(t)\right)$, which for Brownian motion is zero, and $F_R(t)$ is a Gauss distributed stochastic force, which indicates that its mean is zero, i.e. $\langle F_R(t)\rangle = 0$. In the case of Brownian motion, i.e. a heavy particle surrounded by lighter particles with different diffusion times, we must take into account the concept of separation of scales. The interaction between the environment and the particle is

modeled by a friction and a random force, which are correlated (in equilibrium) according to the fluctuation-dissipation theorem. The time scale of the lightweight particles is much smaller than of the tracked particle, considering that the bath is stationary and the random force must take into account the average behavior of the light particles. In other words, it is possible to find a lag-time t', where, in the interval between t and $t+t'$, the change in velocity is minimal, but simultaneously, the random force in $t+t'$ is independent of the value of $F_R(t)$, i.e. $\langle F_R(t)F_R(t+t')\rangle = 0$.

Sometimes, these time scales are comparable, so we can not consider the friction contribution instantaneous. In the 1960s, H. Mori [8] and R. Zwanzig [9,10] posited that the interaction between particles requires a finite amount of time and, using the Langevin equation (LE) (1.1), they introduced the Generalized Langevin equation (GLE)

$$m\ddot{x}(t) = -\int_0^t \Gamma(t')\dot{x}(t-t')dt' - \nabla U\left(x(t)\right) + F_R(t). \tag{1.2}$$

Mori obtained this integro-differential equation via linearly projecting the phase space dynamics of a Hamiltonian system onto a one-dimensional reaction coordinate, using the Liouville operator formalism. The memory kernel $\Gamma(t')$ in Eq. (1.2) encloses the degrees of freedom orthogonal to the reaction coordinate x, and, if we are at equilibrium, the memory kernel is proportional to the autocorrelation of the random force. A peculiar difference between the Langevin equation (1.1) and the GLE (1.2), the former being Markovian, is that the acceleration equation depends solely on the time t, and not also on the previous time t'. Going from Eq. (1.1) to Eq. (1.2) depends on the separation time scale, in other words, if we are able to approximate the interaction between particles as instantaneous. It is instantaneous when the decay of the memory kernel $\Gamma(t)$ is much faster than the velocity time scale. If one substitutes the memory kernel with a delta function in Eq. (1.2), one comes back at Eq. (1.1). As we have already stated, the Langevin equation has widespread applicability in stochastic mechanics, because the reaction coordinate x could be used to describe a particle's position, as well as more abstract objects, such as a vector connecting two particles, an end-to-end vector, or the fluctuating price of an asset.

From Eq. (1.1) and Eq. (1.2) it is clear that it is always easier to work with the first equation, because the memory function does not have a universal description and can become very complicated and thus difficult to express analytically. Several methods exist in the literature to determine $\Gamma(t)$, but none is universal [11, 12], because the methods depend on the type of the studied system.

Model systems can be simulated by solving the LE or GLE numerically.

Solving LE is easier when we find the optimal reaction coordinate, but in some cases, optimal reaction coordinat does not exist, so one has to solve GLE. The numerical simulation is useful to verify an analytical model.

Another noteworthy aspect of the GLE is the relationship between the random force and the memory kernel; as we have already clarified, the random force $F_R(t)$ is Gaussian distributed and, at the point of equilibrium, obeys the fluctuation-dissipation theorem (FDT)

$$\langle F_R(t)F_R(t')\rangle = k_B T\Gamma(t-t'), \tag{1.3}$$

where k_B is the Boltzmann constant.

One process that is often described by the Langevin equation is protein folding, because the dynamics are characterized by the friction coefficient. The process can be modeled by a one-dimensional barrier crossing that divides the folded and the unfolded state. The double-well is a simple potential that describes the crossing process in one dimension. The barrier crossing defines the probability of going to a certain point B starting from point A. This process is affected by various parameters, e.g., the friction coefficient or the mass. As stated above, Markovian dynamics is an approximation where one considers the interaction between the particle and the environment as instantaneous. However, if the time scales between the particle and the environment are comparable, one must additionally consider the non-Markovian dynamics [13, 14]. The protein folding process is a typical example where the time scales are similar. For this reason, the duration of the particle interactions will be finite. Apart from that, the memory time changes the probability of crossing the barrier, inducing an acceleration of the time to cross with respect to the Markovian case for intermidiate memory times and a slow-down for long memory times.

Protein folding is a vital cell process, and the failure of this process, or the misfolding, is the cause of many neurodegenerative diseases, for example, Alzheimer's or Parkinson's Disease [15]. To prevent such misfolding, other proteins are involved in the process, acting as chaperones: these molecules increase the folding efficiency, reducing the probability of different types of aggregation [16]. The stabilizing effect of these chaperones does not occur in a state of equilibrium, because they consume chemical energy [17]. FDT does not hold in this case, and the system is in a condition of non-equilibrium that changes its thermodynamics. This is the condition of Active Matter, where active agents consume energy to produce work. This activity, measured in a state of non-equilibrium, is characteristic of other living systems, such as cell migration or cell division.

1.1 Outline

This thesis will set out to consider the ways in which memory effects influence the dynamics of a one-dimensional potential landscape. Utilizing both simulations as well as analytical calculations, we will investigate how the mean-first passage time (MFPT) over a single barrier modifies its crossing velocity. In particular, we will consider various systems, modifying both the memory kernel and the potential. We will also study systems in which the FDT is violated, because a model far from a state of equilibrium can describe a range of chemical reactions and molecular conformational transition.

In chapter 3, we will simulate the GLE (1.2) for a multi-exponential memory kernel, considering various friction coefficients γ_i and memory times τ_i, in particular for two or three exponentials. Furthermore, we will verify the validity of previous works and, based on a new heuristic formula, generate a general scaling diagram. This diagram will depict the Markovian regime for short memory times and an asymptotic long-memory-time regime. The MFPT grows quadratically in the region of long-memory-time and the scaling variable is γ_i/τ_i^2. Therefore the memory contributions with long memory times τ_i or small amplitudes γ_i are negligible compared to other memory contributions. For the other memory time, we observe an intermediate non-Markovian regime, characterized by acceleration, or by a slowdown of the MFPT, depending on the particle mass.

In chapter 4, we will concentrate on the easiest exponential memory kernel, the single one; the autocorrelation of the random force is proportional to another exponential function, similar to the memory kernel, but with a different relaxation time. Using a harmonic approximation, we will present an analytical result for the MFPT based on the positional autocorrelation function. This calculation generalizes previous works [18, 19] and provides effective parameters that correspond to our simulation data, producing a heuristic formula for a double-well potential. The new MFPT shows a non-Arrhenius behavior, where the non-equilibrium random forces have a relaxation time longer than the friction relaxation time. The effective parameters also describe the spatial and velocity distributions.

Another step to better describe the protein folding process is to consider an asymmetric double-well potential, as we will demonstrate in chapter 5. Using the results of the previous chapter, we will modify the heuristic formula for a potential with various barrier heights on the two sides of the top and separation lengths between the top and the left and the right minima, respectively. We will compare the procedure with the simulation to demonstrate its validity. We will also be able to conclude that the two wells operate independently of one another, and the mean first passage time from the bot-

tom of one well to the top is not influenced by the dynamic of the other well.

In chapter 6, we will analyze another important concept in the context of barrier crossing: the transition path time, i.e., the time taken to reach a target without revisiting the initial position. Additionally in this case, using the effective parameters found in chapter 4, we will develop a heuristic formula for single and double exponential memory kernels. We are therefore demonstrating that the presence of a memory kernel will accelerate this process, in particular when the mass of the particle is small; in other words, the mean of the transition path time (MTPT) in the non-Markovian case is shorter than the MTPT in the Markovian case. For more elevated values of memory time, we will find that it reachs a plateau.

Chapter 2

Methods and Simulations

2.1 Langevin Equation

In this chapter we will discuss in greater detail the theoretical instruments and simulation method that we will apply in the following chapters. As previously mentioned, Langevin developed his equation in 1908 [7], subsequently applying it to the theory of Brownian motion. Brownian motion [1, 20] describes the random dynamics of a particle immersed in a fluid, though it can also be used to describe systems of greater variability, as previously mentioned in the introduction. Langevin started with the Newtonian approach and the motion of a particle immersed in a fluid without the influence of external forces as described by

$$m\dot{v}(t) = -\gamma v(t), \tag{2.1}$$

where m is the particle mass, γ the friction coefficient and $v(t)$ the particle velocity. The solution of this first-order differential equation is

$$v(t) = e^{-\gamma t/m} v(0). \tag{2.2}$$

According to this solution, the velocity of a Brownian particle decays to zero at longer times. But on the other hand, we can calculate that in the canonical ensemble the mean square velocity is

$$\langle v(t)^2 \rangle = k_B T/m, \tag{2.3}$$

from the law of equipartition [21].

This means that the total force applied to the particle comes not only from the frictional force, but also from another "random" force, so the Langevin equation for a Brownian particle therefore becomes

$$m\dot{v}(t) = -\gamma v(t) + F_R(t). \tag{2.4}$$

Both of the forces stem from the interaction of the particle with its environment, also referred to as the "heat bath". The random force is considered to vary extremely rapidly over the time of observation following the Gaussian distribution, therefore the first two moments of the random force averaged out over an infinitesimal time interval are given by

$$\langle F_R(t) \rangle = 0, \tag{2.5}$$
$$\langle F_R(t) F_R(t') \rangle = 2B\delta(t - t'), \tag{2.6}$$

where B is the strength of the random force. The solution of the first-order differential Eq. (2.4) is

$$v(t) = e^{-\gamma t/m} v(0) + \int_0^t dt' e^{-\gamma(t-t')/m} F_R(t')/m. \tag{2.7}$$

Squaring the velocity solution we obtain three terms

$$e^{-2\gamma t/m} v(0)^2, \tag{2.8}$$
$$2e^{-\gamma t/m} v(0) \int_0^t dt' e^{-\gamma(t-t')/m} F_R(t')/m, \tag{2.9}$$
$$\int_0^t dt' e^{-\gamma(t-t')/m} F_R(t')/m \int_0^t dt'' e^{-\gamma(t-t'')/m} F_R(t'')/m. \tag{2.10}$$

Averaging these three terms over time, we observe that the cross term (2.9) disappears and in the term (2.10) we substitute the Eq. (2.6). The final mean squared velocity is

$$\langle v(t)^2 \rangle = e^{-2\gamma t/m} v(0)^2 + \frac{B}{\gamma m} \left(1 - e^{-2\gamma t/m}\right). \tag{2.11}$$

When $t \to +\infty$ the exponential terms disappear and the mean square velocity obeys the law of equipartition (2.3), therefore

$$B = \gamma k_B T, \tag{2.12}$$

the fluctuation-dissipation theorem. This theorem represents the balance between the friction constant and the strength of the random force.

2.2 Generalized Langevin Equation

2.2.1 Projection formalism

A projection $\mathcal{P}$ is an operator with the following properties [22]

- Linear $\mathcal{P}(c_1A + c_2B) = c_1\mathcal{P}A + c_2\mathcal{P}B$
- idempotent $\mathcal{P}^2A = \mathcal{P}A$,

where $c_1, c_2 \in \mathbb{R}$ and A, B are two arbitrary observables.

The projection $\mathcal{Q} = 1 - \mathcal{P}$ projects an observable onto the *complementary* subspace, where 1 is the identity operator. The operator $\mathcal{P}$ projects on the *relevant* subspace. From the definition of idempotency of the two operators,

$$\mathcal{P}\mathcal{Q} = \mathcal{Q}\mathcal{P} = 0. \tag{2.13}$$

2.2.2 Liouville dynamics and projection method

To use the projector operators we must rewrite the dynamic evolution with the Liouville operator. If we take a point $\omega = (\mathbf{r}, \mathbf{p})$ in the phase space Ω, $\mathbf{r}$ is the vector of the Cartesian position and $\mathbf{p}$ the conjugate momentum, the corresponding Hamiltonian is an invariant of motion, given by

$$H(\omega) = \frac{\mathbf{p}^2}{2m} + V(\mathbf{r}), \tag{2.14}$$

where $V(\mathbf{r})$ is a potential. The evolution of the point ω is defined by a linear differential equation, the *Liouville's equation* through

$$\dot{\omega}_t = \mathcal{L}\omega_t, \tag{2.15}$$

$\mathcal{L} = \left(\frac{\mathbf{P}}{m}\nabla_{\mathbf{r}} - (\nabla_{\mathbf{r}}V)\nabla_{\mathbf{p}}\right)$ is the *Liouville operator*. The subscript t defines the location in the phase space of the point ω at time t. Solving the Eq. (2.15)

$$\omega_t = e^{t\mathcal{L}}\omega_0, \tag{2.16}$$

the initial point ω_0 is propagated by the operator $e^{t\mathcal{L}}$.

The same equation governs the evolution of an observable

$$\dot{A}_t = \mathcal{L}A_t, \tag{2.17}$$

where $A_t = A(\omega_t) = A(\omega_0, t)$ an observable that depends on the real-valued function of the phase space and implicitly on time. We thus define an inner

product, as the observables are elements of a Hilbert space, a vector space within an inner product,

$$\langle A_t, B_{t'} \rangle = \int_\Omega d\omega_0 \; \rho_{eq}(\omega_0) A(\omega_0, t) B(\omega_0, t'), \tag{2.18}$$

where $\rho_{eq}(\omega_0) = \frac{1}{Z} e^{-\beta H_0(\omega_0)}$ is the canonical Boltzmann distribution, with $\beta = \frac{1}{k_B T}$ and the partition function $Z = \int_\Omega d\omega_0 e^{-\beta H_0(\omega_0)}$.

Having defined the dynamic evolution, we can decompose the Liouville equation with the projector operators,

$$\ddot{A}_t = e^{t\mathcal{L}} \mathcal{L} \dot{A}_0 = e^{t\mathcal{L}} (\mathcal{P} + \mathcal{Q}) \mathcal{L} \dot{A}_0 = e^{t\mathcal{L}} \mathcal{P}\mathcal{L} \dot{A}_0 + e^{t\mathcal{L}} \mathcal{Q}\mathcal{L} \dot{A}_0. \tag{2.19}$$

$e^{t\mathcal{L}}\mathcal{Q}$ propagates in time the observables that lie on the complimentary space, using that

$$\frac{d}{dt} e^{t\mathcal{L}} \mathcal{Q} = e^{t\mathcal{L}} \mathcal{L}\mathcal{Q} = e^{t\mathcal{L}} \mathcal{P}\mathcal{L}\mathcal{Q} + e^{t\mathcal{L}} \mathcal{Q}\mathcal{L}\mathcal{Q}, \tag{2.20}$$

and solving the inhomogeneous differential equation, we obtain

$$e^{t\mathcal{L}} \mathcal{Q} = \mathcal{Q} e^{t\mathcal{L}\mathcal{Q}} + \int_0^t du \; e^{u\mathcal{L}} \mathcal{P}\mathcal{L}\mathcal{Q} \; e^{(t-u)\mathcal{L}\mathcal{Q}}. \tag{2.21}$$

Using the equivalence $\mathcal{Q} e^{t\mathcal{L}\mathcal{Q}} = e^{t\mathcal{Q}\mathcal{L}} \mathcal{Q}$ and substituting $s = t - u$, we obtain

$$e^{t\mathcal{L}} \mathcal{Q} = e^{t\mathcal{Q}\mathcal{L}} \mathcal{Q} + \int_0^t ds \; e^{(t-s)\mathcal{L}} \mathcal{P}\mathcal{L} \; e^{s\mathcal{Q}\mathcal{L}} \mathcal{Q}. \tag{2.22}$$

The first term lies on the complementary subspace, whereas the second term is a coupling between the two subspaces. Inserting the Eq. (2.22) inside Eq. (2.19), we obtain [8, 9, 23]

$$\ddot{A}_t = e^{t\mathcal{L}} \mathcal{P}\mathcal{L} \dot{A}_0 + \int_0^t ds \; e^{(t-s)\mathcal{L}} \mathcal{P}\mathcal{L} F_R(s) + F_R(t) \tag{2.23}$$

$$F_R(t) = e^{t\mathcal{Q}\mathcal{L}} \mathcal{Q}\mathcal{L} \dot{A}_0 = \mathcal{Q} e^{t\mathcal{L}\mathcal{Q}} \mathcal{L} \dot{A}_0. \tag{2.24}$$

$F_R(t)$ is a function that lays on the complementary space and depends on the initial condition. In the Eq. (2.23) the first term is similar as the term (2.24), but remains on the relevant subspace. The second term is a coupling between the operator $\mathcal{P}$ and the function $\mathcal{L}F_R(t)$. The Eq. (2.23) has the form of the Langevin equation, but to have an explicit expression, we must specify which projection is applied.

2.2.3 The Mori projection

Considering an observable A_t, the Mori projection is given by [8]

$$\mathcal{P}_M A_t = \frac{\langle A_t, B_0\rangle}{\langle B_0^2\rangle} B_0 + \frac{\langle A_t, \dot{B}_0\rangle}{\langle \dot{B}_0^2\rangle}\dot{B}_0, \tag{2.25}$$

where the bracket defines the inner product as in the Eq. (2.18). The Eq. (2.25) projects the observable A_t onto the subspace of all the functions linear in the observable $B_0,\ \dot{B}_0$.

As a projection $\mathcal{P}_M$ is linear and idempotent, but also self-adjoint with respect to the inner product, therefore satisfying the relations

$$\langle \mathcal{P}_M A_t, C_{t'}\rangle = \langle A_t, \mathcal{P}_M C_{t'}\rangle, \tag{2.26}$$

$$\langle \mathcal{P}_M A_t, \mathcal{Q}_M C_{t'}\rangle = 0, \tag{2.27}$$

given two arbitrary observables $A_t, C_{t'}$.

If we substitute in the Eqs. (2.23), (2.24) the Mori projection and we project directly on the interested observable $B_t = A_t,\ \dot{B}_t = \dot{A}_t$, we obtain

$$\ddot{A}_t = -KA_t - \int_0^t ds\Gamma^M(s)\dot{A}_{t-s} + F^R(\omega_0, t). \tag{2.28}$$

$$K = \frac{\langle \dot{A}_0^2\rangle}{\langle A_0^2\rangle} \tag{2.29}$$

$$\Gamma^M(t) = \frac{\langle F^R(0), F^R(t)\rangle}{\langle \dot{A}_0^2\rangle}. \tag{2.30}$$

The first term in the Eq. (2.28) is a force stemming from a potential of quadratic form, the second and the third term are connected via the fluctuation-dissipation theorem. The equation is an exact derivation from the Liouville equation, but the random force is an explicit function of the initial state of the entire system; therefore it can only be computed for very simple systems.

2.2.4 The Zwanzig projection

Similarly to the Mori projection, the Zwanzig projection is linear, idempotent and self-adjoint, but it is nonlinear in the functions $B_0,\ \dot{B}_0$ [9], because

$$P_Z A_t = \frac{\langle \delta[B(\hat{\omega}_0) - B(\omega_0)]\delta[\dot{B}(\hat{\omega}_0) - \dot{B}(\omega_0)], A(\hat{\omega}, t)\rangle}{\langle \delta[B(\hat{\omega}_0) - B(\omega_0)]\delta[\dot{B}(\hat{\omega}_0) - \dot{B}(\omega_0)]\rangle} = \langle A_t\rangle_{B_0,\dot{B}_0}, \tag{2.31}$$

where $\hat{\omega}_0$ are integrated over. Choosing as the projection function the position ($B_0 \to \mathbf{r}_0$) and the linear momentum ($\dot{B}_0 \to \mathbf{p}_0$), the Liouville equation becomes

$$\dot{\mathbf{p}}_t = -\nabla_{\mathbf{r}_t} U_{PMF}(\mathbf{r}_t) + \int_0^t ds \left[\left(\frac{\nabla_{\mathbf{p}_s}}{\beta} - \frac{\mathbf{p}_s}{m} \right) \right]^T \Gamma^Z(t-s, \mathbf{r}_s, \mathbf{p}_s) + F^R(\omega_0, t) \tag{2.32}$$

where the memory kernel has the following shape

$$\beta \Gamma^Z_{i,j}(t-s, \mathbf{r}_s, \mathbf{p}_s) = \langle F^R_i(0), F^R_j(t-s) \rangle_{\mathbf{r}_s, \mathbf{p}_s}. \tag{2.33}$$

In this case the first term in the Eq. (2.32) is a derivative of the potential of mean force (PMF) $U_{\mathrm{PMF}}(\mathbf{r}) = -k_B T \, ln \langle \delta(\mathbf{r}_0 - \mathbf{r}) \rangle$; a force that acts on a particle to provide the equilibrium positional distribution. The advantage of this projection is that we always obtain the correct distribution at equilibrium; when considering the stochastic description the random force has a mean value of 0 [24]. The Zwanzig projection is difficult to apply, because the memory kernel also depends on the particle position $\mathbf{r}_s$ and momentum $\mathbf{p}_s$.

2.2.5 Mori-Zwanzig projection

The GLE mainly used in the literature is,

$$m\ddot{x}(t) = -\int_0^t \Gamma(t') \, \dot{x}(t-t') dt' - \nabla U\left(x(t)\right) + F_R(t). \tag{2.34}$$

It is an approximate GLE, obtained from the Zwanzig projection imposing a memory function independent of the position and the momentum, as in the Eq. (2.30). In this GLE the random force is Gaussian for longer time limits and the memory function depends only upon the value for time, and therefore can be estimated numerically from the trajectory data. It is demonstrated that the Eq. (2.34) reproduces the full system dynamics [14].

2.3 Mean first-passage time

Another important concept, upon which we will expand later, is the mean first-passage time: the average of the time necessary to reach a target point for the first time beginning from a defined position.

2.3.1 Kramers problem high friction

Kramers studied the escape probability of a Brownian particle over a potential barrier [25]. Starting from the Smoluchowski equation

$$\frac{\partial f(x,t)}{\partial t} = D\frac{\partial}{\partial x}e^{-\beta U(x)}\frac{\partial}{\partial x}e^{\beta U(x)}f(x,t), \tag{2.35}$$

the diffusion of the probability distribution $f(x,t)$ in the phase space in an external potential with the diffusion coefficient $D = \frac{k_B T}{\gamma}$. We assume that

$$J = -De^{-\beta U(x)}\frac{\partial}{\partial x}e^{\beta U(x)}f(x,t) = \text{const.}, \tag{2.36}$$

the flux is constant, therefore the process is stationary ($\dot{f} = 0$).

Writing the equality

$$\frac{Je^{\beta U(x)}}{D} = -\frac{\partial}{\partial x}e^{\beta U(x)}f(x,t) \Rightarrow \frac{J}{D}\int_{x_1}^{x_2} e^{\beta U(x)} = -e^{\beta U(x)}f(x,t)\Big|_{x_1}^{x_2}, \tag{2.37}$$

because the flux J and the diffusion coefficient D are assumed constants. We also assume, that at the maximum x_2 we have absorbing boundary conditions, therefore $f(x_2) = 0$. The Eq. (2.37) becomes

$$\frac{J}{D} = \frac{e^{\beta U(x_1)}f(x_1,t)}{\int_{x_1}^{x_2} e^{\beta U(x)}}. \tag{2.38}$$

Expanding the potential $U(x)$ around the maximum x_2,
$U(x) = U_2 - \frac{U_2''}{2}(x - x_2)$, the integral at the denominator is given by,

$$\begin{aligned}\int_{x_1}^{x_2} e^{\beta U(x)} &= e^{\beta U(x_2)}\int_{x_1}^{x_2} e^{-\beta\frac{U_2''}{2}(x-x_2)} \simeq \frac{1}{2}e^{\beta U(x_2)}\int_{-\infty}^{\infty} e^{-\beta\frac{U_2''}{2}(x-x_2)} \\ &= \frac{1}{2}e^{\beta U(x_2)}\sqrt{\frac{2\pi}{\beta U_2''}}.\end{aligned} \tag{2.39}$$

Introducing this expression in the flux, we obtain

$$J = De^{-\beta(U_2-U_1)}\sqrt{\frac{2\beta U_2''}{\pi}}f(x_1). \tag{2.40}$$

The final step is to write explicitly $f(x_1)$. We assume that it is given by the equilibrium distribution and we expand the potential around the minimum x_1, $U(x) = U_1 + U_1''(x - x_1)^2$,

$$f(x_1) = \frac{e^{-\beta U(x_1)}}{\int_{x_0}^{x_2} dx\ e^{-\beta U(x)}} \simeq \frac{U_1''}{2\pi}. \tag{2.41}$$

In conclusion the flux becomes

$$J = \frac{D\sqrt{U_1'' U_2''}}{\pi k_B T} e^{-\beta \Delta U}, \tag{2.42}$$

it depends exponentially on the potential difference and on the curvature of the potential. Substituting the diffusion coefficient, and knowing that the crossing rate k is half of the flux, we obtain

$$k = \frac{\sqrt{U_1'' U_2''}}{2\pi\gamma} e^{-\beta \Delta U}. \tag{2.43}$$

If we consider a double well potential

$$U = U_0 \left(\left(\frac{x}{L} \right)^2 - 1 \right)^2, \tag{2.44}$$

the crossing rate is

$$k = \frac{2\sqrt{2} U_0}{\pi \gamma L^2} e^{-\beta U_0}. \tag{2.45}$$

The inverse of the crossing rate is the mean first-passage time for a Markovian system in high friction limit, $\tau_{MFP} = 1/k$.

2.3.2 Grote-Hynes theory

The Grote-Hynes (GH) theory predicts the barrier crossing time with frequency-dependent friction [26]

$$\tau^{GH} = \frac{2\pi\omega_{max}}{\lambda \omega_{min}} e^{\beta U_0}, \tag{2.46}$$

where $\omega_{max} = \sqrt{|U''_{max}|/m}$ and $\omega_{min} = \sqrt{|U''_{min}|/m}$ are the frequencies at the free energy maximum and minimum respectively. In Eq. (2.46), we recognize the Transition state theory (TST) prediction for the barrier crossing,

$$\tau^{TST} = \frac{2\pi}{\omega_{min}} e^{\beta U_0}. \tag{2.47}$$

For a symmetric double-well potential, the frequencies, respectively, are $\omega_{max} = \sqrt{4\beta U_0/(\tau_D \tau_m)}$ and $\omega_{min} = \sqrt{8\beta U_0/(\tau_D \tau_m)}$. λ is the barrier reactive frequency, solution of the Grote-Hynes equation

$$\lambda^2 + \lambda \frac{\tilde{\Gamma}(\lambda)}{m} = \omega_{max}^2, \tag{2.48}$$

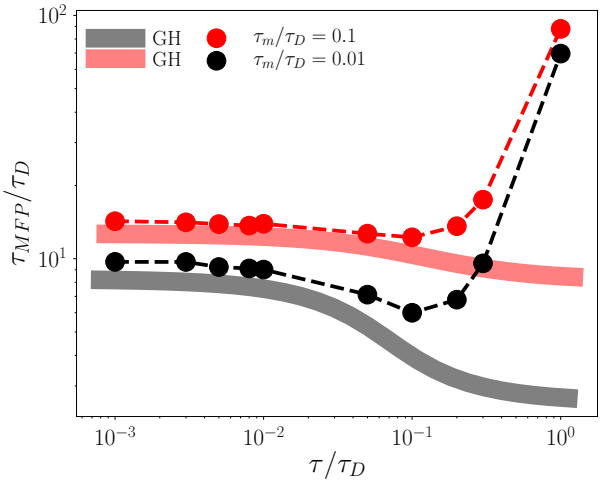

Figure 2.1: MFPT as a function of rescaled τ/τ_D for a symmetric double-well potential Eq. (2.44) with $\beta U_0 = 3$, red for $\tau_m/\tau_D = 0.1$ and black for $\tau_m/\tau_D = 0.01$. The thick lines are the Grote-Hynes theory following the Eq. (2.46). The circles are the simulation data, connected with broken lines.

where $\tilde{\Gamma}(\lambda)$ is the Laplace transform of the friction memory kernel, and in the case of a single exponential memory kernel, it is given by

$$\tilde{\Gamma}(\lambda) = \int_0^\infty \Gamma(t')e^{-\lambda t'}dt' = \frac{\gamma}{1+\tau\lambda}. \tag{2.49}$$

Inserting the Laplace transform of the friction memory kernel into the GH equation (2.48), we obtain a cubic polynomial, which has a real and positive root.

In Fig.2.1, we observe the agreement between the Grote-Hynes Theory, and the simulation data for small values of τ/τ_D, but a deviation for intermediate and high values. To better understand this behavior, we must study the various limits of GH-Theory.

- Markovian limit ($\tau/\tau_D \to 0$), equivalent to the Kramers (Kr) rate for intermediate-high friction.

  In other words $\tilde{\Gamma}(\lambda) = \gamma$, meaning that

$$\lambda = -\frac{\gamma}{2m} \pm \left(\frac{\gamma^2}{4m^2} + \omega_{max}^2\right)^{1/2}, \tag{2.50}$$

  taking the positive root we obtain

$$\tau^{Kr} = \omega_{max}\left[\left(\frac{\gamma^2}{4m^2}+\omega_{max}^2\right)^{1/2}-\frac{\gamma}{2m}\right]^{-1}\tau^{TST}. \tag{2.51}$$

– High friction limit ($\frac{\gamma}{m} \gg 1$)

$$\begin{aligned}\lambda &= \frac{\gamma}{2m}\left(1+\frac{4m^2\omega_{max}^2}{\gamma^2}\right)^{1/2}-\frac{\gamma}{2m}\\ &\simeq \frac{\gamma}{2m}+\frac{m\omega_{max}^2}{\gamma}-\frac{\gamma}{2m}\\ &= \frac{m\omega_{max}^2}{\gamma}.\end{aligned} \tag{2.52}$$

$$\tau_{hf}^{Kr} = \frac{2\pi\gamma}{m\omega_{max}\omega_{min}}e^{\beta U_0}. \tag{2.53}$$

– Low friction limit ($\frac{\gamma}{m} \ll 1$).

$$\tau_{lf}^{Kr} = \tau^{TST}, \tag{2.54}$$

because $\lambda = \omega_{max}$.

- Low mass ($m \to 0$).
  The GH's equation (2.48) becomes

$$\lambda\frac{\gamma}{(1+\tau\lambda)m}-\omega_{max}^2 = 0, \tag{2.55}$$

$$\Rightarrow \lambda = \frac{\omega_{max}^2 m/\gamma}{1-\tau\omega_{max}^2 m/\gamma}. \tag{2.56}$$

$$\tau_{low-mass}^{GH} = \frac{2\pi(1-\omega_{max}^2\tau m/\gamma)}{\omega_{min}\omega_{max}m/\gamma}e^{\beta U_0}, \tag{2.57}$$

  The speed-up regime is recovered for intermediate τ, but the transition time continuously decreases with the increasing memory time, as depicted in Fig.2.1.

- Long memory limit ($\tau/\tau_D \gg 1$), in this limit, the Laplace transform of the memory kernel is

$$\tilde{\Gamma}(\lambda) \simeq \frac{\gamma}{\tau\lambda}, \tag{2.58}$$

$$\Rightarrow \lambda = \omega_{max}\left(1 - \frac{\gamma}{\tau\omega_{max}^2}\right)^{1/2}. \tag{2.59}$$

$$\tau_{long-memory}^{GH} = \frac{2\pi}{\omega_{min}\left(1 - \frac{\gamma}{\tau m\omega_{max}^2}\right)^{1/2}} e^{\beta U_0}, \tag{2.60}$$

for $\tau \to 0$, the transition time is independent of τ and for this reason we observe a constant value in Fig.2.1.

$$\tau_{\tau\to\infty}^{GH} = \frac{2\pi\sqrt{m}}{\sqrt{U''_{min}}}, \tag{2.61}$$

The transition time trends towards zero as $m \to 0$.

2.3.3 Mel'nikov Meshkov theory

The idea behind Me'lnikov Meshkov theory [27] is to derive the Green's function of the Fokker-Planck equation in the form of a system of integral equations. By Fourier transform the equations can then be solved by the Wiener-Hopf method [28]. As a first step we calculate the action of one oscillation of a particle with zero total energy

$$S_1 = \int_{-\sqrt{2}}^{0} \sqrt{-U_0\beta\left((x^2-1)^2 - 1\right)}dx. \tag{2.62}$$

The final expression for the MFPT is

$$\begin{aligned}\frac{\tau_{MFP}}{\tau_D}^{-1} = \frac{\sqrt{8U_0\beta/(\tau_m\tau_D)}}{2\pi}\Bigg(&\sqrt{1 + \frac{1}{4\tau_m^2 4U_0\beta/(\tau_m\tau_D)}} \\ &- \frac{1}{2\tau_m\sqrt{4U_0\beta/(\tau_m\tau_D)}}\Bigg) A(\tau_m, \tau_D, S_1)e^{-\beta U_0},\end{aligned} \tag{2.63}$$

2.3.4 Calculation of the mean first passage time from simulation

There is no unique method of calculating the mean first passage time from simulation, or rather the average time to make a transition between states. One method is to consider the mean first-to-first passage time (MFFPT), in other words the time that a system spends in a certain state. The other method is to consider the mean all-to-first passage time MAFPT, which tells us how long it takes a system to transition from one state to another. In the Fig.2.2 we illustrate the two definitions.

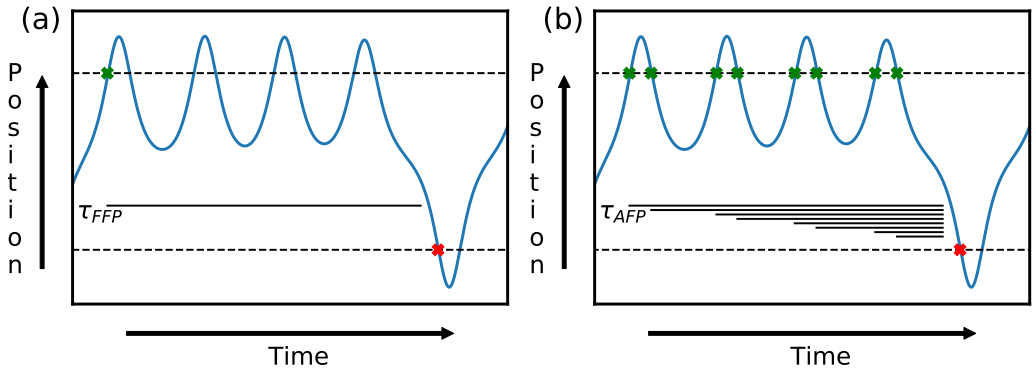

Figure 2.2: Particle trajectory, on the left the definition of the first-to-first passage time, which is the difference in time between the green and the red cross. On the right are shown various all-to-first passage times; the gap times between every green crosses and the red one.

In rare event systems, such as the folding of a protein or a phase transition, it is convenient to consider the all-to-first mean first passage time, in order to reduce the noise and enhance statistical accuracy. The two times are comparable for Markovian systems, but when memory effects are present, the two times diverge. The τ_{MAFP} corresponds to the longest time of dynamics, and the MFFPT in non-Markovian systems scales alongside the mean transition path time.

In the remainder of this thesis we will discuss in greater detail the mean all to first passage time, which we will refer to the MAFPT.

2.4 Langevin simulation methods

In this section, we will explain the equations that we use to simulate the non-Markovian dynamics.

If we consider an exponential memory kernel

$$\Gamma(t) = \frac{\gamma}{\tau} e^{-|t|/\tau}, \tag{2.64}$$

and to efficiently simulate the system, we first derive a dimensionless version of the GLE,

$$
\begin{aligned}
m\ddot{x}(t) &= -\int_{t_0}^{t} \frac{\gamma}{\tau} e^{-\frac{|t-t'|}{\tau}} \dot{x}(t')dt' - \nabla U(x(t)) + F_R(t), \\
m\frac{L}{k_BT}\ddot{x}(t) &= -\int_{t_0}^{t} \frac{L}{k_BT}\frac{\gamma}{\tau} e^{-\frac{|t-t'|}{\tau}} \dot{x}(t')dt' - \frac{L}{k_BT}\nabla U(x(t)) + \frac{L}{k_BT}F_R(t), \\
m\frac{L}{k_BT}\frac{L}{\tau_D^2}\ddot{\tilde{x}}(\tilde{t}) &= -\int_{\tilde{t}_0}^{\tilde{t}} \frac{L}{k_BT}\frac{\gamma}{\tau} e^{-\frac{\tau_D|\tilde{t}-\tilde{t}'|}{\tau}} \frac{L}{\tau_D}\dot{\tilde{x}}(\tilde{t}')\tau_D d\tilde{t}' - \frac{L}{k_BT}\nabla U(x(t)) + \frac{L}{k_BT}F_R(t), \\
\frac{\tau_m}{\tau_D}\ddot{\tilde{x}}(\tilde{t}) &= -\int_{\tilde{t}_0}^{\tilde{t}} \frac{\tau_D}{\tau} e^{-\frac{\tau_D|\tilde{t}-\tilde{t}'|}{\tau}} \dot{\tilde{x}}(\tilde{t}')d\tilde{t}' + \tilde{F}\left[\tilde{x}(\tilde{t})\right] + \tilde{F}_R(\tilde{t}),
\end{aligned}
\tag{2.65}
$$

where $\tilde{t} = t/\tau_D$, $\tilde{x}(\tilde{t}) = x(\tau_D\tilde{t})/L$, and $\tilde{F}(\tilde{x}) = -(k_BT)^{-1}LU'(L\tilde{x})$. Dots in the equations denote derivatives with respect to time. In a state of equilibrium, the generalized Langevin equation Eq. (2.65) can be rewritten as a coupled set of Markovian differential equations,

$$\dot{\tilde{x}}(\tilde{t}\,) = \frac{d\tilde{x}(\tilde{t})}{d\tilde{t}}, \tag{2.66}$$

$$\ddot{\tilde{x}}(\tilde{t}\,) = \frac{\tau_D}{\tau_m}\left(R(\tilde{t}) + \tilde{F}\left[\tilde{x}(\tilde{t})\right]\right), \tag{2.67}$$

$$\dot{R}(\tilde{t}\,) = -\frac{\tau_D}{\tau}\left(R(\tilde{t}) + \dot{\tilde{x}}(\tilde{t}\,) - \tilde{\xi}(\tilde{t})\right). \tag{2.68}$$

Here, $R(\tilde{t})$ is an auxiliary variable and the correlation function of the dimensionless random force $\tilde{\xi}(\tilde{t})$ is given by

$$\langle\tilde{\xi}(\tilde{t})\tilde{\xi}(\tilde{t}')\rangle = 2\delta(\tilde{t}-\tilde{t}'). \tag{2.69}$$

Solving the inhomogeneous differential Eq. (2.68) we obtain

$$R(\tilde{t}) = -\frac{\tau_D}{\tau}\int_{\tilde{t}_0}^{\tilde{t}} \exp\left[-\frac{\tau_D}{\tau}(\tilde{t}-\tilde{t}')\right]\left(\dot{\tilde{x}}(\tilde{t}') - \tilde{\xi}(\tilde{t}')\right)d\tilde{t}'. \tag{2.70}$$

Substituting this result into Eq. (2.67), we obtains Eq. (2.65), the rescaled equilibrium version of the GLE (2.34) [19], and where the random force is given by

$$\tilde{F}_R(\tilde{t}) = \frac{\tau_D}{\tau}\int_{\tilde{t}_0}^{\tilde{t}} \exp\left[-\frac{\tau_D}{\tau}(\tilde{t}-\tilde{t}')\right]\tilde{\xi}(\tilde{t}')d\tilde{t}'. \tag{2.71}$$

Calculating the random force autocorrelation

$$
\begin{aligned}
&\langle \tilde{F}_R(\tilde{t})\tilde{F}_R(\tilde{t}')\rangle = \\
&\left(\frac{\tau_D}{\tau}\right)^2 \int_{\tilde{t}_0}^{\tilde{t}} dy \int_{\tilde{t}_0}^{\tilde{t}'} \exp\left[-\frac{\tau_D}{\tau}(\tilde{t}-y)\right] \exp\left[-\frac{\tau_D}{\tau}(\tilde{t}'-y')\right] \langle \tilde{\xi}(y)\tilde{\xi}(y')\rangle dy' \\
&= 2\left(\frac{\tau_D}{\tau}\right)^2 \int_{\tilde{t}_0}^{\tilde{t}} dy \int_{\tilde{t}_0}^{\tilde{t}'} \exp\left[-\frac{\tau_D}{\tau}(\tilde{t}-y)\right] \exp\left[-\frac{\tau_D}{\tau}(\tilde{t}'-y')\right] \delta(y-y')dy' \\
&= 2\left(\frac{\tau_D}{\tau}\right)^2 \exp\left[-\frac{\tau_D}{\tau}(\tilde{t}+\tilde{t}')\right] \int_{\tilde{t}_0}^{\min\{\tilde{t},\tilde{t}'\}} \exp\left[2\frac{\tau_D}{\tau}y\right] dy \\
&= 2\left(\frac{\tau_D}{\tau}\right)^2 \exp\left[-\frac{\tau_D}{\tau}(\tilde{t}+\tilde{t}')\right] \frac{\tau}{2\tau_D}\left(\exp\left[2\frac{\tau_D}{\tau}\min\{\tilde{t},\tilde{t}'\}\right] - \exp\left[2\frac{\tau_D}{\tau}\tilde{t}_0\right]\right) \\
&= \frac{\tau_D}{\tau}\left(\exp\left[-\frac{\tau_D}{\tau}|\tilde{t}-\tilde{t}'|\right] - \exp\left[-\frac{\tau_D}{\tau}(\tilde{t}+\tilde{t}'-2\tilde{t}_0)\right]\right),
\end{aligned}
\tag{2.72}
$$

for $\tilde{t}+\tilde{t}' \gg 2\tilde{t}_0$ we have

$$
\langle \tilde{F}_R(\tilde{t})\tilde{F}_R(\tilde{t}')\rangle = \frac{\tau_D}{\tau}\exp\left[-\frac{\tau_D}{\tau}|\tilde{t}-\tilde{t}'|\right]. \tag{2.73}
$$

This is the rescaled version of Eq. (1.2) for the equilibrium case. In the simulations we use Eqs. (2.66)-(2.68) in conjunction with the 4th order Runge-Kutta method [29, 30]. The time step is fixed at

$$
\Delta\tilde{t} = \Delta t/\tau_D \cdot \min\{\tau_m/\tau_D, \tau/\tau_D, \tau_R/\tau_D\}. \tag{2.74}
$$

In this thesis we will take in consideration different memory kernels, in the following sections we take in consideration how the Markovian embedding changes for various memory function.

2.4.1 Multi-exponential memory kernel

The function of a multi-exponential memory kernel is

$$
\Gamma(t) = \sum_{i=1}^{N} \frac{\gamma_i}{\tau_i} e^{-t/\tau_i}. \tag{2.75}
$$

The Markovian embedding for the multi-exponential memory kernel can be written as

$$\dot{\tilde{x}}(\tilde{t}\,) = \frac{d\tilde{x}(\tilde{t})}{d\tilde{t}}, \tag{2.76}$$

$$\frac{\tau_m}{\tau_D}\ddot{\tilde{x}}(\tilde{t}\,) = \sum_{i=1}^{N}\left[R_i(\tilde{t}) + \tilde{F}\left(\tilde{x}(\tilde{t}\,)\right)\right], \tag{2.77}$$

$$\dot{R}_i(\tilde{t}\,) = -\frac{\tau_D}{\tau_i}\left[R_i(\tilde{t}\,) + \frac{\gamma_i}{\gamma}\dot{\tilde{x}}(\tilde{t}\,) - \sqrt{\frac{\gamma_i}{\gamma}}\tilde{\xi}_i(\tilde{t}\,)\right] \quad 1 \le i \le N, \tag{2.78}$$

where $\tilde{t} = t/\tau_D$, $\tilde{x}(\tilde{t}) = x(\tau_D\tilde{t})/L$, the R_i are auxiliary variables, $\tilde{F}(\tilde{x}) = (k_BT)^{-1}LU'(L\tilde{x})$, dots here denote derivatives with respect to $\tilde{t}$, and the correlators of the dimensionless random forces $\tilde{\xi}_i(\tilde{t}) := (k_BT)^{-1}L\,f_{R_i}(\tau_D\tilde{t})$ are given by

$$\langle\tilde{\xi}_i(\tilde{t})\tilde{\xi}_j(\tilde{t}')\rangle = 2\delta(\tilde{t}-\tilde{t}')\delta_{ij}. \tag{2.79}$$

Solving the inhomogeneous harmonic oscillator Eq. (2.78) for the auxiliary variable $\tilde{R}_i$, substituting the result into Eq. (2.77), it is seen that Eqs. (2.76-2.79) are equivalent to the GLE with multi-exponential memory kernel [18].

2.4.2 GLE out of equilibrium

As already said before, a GLE is ouf of equilibrium when the FDT is violated, for this reason we consider a single exponential friction memory kernel Γ_V and for the random force correlator we take another exponential memory function with different memory time Γ_R,

$$\Gamma_V(t) = \frac{\gamma_V}{\tau_V}e^{-\frac{|t|}{\tau_V}}, \tag{2.80}$$

$$\Gamma_R(t) = \frac{\gamma_R}{\tau_R}e^{-\frac{t}{\tau_R}} \quad \text{for} \quad t > 0 \tag{2.81}$$

The dimensionless version of the GLE is

$$\frac{\tau_m}{\tau_D}\ddot{\tilde{x}}(\tilde{t}) = -\int_{\tilde{t}_0}^{\tilde{t}}\frac{\tau_D}{\tau_V}e^{-\frac{\tau_D|\tilde{t}-\tilde{t}'|}{\tau_V}}\dot{\tilde{x}}(\tilde{t}')d\tilde{t}' + \tilde{F}\left[\tilde{x}(\tilde{t})\right] + \tilde{F}_R(t). \tag{2.82}$$

To simulate the non-equilibrium GLE, we need to split the auxiliary variable $R(\tilde{t})$ into two variables $R_V(\tilde{t})$ and $R_R(\tilde{t})$ and use the coupled set of

Markovian equations

$$\dot{\tilde{x}}(\tilde{t}\,) = \frac{d\tilde{x}(\tilde{t})}{d\tilde{t}}, \tag{2.83}$$

$$\ddot{\tilde{x}}(\tilde{t}\,) = \frac{\tau_D}{\tau_m}\left(R_V(\tilde{t}) + R_R(\tilde{t}) + \tilde{F}\left[\tilde{x}(\tilde{t})\right]\right), \tag{2.84}$$

$$\dot{R}_V(\tilde{t}\,) = -\frac{\tau_D}{\tau_V}\left(R_V(\tilde{t}) + \dot{\tilde{x}}(\tilde{t}\,)\right), \tag{2.85}$$

$$\dot{R}_R(\tilde{t}\,) = -\frac{\tau_D}{\tau_R}\left(R_R(\tilde{t}) - \tilde{\xi}(\tilde{t})\right). \tag{2.86}$$

Solving the inhomogeneous differential Eqs. (2.85) and (2.86), we obtain

$$R_V(\tilde{t}) = -\frac{\tau_D}{\tau_V}\int_{\tilde{t}_0}^{\tilde{t}} \exp\left[-\frac{\tau_D}{\tau_V}(\tilde{t}-\tilde{t}')\right]\dot{\tilde{x}}(\tilde{t}')d\tilde{t}', \tag{2.87}$$

$$R_R(\tilde{t}) = \frac{\tau_D}{\tau_R}\int_{\tilde{t}_0}^{\tilde{t}} \exp\left[-\frac{\tau_D}{\tau_R}(\tilde{t}-\tilde{t}')\right]\tilde{\xi}(\tilde{t}')d\tilde{t}'. \tag{2.88}$$

Inserting these results into Eq. (2.84) we arrive at the rescaled GLE (2.82), where in this case the random force and its correlation are given by

$$\tilde{F}_R(\tilde{t}) = \frac{\tau_D}{\tau_R}\int_{\tilde{t}_0}^{\tilde{t}} \exp\left[-\frac{\tau_D}{\tau_R}(\tilde{t}-\tilde{t}')\right]\tilde{\xi}(\tilde{t}')d\tilde{t}', \tag{2.89}$$

$$\langle \tilde{F}_R(\tilde{t})\tilde{F}_R(\tilde{t}')\rangle = \frac{\tau_D}{\tau_R}\exp\left[-\frac{\tau_D}{\tau_R}|\tilde{t}-\tilde{t}'|\right]. \tag{2.90}$$

Chapter 3

Barrier crossing in the presence of multi-exponential memory functions

3.1 Introduction

Most biological and chemical processes work at the nano-scale, such as chemical reactions and protein folding. The dynamics of the molecules involved are stochastic processes in a liquid governed by thermal noise. These systems are studied by either the Langevin or the Fokker-Plank equations. In the Markovian limit, the orthogonal degrees of freedom reach a state of relaxation more rapidly than the diffusive and inertial time scales of the reaction coordinate [11, 31–35]. However, the adiabatic approximation, in which one neglects the relaxation of these degrees of freedom, is not always valid, as is the case for dihedral barrier crossing, reactions in peptides and alkalis, as well as for ion-pairing kinetics [36–42]. Sometimes, the characteristic times for the reaction coordinate and the environment are similar; we must, therefore, include memory effects to characterize the dynamics of the reaction coordinate correctly. In other words, we are dealing with a non-Markovian process. In most systems, a single time scale is not sufficient, and it is necessary to consider several memory time scales in order to produce an accurate description, depending on the complexity of the system [31, 36, 43–46].

Often, these processes can be described as a barrier-crossing in a one-dimensional landscape [25, 47–55], and they are mainly studied in the framework of the generalized Langevin equation (GLE) [8, 9, 26, 55–58]

$$m\ddot{x}(t) = -\int_0^t \Gamma(t-t')\dot{x}(t')dt' - U'\left[x(t)\right] + F_R(t), \tag{3.1}$$

where m is the effective mass of the reaction coordinate x, $\Gamma(t)$ is the memory kernel function and $U'(x)$ is the derivative of the potential $U(x)$. $F_R(t)$ denotes the Gaussian time-dependent random force with $\langle F_R(t)\rangle = 0$. At equilibrium, which is the scenario we will consider in this chapter, the relationship between the friction kernel $\Gamma(t)$ and the autocorrelation of the random force is given by

$$\langle F_R(t)F_R(t')\rangle = k_B T\Gamma(|t-t'|), \tag{3.2}$$

where T is the temperature and k_B is the Boltzmann constant. To describe the barrier crossing, we will choose a symmetrical double-well potential

$$U(x) = U_0\left[\left(\frac{x}{L}\right)^2 - 1\right]^2. \tag{3.3}$$

The separation between the two wells is $2L$, and the barrier height is given by U_0, as shown in Fig.3.1a). In the main part of this discussion, we will use $U_0 = 3k_BT$.

Considering a memory kernel expressed as a sum of N exponentials

$$\Gamma(t) = \sum_{i=1}^{N} \frac{\gamma_i}{\tau_i} e^{-t/\tau_i}, \tag{3.4}$$

where τ_i and γ_i are the i-th memory time and friction coefficient. Accordingly, the random force in Eq. (3.1) can be decomposed in

$$F_R(t) = \sum_{i=1}^{N} f_{R_i}(t), \tag{3.5}$$

where

$$\langle f_{R_i}(t)f_{R_j}(t')\rangle = k_B T\frac{\gamma_i}{\tau_i} e^{-|t-t'|/\tau_i}\delta_{ij} \quad \forall i,j. \tag{3.6}$$

The integral over the memory function $\gamma = \int_0^\infty \Gamma(t)dt = \sum_{i=1}^{N}\gamma_i$ defines the total friction coefficient and, by construction, is independent of the memory times.

The most important characteristic of these systems is the mean first-passage time (MFPT), the mean of the time necessary to first reach a minimum of the double well potential starting from the other minimum. As illustrated in Fig.3.1b), the MFPT is the average time between each blue and red lines.

In Ref. [18], for single-exponential memory ($N = 1$), it was proven that the mean first-passage time τ_{MFP} is a function of the memory time τ and

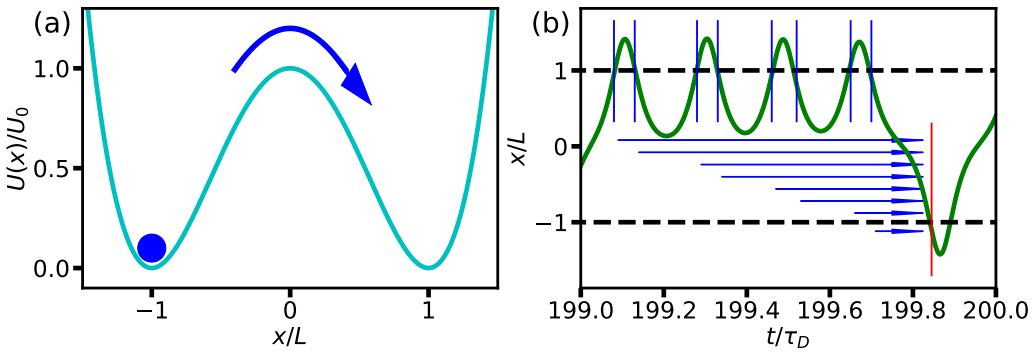

Figure 3.1: a) Picture of a double well potential as defined in the Eq. (3.3) with a massive particle. The first passage time is the time required for a massive particle to cross the minimum, for example, $x/L = -1$, and reach the other minimum ($x/L = 1$) for the first time. In b), we see the illustration of how the first-passage times (FPTs) are calculated; the blue vertical lines depict the crossing of the minimum $x/L = 1$, and the red vertical line denotes the initial crossing of the other minimum $x/L = -1$. The difference between the red line and each blue line provides us with a sample for the FPT. The mean first-passage time (MFPT) is obtained by taking an average of all the values of FPT. The parameters used for the depicted trajectory are $\tau_m/\tau_D = 0.001$, $\tau_1/\tau_D = 1$, $\tau_2/\tau_D = 10$, $\gamma_2/\gamma_1 = 2$ and barrier height $\beta U_0 = 3$.

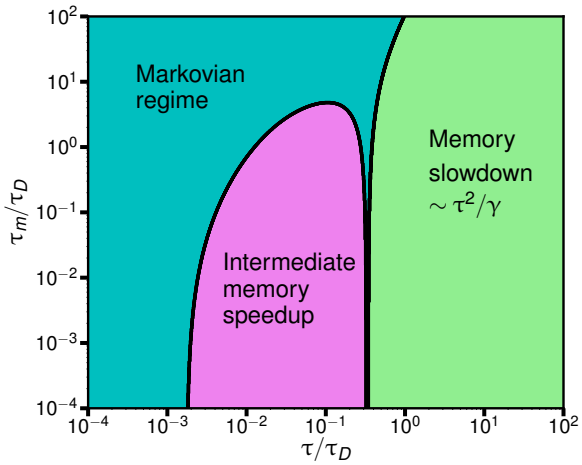

Figure 3.2: Scaling behaviour of the MFPT as a funtion of τ_m/τ_D on the y-scale and of τ/τ_D on the x-scale. The transition between the Markovian regime (blue area) and the intermediate memory speedup (purple area) is defined when the MFPT is 5% smaller than the Markovian time. The green area is the memory slowdown, that means that τ_{MFP}/τ_D is higher than the Markovian time. The asympotic behavior is τ^2/γ.

the friction coefficient γ, with an asymptotic behavior $\tau_{MFP} \simeq \tau^2/\gamma$ for long values of memory time as shown in the Fig.3.2 in the light-green area. In fact, in Fig.3.2 we show a phase diagram for the behaviour of the MFPT as a function of τ_m/τ_D and the memory time. The barrier-crossing kinetics are modified in the presence of the slowly decaying memory, even when the MFPT is much longer than the memory time. This simply means that time-scale separation, where the memory time modifies the MFPT only when they have similar values, is no longer valid. On the other hand, in the friction-dominated regime and for intermediate memory time, we are able to observe a speed-up regime of the MFPT (purple in Fig.3.2), meaning that the barrier-crossing kinetics are faster than those observed in the Markovian model. The value of the memory time determines whether the barrier-crossing process will accelerate or decelerate.

For a system with a bi-exponential memory kernel ($N = 2$), where the friction amplitudes contribute equally ($\gamma_1 = \gamma_2 = \gamma$), it was previously demonstrated that the MFPT is dominated by the shorter memory time [19], provided that one of the two memories is larger than the intrinsic diffusion time.

By examining the trajectories in Fig.3.3, we can visualize how the system is altered when the memory times are modified. In the figure, we depict

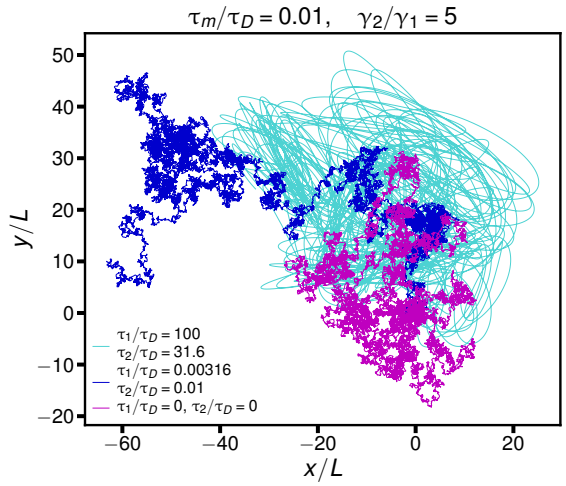

Figure 3.3: Two-dimensional particle trajectories for $\tau_m/\tau_D = 0.01$ and $\gamma_2/\gamma_1 = 5$ without an external potential for the Markovian case $\tau_1/\tau_D = \tau_2/\tau_D = 0$ (magenta), for bi-exponential memory with $\tau_1/\tau_D = 0.00316, \tau_2/\tau_D = 0.01$ (blue) and $\tau_1/\tau_D = 100, \tau_2/\tau_D = 31.6$ (light blue).

the trajectories in 2-D of three particles without an external potential with various memory times. In magenta, a particle with Markovian dynamics, in blue short memory times ($\tau_1/\tau_D = 0.00316$, $\tau_1/\tau_D = 0.01$) and in light blue with long memory times ($\tau_1/\tau_D = 100$, $\tau_1/\tau_D = 31.6$). In particular, the free particle has a different dynamic even when introducing lower values of memory time (blue line) compared the Markovian case (magenta line).

This chapter will consider a position-independent memory function as a sum of two exponentials with different memory times and friction coefficients. Furthermore, we will take into account the sum of three exponentials. By comparing our simulation data with the previous formula (for the bi-exponential memory kernel in a limited case), we are able to confirm the validity of a previously [19] suggested heuristic formula for the mean first-passage time, τ_{MFP}.

3.2 Setup

In order to analyze a general non-Markovian system according to Eq. (3.1), we introduce two time-scales

$$\tau_D = \frac{L^2\gamma}{k_B T}, \tag{3.7}$$

$$\tau_m = \frac{m}{\gamma}, \tag{3.8}$$

where τ_D and τ_m represent the diffusion and inertial times, respectively. The diffusion time depends on the separation between the two potential wells $2L$, the friction coefficient γ, and the temperature T. The inertial time is proportional to the mass m and inversely proportional to the friction coefficient. Using the two time-scales defined in Eq. (3.7) and (3.8), we rewrite Eq. (3.1) as

$$\frac{\tau_m}{\tau_D}\ddot{\tilde{x}}(\tilde{t}) = -\sum_{i=1}^{N}\frac{\tau_D}{\tau_i}\int_0^{\tilde{t}}\frac{\gamma_i}{\gamma}e^{-\frac{\tau_D}{\tau_i}}\dot{\tilde{x}}(\tilde{t}')d\tilde{t}' + 4\frac{U_0}{k_B T}\tilde{x}(1-\tilde{x}^2) + \tilde{F}_R(\tilde{t}), \tag{3.9}$$

where $\tilde{t} = t/\tau_D$ and $\tilde{x}(\tilde{t}) = x(\tau_D\tilde{t})/L$ are the dimensionless time and particle position respectively, we define the dimensionless random force as $\tilde{F}_R(\tilde{t}) = LF_R(\tau_D\tilde{t})/k_B T$. It is, therefore, clear that the problem is accurately described by the rescaled potential barrier $U_0/k_B T$ and the characteristic time scales τ_D, τ_m, and τ_i. To simulate numerically Eq. (3.9), we must first rewrite it as a set of Markovian embedding equations, adding N auxiliary variables $R_i(\tilde{t})$ [59], as

$$\begin{aligned}
&\frac{d}{d\tilde{t}}\tilde{x}(\tilde{t}) = \dot{\tilde{x}}(\tilde{t}),\\
&\frac{d}{d\tilde{t}}\dot{\tilde{x}}(\tilde{t}) = \frac{\tau_D}{\tau_m}\left(\sum_{i=1}^{N}R_i(\tilde{t}) + 4\frac{U_0}{k_B T}\tilde{x}(1-\tilde{x}^2)\right),\\
&\frac{d}{d\tilde{t}}\dot{R}_i(\tilde{t}) = -\frac{\tau_D}{\tau_i}\left(R_i(\tilde{t}) + \frac{\gamma_i}{\gamma}\dot{\tilde{x}}(\tilde{t}) - \xi_i(\tilde{t})\right), \quad \text{for} \quad i \in [1...N]
\end{aligned} \tag{3.10}$$

where

$$R_i(\tilde{t}) = -\frac{\tau_D}{\tau_i}\int_0^{\tilde{t}} e^{-\frac{\tau_D}{\tau_i}}\left(\frac{\gamma_i}{\gamma}\dot{\tilde{x}}(\tilde{t}') - \xi(\tilde{t}')\right)d\tilde{t}'. \tag{3.11}$$

Here $\xi_i(\tilde{t})$ are random variables, with

$$\begin{aligned}
\langle\xi_i(\tilde{t})\rangle &= 0,\\
\langle\xi_i(\tilde{t})\xi_j(\tilde{t}')\rangle &= 2\frac{\gamma_i}{\gamma}\delta(\tilde{t}-\tilde{t}')\delta_{ij}.
\end{aligned} \tag{3.12}$$

In chapter 2, we show that the set of Eqs. (3.10), (3.11), and (3.12) is equivalent to Eq. (3.9). From our simulations, we collect all values of first passage time τ_{FP}; the time that the particle needs to reach the minimum $x/L = 1$ crossing the minimum $x/L = -1$. Since we are considering a symmetric potential, we can also count the crossing time from the minimum $x/L = -1$ to $x/L = 1$. The MFPT is the average of these values.

3.3 First passage trajectories and distributions

In Fig.3.4, we depict a number of simulation trajectories, for an one-dimensional system with a double-well potential. First, this figure shows the importance of considering a range of friction coefficients. All the trajectories are for $\tau_1/\tau_D = 1$ and $\tau_2/\tau_D = 10$, in the upper row the plots are characterized by $\tau_m/\tau_D = 0.001$ (high friction) and in the bottom row by $\tau_m/\tau_D = 10$ (low friction). From left to right, we have various ratios between the friction coefficients $\gamma_2/\gamma_1 = 100$, $\gamma_2/\gamma_1 = 2$ and $\gamma_2/\gamma_1 = 0.01$, respectively.

We are thus able to observe a variety of behaviors in the trajectories when we transition from a) to c) and from d) to f), where the ratio between γ_2/γ_1 decreases. In fact, from left to right, the mean first passage time decreases because we see more transition between the two minima.

In Fig.3.5, we plot the rescaled first-passage time distribution in a semi-logarithmic representation, with the same parameters as in Fig.3.4. We are, therefore, able to observe that the distributions follow an exponential distribution. For all simulation data, we further check whether the simulation distribution has an exponential behavior in order to be sure that our simulations are equilibrated and sufficiently long,

$$\rho(\tau_{FP}) = \frac{1}{\tau_{MFP}} \exp(-\tau_{FP}/\tau_{MFP}), \tag{3.13}$$

analytically depicted with red lines in Fig.3.5.

3.4 Bi-exponential and triple-exponential memory kernel

The aim of this section is to find a heuristic formula for MFPT with a multi-exponential memory kernel. For this, we first study the case for a bi-exponential memory kernel with a fixed ratio γ_2/γ_1. We run simulations for the Markovian embedding (3.10) and extract the MFPT. We compare them with a previously proposed heuristic crossover formula [19]

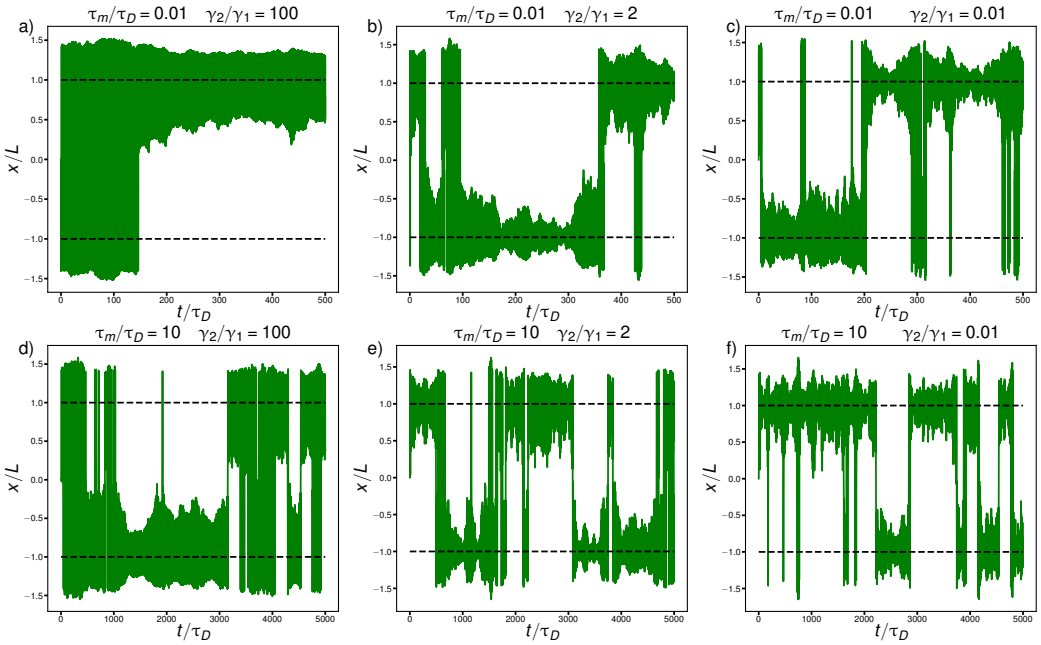

Figure 3.4: Simulation trajectories in one dimension for a barrier crossing potential with height $\beta U_0 = 3$ for memory times $\tau_1/\tau_D = 1$ and $\tau_2/\tau_D = 10$. In the upper row (a-c) are trajectories for high friction with $\tau_m/\tau_D = 0.01$, while in the lower row (d-f) for low friction with $\tau_m/\tau_D = 10$. Each column corresponds to a different ratio γ_2/γ_1 equal to 100 (a,d), 2 (b,e), or 0.01 (c,f). The black dashed lines indicate the positions of the two potential minima.

$$\tau_{MFP} = \sum \tau^i_{OD} + \Big(\sum 1/\tau^i_{ED}\Big)^{-1}, \tag{3.14}$$

which is the sum of the overdamped contribution to the MFPT

$$\frac{\tau^i_{OD}}{\tau_D} = \frac{\gamma_i e^{\beta U_0}}{\gamma \beta U_0}\left[\frac{\pi}{2\sqrt{2}}\frac{1}{1+10\beta U_0 \tau_i/\tau_D} + \sqrt{\beta U_0 \frac{\tau_m}{\tau_D}}\right], \tag{3.15}$$

and the energy-diffusion contribution

$$\frac{\tau^i_{ED}}{\tau_D} = \frac{\gamma e^{\beta U_0}}{\gamma_i \beta U_0}\left[\frac{\tau_m}{\tau_D} + 4\beta U_0\Big(\frac{\tau_i}{\tau_D}\Big)^2 + \sqrt{\beta U_0 \frac{\tau_m}{\tau_D}}\right]. \tag{3.16}$$

In Fig.3.6 we observe a close agreement between the analytical expression (3.14) and the simulation data (stars) of the rescaled MFPT τ_{MFP}/τ_D as a function of τ_1/τ_D and for fixed values of τ_2/τ_D, γ_2/γ_1, and U_0/k_BT. In particular, for $\tau_1/\tau_D \gg 1$, we observe that the MFPT is constant with

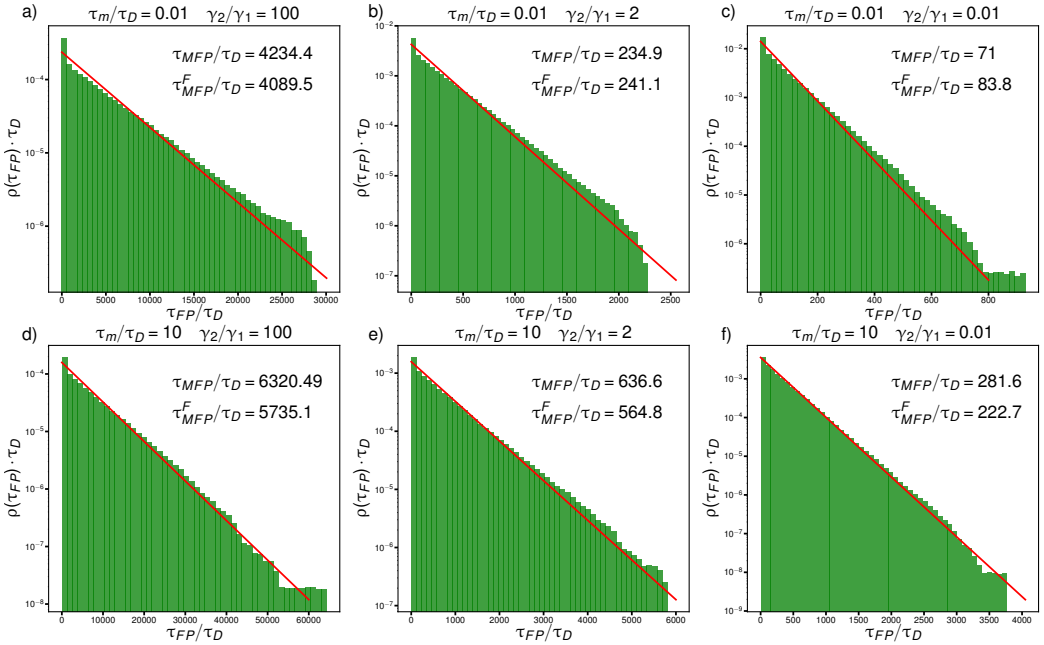

Figure 3.5: First passage time distribution for barrier crossing. The parameters used for the simulation are the same as in Fig.3.4: the potential height is fixed $\beta U_0 = 3$ and the memory times as $\tau_1/\tau_D = 1$ and $\tau_2/\tau_D = 10$. The upper row corresponds to high friction $\tau_m/\tau_D = 0.01$, and the bottom row to low friction. Various ratios of the two friction coefficients correspond to $\gamma_2/\gamma_1 = 100$ in a) and d), $\gamma_2/\gamma_1 = 2$ in b) and e), and $\gamma_2/\gamma_1 = 0.01$ in c) and f), respectively. The green histograms denote the rescaled probability distribution $\rho(\tau_{FP})$, and on every plot, the respective MFPT is indicated, as well as the average of all the samples and the MFPT from the Eq. (3.14). The red lines highlight the exponential decay explained in Eq. (3.13).

respect to τ_1/τ_D, as was already observed in the previous work [19]. The black lines on the right of the figure show the MFPT for a single exponential memory kernel ($\gamma_1 = 0$); taking this into account, we rescale the MFPT in order to compare the expressions for the single- and bi-exponential MFPT, respectively

$$\frac{\tau_{MFP_2}}{\tau_{D_2}}\frac{\gamma_2}{\gamma} = \frac{\tau_{MFP_2}}{\tau_D}, \tag{3.17}$$

where in $\tau_{D_2} = L^2\gamma_2/k_BT$ instead of γ there is γ_2. The dash-dotted line on the bottom left-hand side of the figure depicts the Markovian limit $\gamma_1 = \gamma_2 = 0$. For the values of $\tau_2/\tau_D = 0.1$ and $\tau_2/\tau_D = 0.316$, we observe a near-constant behavior for $\tau_1/\tau_D \ll 1$ as well as $\tau_1/\tau_D \gg 1$. These two lines agree closely with the dashed line. This means that the MFPT is dominated by the

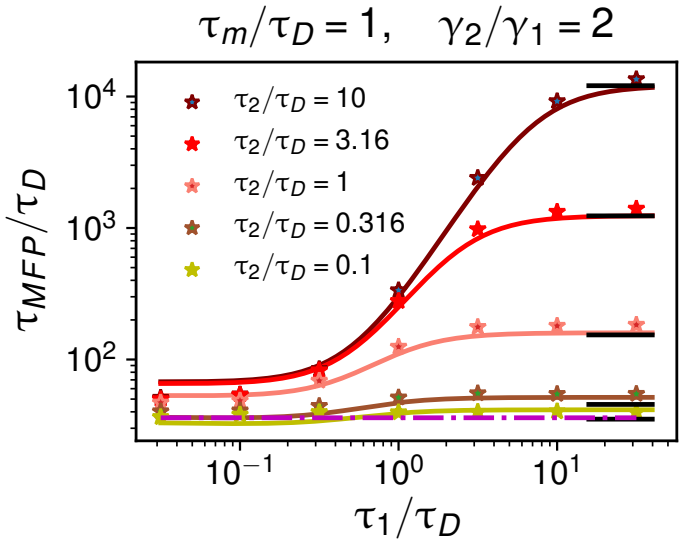

Figure 3.6: Rescaled MFPT for bi-exponential memory kernel τ_{MFP}/τ_D as a function of τ_1/τ_D for several values of τ_2/τ_D and fixed $\tau_m/\tau_D = 1$, $\gamma_2/\gamma_1 = 2$, and $U_0/k_BT = 3$. The stars denote the simulation results, and the colored lines represent the heuristic formula Eq. (3.14). The horizontal dashed line represents the Markovian limit, corresponding to $\gamma_1 = \gamma_2 = 0$. The black horizontal lines for high τ_1/τ_D values denote the heuristic formula for a single exponential memory kernel, i.e., $\gamma_1 = 0$.

overdamped contribution in Eq. (3.15), this contribution being almost equal to the Markovian expression.

In the following paragraph, we analyze the influence of the ratio between the two friction coefficients γ_2/γ_1. In Fig.3.7, we plot the rescaled MFPT as a function of γ_2/γ_1 for various values of τ_m/τ_D. In Fig.3.7a) fixing $\tau_1/\tau_D = 1$ and $\tau_2/\tau_D = 10$, we observe a plateau for both $\gamma_2/\gamma_1 \gg 1$ and $\gamma_2/\gamma_1 \ll 1$. The black horizontal lines depict the single exponential result for $\gamma_2 = 0$ on the left, and $\gamma_1 = 0$ on the right; when the amplitude of either exponential contribution to the memory kernel is lower than the other, its effect on the MFPT disappears, as follows from the agreement between the colored lines and the black lines. In Fig.3.7a), we observe a number of discrepancies between the simulation data and the formula (3.14), particularly for small values of γ_2/γ_1, though generally, the formula describes the simulation data accurately. In Fig.3.7b), we observe the same behavior as in Fig.3.7a) with constant values for small and large γ_2/γ_1. In this case, however, we observe a more extended range of values of MFPT; here $\tau_1/\tau_D = 0.316$ and $\tau_2/\tau_D = 31.6$, therefore the ratio between these two memory times is 100, and in

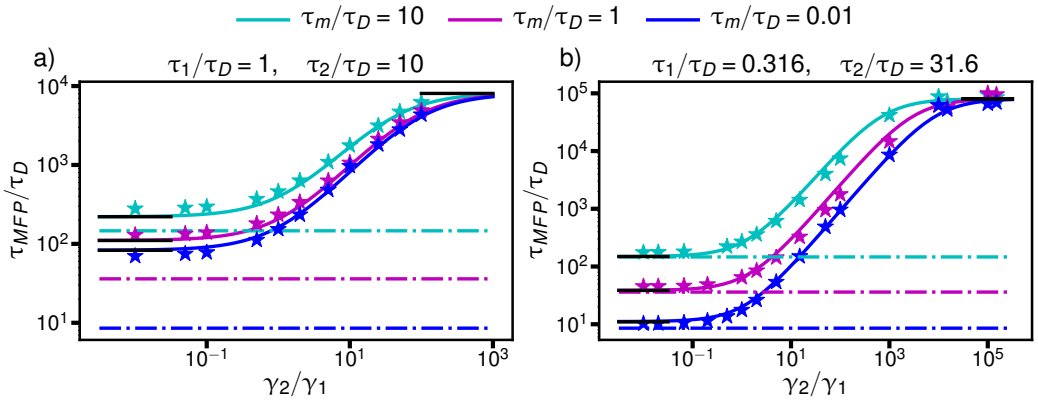

Figure 3.7: Mean first-passage time for bi-exponential memory and $U_0/k_BT = 3$: (a) τ_{MFP}/τ_D for fixed $\tau_1/\tau_D = 1$, $\tau_2/\tau_D = 10$ as a function of γ_2/γ_1 for several values of τ_m/τ_D, (b) τ_{MFP}/τ_D for fixed $\tau_1/\tau_D = 0.316$, $\tau_2/\tau_D = 31.6$ as a function of γ_2/γ_1 for several values of τ_m/τ_D. The stars illustrate the simulation results, while the colored lines represent the heuristic formula Eq. (3.14). The horizontal dash-dotted lines represent the Markovian limit, corresponding to $\gamma_1 = \gamma_2 = 0$. The horizontal black lines denote the heuristic formula for a single exponential memory kernel for $\gamma_2 = 0$ on the left and $\gamma_1 = 0$ on the right.

Fig.3.7a) it is 10. In order to understand the importance of the effect of memory on the MFPT, we compare the Markovian and non-Markovian cases, where the dash-dotted lines depict the Markovian case. From Fig.3.7, we intuit that the scaling variable (that describes the relative importance of exponential memory contributions) is proportional to γ_i/τ_i^2, which we will derive in more detail in the following paragraph.

Having discussed the bi-exponential case, we next analyze the tri-exponential memory kernel. In Fig.3.8 we depict the MFPT for fixed $\tau_m/\tau_D = 1$, $\tau_1/\tau_D = 0.316$, $\tau_2/\tau_D = 1$, $\tau_3/\tau_D = 3.16$ and $U_0/k_BT = 3$. In Fig.3.8a), we plot the MFPT as a function of γ_2/γ_1 for various values of γ_3/γ_1 and in Fig.3.8b) as a function of γ_1/γ_2 for various values of γ_3/γ_2. In both panels, we observe an agreement between the data, the symbols, and the analytical expression (3.14), as depicted by the colored lines. We can, therefore, conclude that the analytical expression accurately describes the tri-exponential memory kernel as well as the bi-exponential, thus providing an accurate description for a generic multi-exponential memory kernel. The data exhibit an asymptotic behavior on the left and right of the two plots. In particular, when one of the amplitudes of the memory kernel goes to infinity, ($\gamma_2/\gamma_1 \to \infty$ in Fig.3.8a) and $\gamma_1/\gamma_2 \to \infty$ in Fig.3.8b)), the MFPT reaches the single expo-

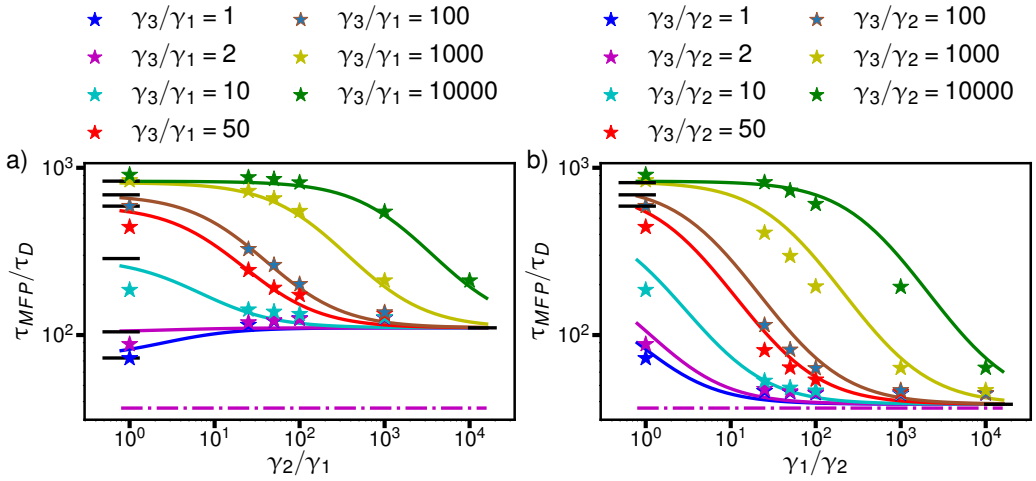

Figure 3.8: Mean first-passage time for tri-exponential memory. In a), we plot the simulation results for the rescaled MFPT τ_{MFP}/τ_D as a function of γ_2/γ_1 for fixed $\tau_m/\tau_D = 1$, $\tau_1/\tau_D = 0.316$, $\tau_2/\tau_D = 1$, $\tau_3/\tau_D = 3.16$ and $U_0/k_BT = 3$. The colored stars represent the results for various values of γ_3/γ_1. The colored lines represent the heuristic formula 3.14. In b), τ_{MFP}/τ_D is shown as a function of γ_1/γ_2 for fixed $\tau_m/\tau_D = 1$, $\tau_1/\tau_D = 0.316$, $\tau_2/\tau_D = 1$, $\tau_3/\tau_D = 3.16$. The different colored stars denote the results for the various fixed values of γ_3/γ_2. The colored lines represent the heuristic formula 3.14. In both plots, the horizontal black lines to the right represent the heuristic formula for single exponential memory, in a) for $\gamma_1 = \gamma_3 = 0$ and in b) for $\gamma_2 = \gamma_3 = 0$, while the horizontal black lines to the left represent the heuristic formula for double exponential memory.

nential limit on the right. On the left we see the bi-exponential limits, for $\gamma_2/\gamma_1 \to 0$ in 3.8a) and $\gamma_1/\gamma_2 \to 0$ in 3.8b) respectively. Both limits are depicted with black lines, while the dashed lines denote the Markovian limit.

After checking the close agreement between the formula (3.14) and bi-exponential kernel data for various memory times, friction coefficients, and inertial times, we additionally compare its validity for different weight potentials, as in Fig.3.9. In this figure, we plot the rescaled MFPT as a function of U_0/k_BT for various γ_2/γ_1 and fixed $\tau_m/\tau_D = 1$, $\tau_1/\tau_D = 10$ and $\tau_2/\tau_D = 1$. The formula (3.14) accurately describes the data, dominated by the Arrhenius term $\tau_{MFP} \simeq e^{\beta U_0}$ when the barrier height satisfies $U_0/k_BT \geq 2$.

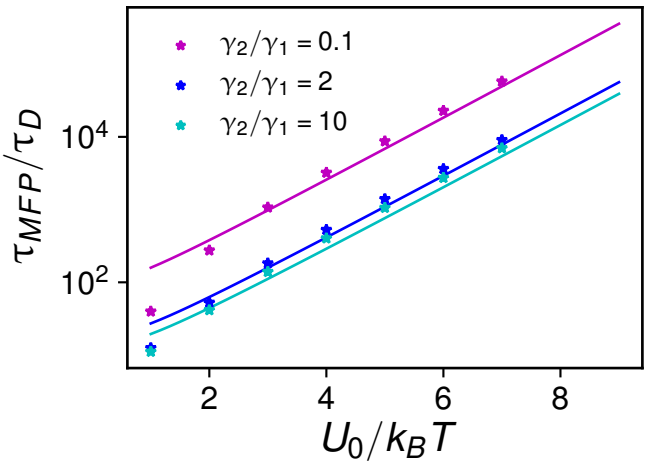

Figure 3.9: Bi-exponential memory. Simulation results for the rescaled MFPT τ_{MFP}/τ_D as a function of the rescaled barrier height U_0/k_BT for $\tau_m/\tau_D = 1$, $\tau_1/\tau_D = 10$ and $\tau_2/\tau_D = 1$ and different values of $\gamma_2/\gamma_1 = 0.1, 2, 10$. The stars and lines depict the simulation data and the heuristic formula (3.14), respectively.

3.5 Scaling diagrams

In the previous section, we learned that the expression (3.14) agrees with the simulation data when $U_0/k_BT \geq 2$. We will now analyze the behavior of MFPT for multi-exponential memory kernels in the case of various friction coefficients based on Eq. (3.14). Studying Eq. (3.14) we observe that, when all the memory times are $\tau_i/\tau_D \gg 1$, the MFPT scales as

$$\frac{\tau_{MFP}}{\tau_D} \propto 4e^{\beta U_0}\left[\sum_i \left(\frac{\tau_D}{\tau_i}\right)^2 \frac{\gamma_i}{\gamma}\right]^{-1}. \tag{3.18}$$

In particular, the MFPT is dominated by the exponential term for which $\left(\frac{\tau_D}{\tau_i}\right)^2 \frac{\gamma_i}{\gamma}$ is the largest. We, therefore, consider that the slower energy exchange between the particle and the heat bath dominates the barrier crossing in the energy-diffusion limit. In the limit $\tau_i/\tau_D \gg 1$ for $\forall i$, the barrier crossing rate is a sum of every individual rate. Therefore, the shortest memory time is the most relevant in the sum because it exchanges energy quickly [60]. In Fig.3.10a) and b), we create scaling diagrams of the MFPT for bi-exponential memory kernels as a function of $\left(\frac{\tau_1}{\tau_D}\right)^2 \frac{\gamma}{\gamma_1}$ and $\left(\frac{\tau_2}{\tau_D}\right)^2 \frac{\gamma}{\gamma_2}$, in the high friction limit $\tau_m/\tau_D = 0.01$ in panel a) and in the low friction

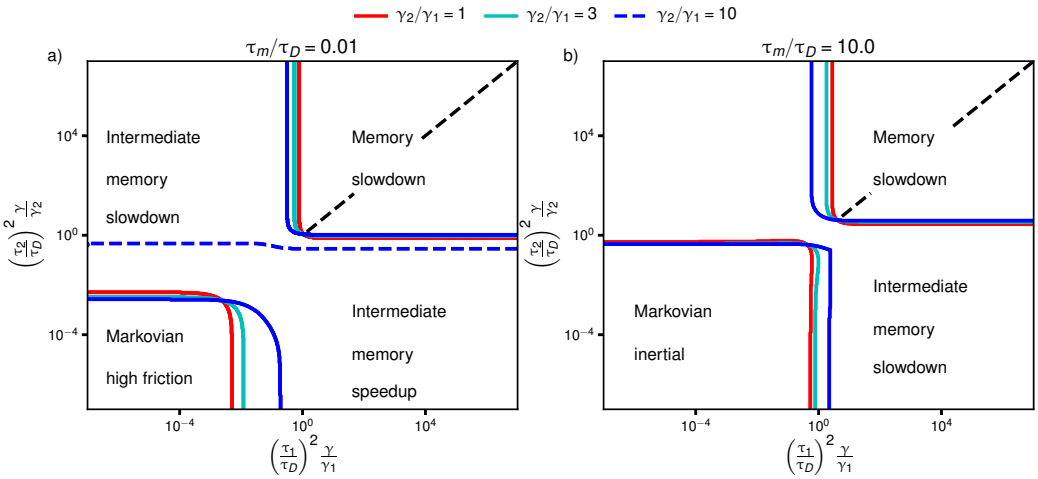

Figure 3.10: a) and b) scaling diagrams for the MFPT in the presence of bi-exponential memory, based on the heuristic formula (3.14) as a function of the scaling variables $(\tau_1/\tau_D)^2\gamma/\gamma_1$ and $(\tau_2/\tau_D)^2\gamma/\gamma_2$ for three ratios of the friction coefficients $\gamma_2/\gamma_1 = 1, 3, 10$ and $U_0/k_BT = 3$. The transition from the Markovian regime to the intermediate memory-speed-up regime is located where τ_{MFP} is smaller by 5% than the value in the Markovian limit ($\tau_1 = \tau_2 = 0$). The transition from the Markovian regime to the intermediate memory-slowdown regime is defined where τ_{MFP} is larger by 5% than the value in the Markovian limit. The asymptotic memory slowdown regime is defined where τ_{MFP} is 10 times the value of the Markovian limit. The dashed blue line in a) represents the transition between the intermediate memory-speed-up regime and the intermediate memory-slowdown regime. This transition is only seen for $\gamma_2/\gamma_1 = 10$. Results are also shown for the high friction case $\tau_m/\tau_D = 0.01$ in a) and for the low friction regime $\tau_m/\tau_D = 10$ in b). The dashed black diagonal lines in a) and b) in the asymptotic memory-slowdown regime indicate the crossover from the τ_1-dominated barrier crossing for $\tau_1^2/\gamma_1 \ll \tau_2^2/\gamma_2$, to the τ_2-dominated barrier crossing for $\tau_2^2/\gamma_2 \ll \tau_1^2/\gamma_1$. We are therefore able to observe that the Markovian regime is entered when both $(\tau_1/\tau_D)^2\gamma/\gamma_1$ and $(\tau_2/\tau_D)^2\gamma/\gamma_2$ exhibit lower values. Conversely, the asymptotic memory-slowdown regime is entered when both $(\tau_1/\tau_D)^2\gamma/\gamma_1$ and $(\tau_2/\tau_D)^2\gamma/\gamma_2$ exhibit higher values. The two asymptotic regimes are separated by intermediate slowdown or speed-up regimes. The minor deviation between the scaling boundaries for the three different ratios of the friction coefficients $\gamma_2/\gamma_1 = 1, 3, 10$ demonstrates that the scaling diagram in terms of the scaling variables $(\tau_1/\tau_D)^2\gamma/\gamma_1$ and $(\tau_2/\tau_D)^2\gamma/\gamma_2$, accurately describes the global behavior, leading to a diagram almost independent of γ_2/γ_1.

limit $\tau_m/\tau_D = 10$ in panel b) for various values of γ_2/γ_1. The figures are based on the numerical analysis of the heuristic formula (3.14). In Fig.3.10a) and b) for lower values of $\left(\frac{\tau_1}{\tau_D}\right)^2 \frac{\gamma}{\gamma_1} \to 0$ and $\left(\frac{\tau_2}{\tau_D}\right)^2 \frac{\gamma}{\gamma_2} \to 0$ we are in the Markovian regime ($\tau_1 = \tau_2 = 0$), in high friction (Fig.3.10a)) and inertial regime (Fig.3.10b)). Both diagrams illustrate the memory slowdown regime, reached when the MFPT is 10 times the Markovian value. With the diagonal dashed black line, we depict the cross-over from the asymptotic scaling behavior $\tau_{MFP} \sim \tau_1^2$ for $\tau_1^2/\gamma_1 \ll \tau_2^2/\gamma_2$ to the other asymptotic behavior $\tau_{MFP} \sim \tau_2^2$ for $\tau_2^2/\gamma_2 \ll \tau_1^2/\gamma_1$. We are thus able to observe the intermediate memory acceleration and the intermediate memory slowdown regimes between the two regimes. The intermediate memory acceleration regime is obtained if the MFPT is smaller than in the Markovian case, and the transition is located where the MFPT is smaller than the Markovian limiting result by 5%. The intermediate memory speed-up regime was also observed for a single memory kernel [18], and we can, therefore, interpret it as acceleration from the memory friction following an unsuccessful barrier-crossing attempt, which pushes the particle towards the barrier. Similarly to the acceleration, we can define the intermediate memory slowdown regime by a τ_{MFP} that is larger than the Markovian limiting result by 5%. In a) we observe both the intermediate memory speed-up and slowdown regimes, but only for the friction coefficient $\gamma_2/\gamma_1 = 10$, for this reason, in Fig.3.10a) we see only the intermediate slowdown regime, depicted with the blue dashed line. The intermediate regimes decrease in size with the ratio's increase between the friction coefficients, particularly in the direction of $(\tau_1/\tau_D)^2\gamma/\gamma_1$. To better understand the behavior of the MFPT in Fig.3.11a) and b), we fix the value of $(\tau_1/\tau_D)^2\gamma/\gamma_1 = 10^{-4}$ for the high and low friction cases. In a), we observe that small values of $(\tau_2/\tau_D)^2\gamma/\gamma_2$ τ_{MFP}/τ_D have the same value as in the Markovian case (black dashed line), and then the value decreases. After reaching its minimum value, the MFPT for the friction coefficients $\gamma_2/\gamma_1 = 3$ and $\gamma_2/\gamma_1 = 10$ increases and becomes constant as $(\tau_2/\tau_D)^2\gamma/\gamma_2$ increases. It is clear that the intermediate memory slowdown regime will only be reached for $\gamma_2/\gamma_1 = 10$ as the MFPT exhibits higher values than the Markovian case. Furthermore, in b), for small values of $(\tau_2/\tau_D)^2\gamma/\gamma_2$, the MFPT is equal to the value in the Markovian case. Increasing $(\tau_2/\tau_D)^2\gamma/\gamma_2$ the MFPT grows for every friction coefficient, subsequently becoming constant because the term $(\tau_1/\tau_D)^2\gamma/\gamma_1$ predominates.

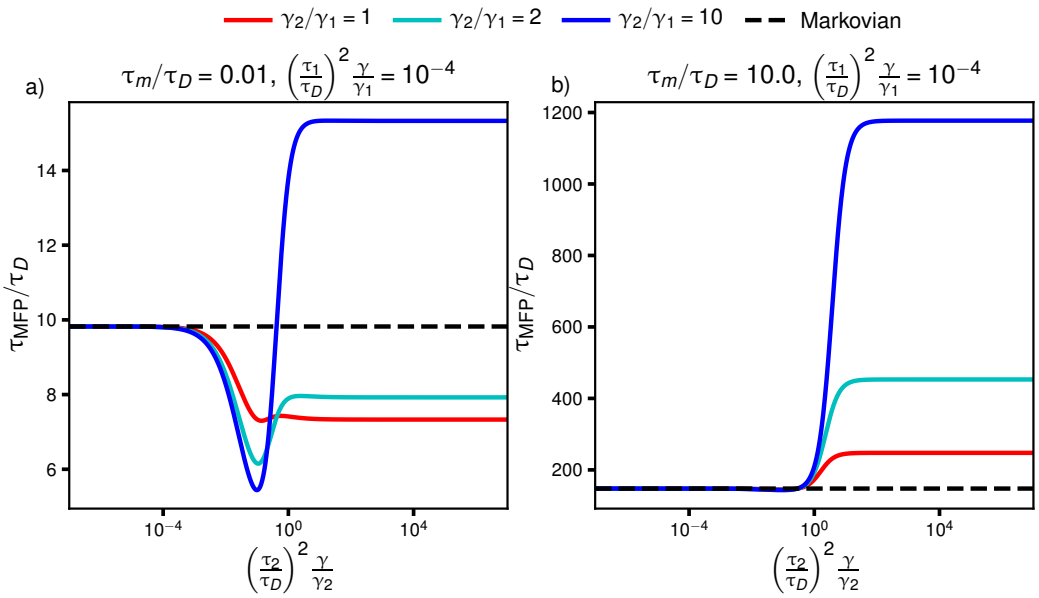

Figure 3.11: In a) and b), the rescaled MFPT τ_{MFP}/τ_D is plotted according to Eq. (3.14) as a function of $(\tau_2/\tau_D)^2\gamma/\gamma_2$ for fixed $(\tau_1/\tau_D)^2\gamma/\gamma_1 = 10^{-4}$ for the ratios γ_2/γ_1 for $\tau_m/\tau_D = 0.01$ in a) and for $\tau_m/\tau_D = 10$ in b). The dashed horizontal lines denote the Markovian limit, obtained from Eq. (3.14) by setting $\tau_1 = \tau_2 = 0$.

3.6 Conclusion

In summary, having simulated the barrier crossing of a massive particle in a one-dimensional double-well potential, we have studied that the dynamics of the particle governed by the generalized Langevin equation with both bi- and tri-exponential memory kernels, as well as varying amplitudes. Comparing the numerical simulation with the heuristic expression (3.14) demonstrates a good agreement between the formula and the simulations. The expression was already previously introduced [19], but for the specific case of bi-exponential memory with $\gamma_1 = \gamma_2$. In the section 3.4, we primarily focus on the effect of the various friction coefficients and memory times on the MFPT and are thus able to conclude that τ_{MFP}/τ_D is dominated by the scaling variable $(\tau_i/\tau_D)^2\gamma/\gamma_i$, the rescaled ratio of the individual friction coefficient γ_i and the squared memory time τ_i^2. In the section 3.5, using Eq. (3.14), we describe the general behavior of the MFPT for a bi-exponential memory kernel with scaling variables. In the scaling diagrams in Fig.3.10, we observe that the MFPT reaches the same values as in the Markovian regime for small values of the two scaling variables. We reach the asymptotic memory slowdown

regime when both scaling variables have high values. Between the Markovian regime and the asymptotic memory slow-down regimes, we observe two intermediate areas for both higher and lower values of the MFPT than in the Markovian case, depending on the various parameters (mass and friction coefficients). In conclusion, we characterize MFPT for bi- and triple-exponential memory kernels and various friction coefficients via the formula (3.14), thus observing that for the non-Markovian regime, the dominant contribution is the smallest scaling variable $(\tau_i/\tau_D)^2\gamma/\gamma_i$; thus, we are able to understand the importance of considering different friction amplitudes, due to their influence upon the scaling variable.

Chapter 4

Barrier crossing for systems far from equilibrium

4.1 Introduction

The majority of biological systems do not exist in a state of equilibrium [61] because an external time-dependent force is often present, by which energy from the environment is injected into the system [62–64]. As an example of such systems, let us consider the zipping of a DNA or RNA hairpin [65]. The two minima of a double-well potential can be used to describe the transition between the zipped/unzipped configuration and an external force that brings the system out of equilibrium [65–68]. The theory of off-equilibrium systems behavior is not well understood.

Non-equilibrium reaction kinetics is a fascinating area of study that explores the dynamic processes, e.g., chemical reactions, far from equilibrium. In these systems, non-thermal forces are crucial in determining barrier-crossing dynamics in a reaction coordinate space. The concepts of non-equilibrium statistical mechanics, rare events, and non-Markovian dynamics have been observed in these systems [69, 70]. As examples, we can cite metastable evolutionary dynamics [71], barrier effects on motion patterns of mammals [72] and cancer cells [73], protein folding under non-equilibrium conditions [74], and chemical reactions in the presence of strong time-dependent electric fields [75].

For many years, much attention has been devoted to the mean first-passage time (MFPT), i.e., the time necessary for a particle to cross a barrier of height U_0 in a double-well potential [47, 76, 77]. One of the initial results was the Arrhenius law that demonstrates that the barrier escape time satisfies $\tau_{MFP} \sim e^{(U_0/k_BT)}$ [78]. To describe a Markovian system, Kramers

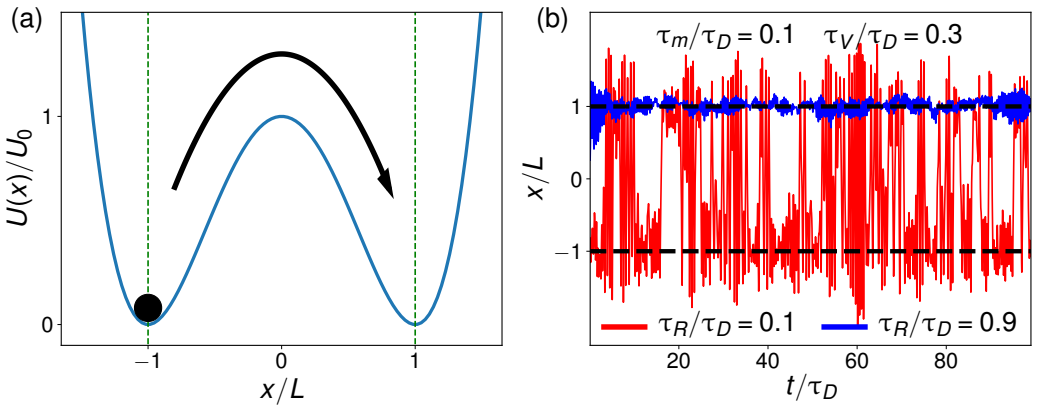

Figure 4.1: a) Double-well potential in Eq. (4.3). b) Non-equilibrium trajectories for moderate barrier height $\beta U_0 = 3$, low rescaled mass $\tau_m/\tau_D = 0.1$ and friction memory time $\tau_V/\tau_D = 0.3$. The red trajectory represents random correlation time $\tau_R/\tau_D = 0.1$ and shows many barrier crossing events, the blue trajectory is for $\tau_R/\tau_D = 0.9$ and shows no barrier-crossing event.

discovered, in the low and high friction limit, an expression [25] where the pre-exponential factor depends on the ratio of mass over friction [27, 55]. This formula describes reaction-diffusion processes [79], chemical reactions [80], protein folding [76, 81, 82] and nucleic-acid hairpin formation [66]. In certain systems such as molecular conformational dynamics [32, 83], chemical reaction kinetics [77] and protein folding [38, 39, 84, 85], as well as colloidal dynamics in viscoelastic materials [86], the memory time can not be neglected, and this causes substantial modification of the pre-exponential factor in the MFPT [18, 19, 26, 47, 57, 87, 88]. But for the system at the equilibrium state, Markovian and non-Markovian formulae do not modify the Arrhenius exponential, therefore if the pre-exponential factor does not correspond with the Arrhenius exponential, means that the system is far from equilibrium.

In this chapter, we will discuss a non-Markovian, non-equilibrium barrier-crossing process in one dimension, as is shown in Fig.4.1a). We must consider two different relaxation times of the friction memory kernel and the random force [40, 69, 70]; therefore violating the fluctuation-dissipation theorem [68, 89–92]. We investigate the behavior of MFPT out of equilibrium [40, 69, 70, 93]. In particular, we observe that the MFPT increases rapidly when the ratio between the memory time of the random force and the memory time in the memory kernel is greater than 1. On the other hand, when the ratio is smaller than 1, the MFPT decreases slowly, as we observe in Fig.4.1b) because the state of non-equilibrium modifies the Arrhenius factor itself. We have depicted two non-equilibrium simulation trajectories in

Fig.4.1b) to better describe what we stated above. We see that when the ratio between the random correlation and the time in the memory kernel is less than 1 (red trajectory), many barrier-crossing events take place. In the same simulation time for the blue trajectory any barrier crossing occurs, where the ratio between the memory times is greater than 1, all the other parameters remain the same, so we can conclude that increasing the random-force correlation time will also increase the barrier-crossing time. We must, therefore, introduce an effective temperature [94], proportional to the square of the friction and random relaxation-time ratio. The effective temperature corresponds to the simulation data and characterizes the non-equilibrium position and velocity distributions. A similar effective temperature was also introduced in previous work to describe the modification of the transition path time at the point of non-equilibrium [95].

4.2 Setup

Our model is based on the generalized Langevin equation (GLE)

$$m\ddot{x}(t) = -\int_{t_0}^{t} \Gamma_V(t-t')\dot{x}(t')dt' - \nabla U(x(t)) + F_R(t), \tag{4.1}$$

where m is the particle mass, $\Gamma_V(t)$ the friction memory kernel, t_0 some initial time and $F_R(t)$ denotes the random force characterized by a general autocorrelation

$$\langle F_R(t)F_R(t')\rangle = \beta^{-1}\Gamma_R(t-t'), \tag{4.2}$$

where β is a numerical constant. We choose the double-well potential,

$$U(x) = U_0\left[\left(\frac{x}{L}\right)^2 - 1\right]^2, \tag{4.3}$$

where $2L$ is the separation between the minima and U_0 is the barrier height as in Fig.4.1a).

At equilibrium, the fluctuation-dissipation theorem asserts $\Gamma_R(t) = \Gamma_V(t)$ and $\beta^{-1} = k_BT$, which is equal to the thermal energy of the heat bath. In a general non-equilibrium scenario, $\Gamma_R(t)$ and $\Gamma_V(t)$ are independent functions, which we describe as single exponentials

$$\Gamma_R(t) = \frac{\gamma_R}{\tau_R}e^{-\frac{t}{\tau_R}} \quad \text{for} \quad t > 0 \tag{4.4}$$

$$\Gamma_V(t) = \frac{\gamma_V}{\tau_V}e^{-\frac{|t|}{\tau_V}}, \tag{4.5}$$

and β is not associated with a heat-bath temperature. With no loss of generality, we can consider equal prefactors $\gamma_R = \gamma_V = \gamma$, since different prefactors can be absorbed into the definition of β in Eq. (4.2). For different random and friction memory times, $\tau_R \neq \tau_V$, the fluctuation-dissipation theorem is irrevocably violated, and thus the system is out of equilibrium [96–98]. The two remaining time scales to characterize the model are the inertial time $\tau_m = m/\gamma$ and the diffusion time $\tau_D = L^2\gamma\beta$.

4.3 Calculation of the positional autocorrelation function

We will first present our analytical results for the MFPT, which are based on the positional autocorrelation function $C(t) = \langle x(t)x(0)\rangle$. For this, we will employ a harmonic approximation of Eq. (4.1) and use $U_{\rm har}(x) = Kx^2/2$, where K is the second derivative of the double-well potential, $K = U''(L) = 8U_0/L^2$. Fourier transforming Eq. (4.1) for $t_0 \to -\infty$ and solving for $\tilde{x}(\omega)$, we obtain

$$\tilde{x}(\omega) = \frac{\tilde{F}_R(\omega)}{K - m\omega^2 + i\omega\tilde{\Gamma}_V^+(\omega)} \equiv \tilde{\chi}(\omega)\tilde{F}_R(\omega), \tag{4.6}$$

which defines the response function $\tilde{\chi}(\omega)$. The half-sided Fourier transform $\tilde{\Gamma}_V^+(\omega)$ of the memory kernel $\Gamma_V(t)$ is given by

$$\tilde{\Gamma}_V^+ = \int_0^\infty dt e^{-i\omega t}\Gamma_V(t) = \frac{\gamma}{1 + i\omega\tau_V}, \tag{4.7}$$

while the Fourier transform of the symmetric random force correlation $\Gamma_R(t)$ is

$$\tilde{\Gamma}_R(\omega) = \tilde{\Gamma}_R^+(\omega) + \tilde{\Gamma}_R^+(-\omega) = \frac{2\gamma}{1 + \omega^2\tau_R^2}. \tag{4.8}$$

Using the Fourier transform of the generalized Langevin equation (4.6) we can write the autocorrelation function as

$$\begin{aligned} C(t) \equiv \langle x(t)x(0)\rangle &= \int \frac{d\omega}{2\pi} e^{i\omega t} \int \frac{d\omega\prime}{2\pi} \langle \tilde{x}(\omega)\tilde{x}(\omega\prime)\rangle \\ &= \int \frac{d\omega}{2\pi} e^{i\omega t} \int \frac{d\omega\prime}{2\pi} \tilde{\chi}(\omega)\tilde{\chi}(\omega\prime)\langle \tilde{F}_R(\omega)\tilde{F}_R(\omega\prime)\rangle \\ &= k_B T \int \frac{d\omega}{2\pi} e^{i\omega t} \int \frac{d\omega\prime}{2\pi} 2\pi\delta(\omega + \omega\prime)\tilde{\Gamma}_R(\omega)\tilde{\chi}(\omega)\tilde{\chi}(\omega\prime) \\ &= k_B T \int \frac{d\omega}{2\pi} e^{i\omega t}\tilde{\Gamma}_R(\omega)\tilde{\chi}(\omega)\tilde{\chi}(-\omega), \end{aligned} \tag{4.9}$$

where we used $\langle \tilde{F}_R(\omega)\tilde{F}_R(\omega\prime)\rangle = k_B T 2\pi\delta(\omega+\omega\prime)\tilde{\Gamma}_R(\omega)$. From this, the Fourier transform of the autocorrelation function follows as

$$\tilde{C}(\omega) = \beta^{-1}\tilde{\Gamma}_R(\omega)\tilde{\chi}(\omega)\tilde{\chi}(-\omega). \tag{4.10}$$

Inserting the Fourier transform of the random force kernel $\Gamma_R(t)$, $\tilde{\Gamma}_R(\omega) = 2\gamma/(1+\omega^2\tau_R^2)$, in Eq. (4.10) we obtain

$$\tilde{C}(\omega) = \frac{2\gamma\beta^{-1}(1+\omega^2\tau_R^2)^{-1}}{\left(K-\omega^2\left[m-\frac{\tau_V\gamma}{1+\tau_V^2\omega^2}\right]\right)^2+\frac{\omega^2\gamma^2}{(1+\omega^2\tau_V^2)^2}} \tag{4.11}$$

which can be rewritten in a form that corresponds to the standard result for the memory-less harmonic oscillator in equilibrium

$$\tilde{C}(\omega) = \frac{2\gamma_{\text{eff}}\beta_{\text{eff}}^{-1}}{(K-m_{\text{eff}}\omega^2)^2+\omega^2\gamma_{\text{eff}}^2} \tag{4.12}$$

where we have introduced an effective frequency-dependent friction, mass, and temperature

$$\gamma_{\text{eff}} = \frac{\gamma}{1+\tau_V^2\omega^2}, \tag{4.13a}$$

$$m_{\text{eff}} = m - c_1\tau_V\gamma_{\text{eff}}, \tag{4.13b}$$

$$\beta_{\text{eff}} = \frac{1+\omega^2\tau_R^2}{1+\omega^2\tau_V^2}\beta, \tag{4.13c}$$

where c_1 is a numerical constant that takes into account the approximation of the harmonic potential. In other studies [18], this mapping was introduced, but for the equilibrium case for asymptotic limits of high and low frequency. In this chapter, we use the mapping for a system far from equilibrium and for arbitrary frequency. For $\tau_R = \tau_V$ equilibrium is recovered and $\beta_{\text{eff}} = \beta$, and for $\tau_R = \tau_V = 0$ the Markovian limit is recovered and $\gamma_{\text{eff}} = \gamma$ and $m_{\text{eff}} = m$. Note that the potential curvature K is not renormalized.

4.3.1 Low-friction limit

In low friction limit, i.e. for $\gamma_{\text{eff}} = 0$, Eq. (4.12) is dominated by the pole

$$\omega_L^2 = K/m_{\text{eff}} \quad \text{for} \quad \frac{Km_{\text{eff}}}{\gamma_{\text{eff}}^2} > 1. \tag{4.14}$$

Inserting Eq. (4.14) into Eq. (4.13a), we arrive at a quadratic equation

$$\gamma_{\text{eff}} = \frac{\gamma}{1+\frac{\tau_V^2 K}{m-c_1\tau_V\gamma_{\text{eff}}}}$$
$$\gamma_{\text{eff}}(m - c_1\tau_V\gamma_{\text{eff}} + \tau_V^2 K) = \gamma(m - c_1\tau_V\gamma_{\text{eff}})$$
$$\gamma_{\text{eff}}^2 - \gamma_{\text{eff}}\left(\frac{m}{c_1\tau_V} + \frac{1}{c_1}\tau_V K + \gamma\right) + \frac{\gamma m}{c_1\tau_V} = 0$$
$$\gamma_{\text{eff}} = \frac{m}{2c_1\tau_V} + \frac{\tau_V K}{2c_1} + \frac{\gamma}{2} \pm \sqrt{\left(\frac{m}{2c_1\tau_V} + \frac{\tau_V K}{2c_1} + \frac{\gamma}{2}\right)^2 - \frac{\gamma m}{c_1\tau_V}}$$
$$\gamma_{\text{eff}} = \frac{m}{2c_1\tau_V} + \frac{\tau_V K}{2c_1} + \frac{\gamma}{2} \pm \sqrt{\left(\frac{m}{2c_1\tau_V} + \frac{\tau_V K}{2c_1} - \frac{\gamma}{2}\right)^2 + \frac{1}{c_1}\tau_V K\gamma}.$$

In the limit $\tau_V \to 0$ we obtain

$$\gamma_{\text{eff}} = \frac{m}{2c_1\tau_V} + \frac{\tau_V K}{2c_1} + \frac{\gamma}{2} \pm \frac{m}{2c_1\tau_V}\left[\left(1 + \frac{\tau_V^2 K}{m} - \frac{c_1\tau_V\gamma}{m}\right)^2 + \frac{4c_1\tau_V^3 K\gamma}{m^2}\right]^{1/2}$$
$$\gamma_{\text{eff}} \simeq \frac{m}{2c_1\tau_V} + \frac{\tau_V K}{2c_1} + \frac{\gamma}{2} \pm \frac{m}{2c_1\tau_V}\left[1 - \frac{2c_1\tau_V\gamma}{m} + \frac{2\tau_V^2 K}{m} + \frac{c_1^2\tau_V^2\gamma^2}{m^2} + \frac{2c_1\tau_V^3 K\gamma}{m^2}\right]^{1/2}$$
$$\gamma_{\text{eff}} \simeq \frac{m}{2c_1\tau_V} + \frac{\tau_V K}{2c_1} + \frac{\gamma}{2} \pm \frac{m}{2c_1\tau_V}\left(1 - \frac{c_1\tau_V\gamma}{m} + \frac{\tau_V^2 K}{m} + \frac{2c_1\tau_V^3 K\gamma}{m^2}\right), \tag{4.15}$$

and taking the minus sign

$$\Rightarrow \gamma_{\text{eff}} \simeq \gamma - \gamma\frac{\tau_V^2 K}{m}. \tag{4.16}$$

In the limit $\tau_V \to \infty$ we obtain

$$\gamma_{\text{eff}} = \frac{m}{2c_1\tau_V} + \frac{\tau_V K}{2c_1} + \frac{\gamma}{2} \pm \frac{\tau_V K}{2c_1}\left[\left(1 + \frac{c_1\gamma}{\tau_V K} + \frac{m}{\tau_V^2 K}\right)^2 - \frac{4c_1\gamma m}{\tau_V^3 K^2}\right]^{1/2}$$
$$\gamma_{\text{eff}} \simeq \frac{m}{2c_1\tau_V} + \frac{\tau_V K}{2c_1} + \frac{\gamma}{2} \pm \frac{\tau_V K}{2c_1}\left[1 + \frac{2c_1\gamma}{\tau_V K} + \frac{2m}{\tau_V^2 K} + \frac{c_1^2\gamma^2}{\tau_V^2 K^2} + \frac{2c_1\gamma m}{\tau_V^3 K^2} - \frac{4c_1\gamma m}{\tau_V^3 K^2}\right]^{1/2}$$
$$\gamma_{\text{eff}} \simeq \frac{m}{2c_1\tau_V} + \frac{\tau_V K}{2c_1} + \frac{\gamma}{2} \pm \frac{\tau_V K}{2c_1}\left[1 + \frac{2c_1\gamma}{\tau_V K} + \frac{2m}{\tau_V^2 K} + \frac{c_1^2\gamma^2}{\tau_V^2 K^2} - \frac{2c_1\gamma m}{\tau_V^3 K^2}\right]^{1/2}$$
$$\gamma_{\text{eff}} \simeq \frac{m}{2c_1\tau_V} + \frac{\tau_V K}{2c_1} + \frac{\gamma}{2} \pm \frac{\tau_V K}{2c_1}\left(1 + \frac{c_1\gamma}{\tau_V K} + \frac{m}{\tau_V^2 K} - \frac{2c_1\gamma m}{\tau_V^3 K^2}\right), \tag{4.17}$$

and taking the minus sign

$$\Rightarrow \gamma_{\text{eff}} \simeq \frac{\gamma m}{\tau_V^2 K}. \tag{4.18}$$

Combining the two limits Eqs. (4.16)-(4.18), we obtain the expression

$$\gamma_{\text{eff}}^L = \frac{\gamma}{1 + \frac{c_2 \tau_V^2 K}{m}}, \tag{4.19}$$

where c_2 is a numerical constant. Inserting Eq. (4.19) into Eq. (4.13b), we obtain the expression

$$m_{\text{eff}}^L = m - \frac{c_1 \tau_V \gamma}{1 + c_2 \tau_V^2 K/m}. \tag{4.20}$$

Inserting Eqs. (4.19) and (4.20) into Eq. (4.13c) we obtain

$$\begin{aligned} \frac{\beta_L}{\beta} &= \frac{1 + \omega_L^2 \tau_R^2}{1 + \omega_L^2 \tau_V^2} = \frac{\tau_R^2 + m/K - c_1 \tau_V \gamma_{\text{eff}}^L / K}{\tau_V^2 + m/K - c_1 \tau_V \gamma_{\text{eff}}^L / K} \\ &= \frac{\tau_R^2 + m/K - c_1 \tau_V \gamma / (K + c_2 \tau_V^2 K^2/m)}{\tau_V^2 + m/K - c_1 \tau_V \gamma / (K + c_2 \tau_V^2 K^2/m)}. \end{aligned} \tag{4.21}$$

4.3.2 High-friction limit

In the high friction limit, i.e. for $m_{\text{eff}} = 0$, Eq. (4.12) is dominated by the pole

$$\omega_H^2 = -K^2/\gamma_{\text{eff}}^2 \quad \frac{K m_{\text{eff}}}{\gamma_{\text{eff}}^2} < 1. \tag{4.22}$$

Inserting this expression into Eq. (4.13) we obtain

$$\begin{aligned} \gamma_{\text{eff}} &= \frac{\gamma}{1 - \tau_V^2 K^2/\gamma_{\text{eff}}^2} = \frac{\gamma \gamma_{\text{eff}}^2}{\gamma_{\text{eff}}^2 - \tau_V^2 K^2} \\ \gamma_{\text{eff}}^2 &- \gamma \gamma_{\text{eff}} - \tau_V^2 K^2 = 0 \\ \gamma_{\text{eff}} &= \frac{\gamma}{2} \pm \sqrt{\frac{\gamma^2}{4} + \tau_V^2 K^2} \quad \text{taking the positive sign} \\ \Rightarrow \gamma_{\text{eff}}^H &= \frac{\gamma}{2} \left[1 + \left(1 + \frac{4 c_3 \tau_V^2 K^2}{\gamma^2} \right)^{1/2} \right], \end{aligned} \tag{4.23}$$

where c_3 is a numerical constant. Inserting Eq. (4.23) into Eq. (4.13c), we obtain

$$\frac{\beta_H}{\beta} = \frac{1+\omega_H^2\tau_R^2}{1+\omega_H^2\tau_V^2} = \frac{\tau_R^2 - (\gamma_{\text{eff}}^H/K)^2}{\tau_V^2 - (\gamma_{\text{eff}}^H/K)^2}$$
$$= \frac{1 - \left\{ K\tau_R / \left[\frac{\gamma}{2} \left(1 + \left(1 + \frac{4c_3\tau_V^2 K^2}{\gamma^2} \right)^{1/2} \right) \right] \right\}^2}{1 - \left\{ K\tau_V / \left[\frac{\gamma}{2} \left(1 - \left(1 + \frac{4c_3\tau_V^2 K^2}{\gamma^2} \right)^{1/2} \right) \right] \right\}^2}. \tag{4.24}$$

4.4 MFPT formula at equilibrium

We use the mapping introduced above to obtain an approximate expression for MFPT for a non-equilibrium, non-Markovian system in a double well potential. The first step is to find an expression for an equilibrium ($\tau_V = \tau_R$) and Markovian system ($\tau_V = \tau_R = 0$). From Eq. (4.13c) we see that $\beta_{\text{eff}} = \beta$ and knowing the Kramers limits

$$\text{High friction} \quad \tau_{MFP} = e^{\beta U_0} 2\sqrt{2}\pi \frac{\gamma}{K}, \tag{4.25a}$$
$$\text{Low friction} \quad \tau_{MFP} = e^{\beta U_0} 3\pi \frac{m}{8\sqrt{2}\beta U_0 \gamma}, \tag{4.25b}$$

we build a heuristic formula

$$\tau_{\text{MFP}} = e^{\beta U_0} \left[\frac{1}{\beta U_0} \frac{3\pi}{8\sqrt{2}} \frac{m}{\gamma} + 2\sqrt{2}\pi \frac{\gamma}{K} + 4\sqrt{2\frac{m}{K}} \right]. \tag{4.26}$$

In Eq. (4.26), we summarized the Eqs. (4.25) and added a crossover term. We show in Fig.4.2 the Eq. (4.26) with a broken black line, and the two Kramers limits with the red lines. The stars depict the simulation data for three different barrier heights; the simulation method is described in chapter 2. Equation (4.26) describes the simulation data and agrees with the Melnikov-Meshkov theory (orange line), which is exact for the high-barrier limit, as shown in chapter 2.

The second step is to relax the Markovian condition and consider the more generic non-Markovian case; to this end, we insert the effective friction and mass from Eqs. (4.13) in Eq. (4.26).

In the low friction limit, the inertial time is given by

$$\frac{m_{\text{eff}}^L}{\gamma_{\text{eff}}^L} = \frac{m}{\gamma} - c_1\tau_V + c_2\tau_V^2 K\gamma. \tag{4.27}$$

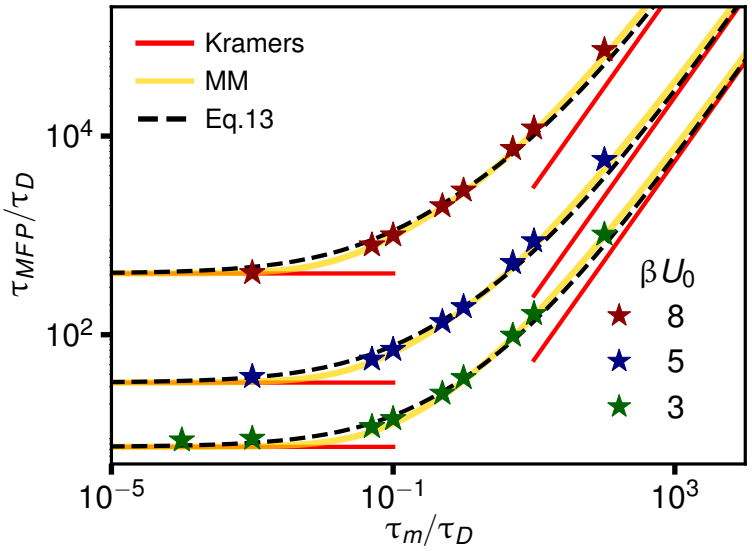

Figure 4.2: MFPT in the equilibrium Markovian limit as a function of τ_m/τ_D for three different βU_0. Comparison of simulation results (symbols), Eq. (4.26) (dashed lines) and the Melnikov-Meshkov (MM) theory [27] (colored lines). The red straight lines show the Kramers limits [25, 99].

The expression shows two different behaviors for various values of memory time: for lower memory time values, we obtain an acceleration of the barrier crossing, and for a higher value, a deceleration in the MFPT [18]. We must, therefore, combine the memory acceleration term with the overdamped contribution in Eq. (4.26) to avoid singular behavior.

$$\gamma/K - c_1\tau_V/(\beta U_0) \approx \gamma/K/(1 + c_1 K\tau_V/(\gamma\beta U_0)), \tag{4.28}$$

this new term provides a better description of the numerical data.

Inserting, also, the high friction term (4.23) in the Eq. (4.26), we obtain

$$\begin{aligned}\tau_{MFP} = e^{\beta U_0}\Bigg[&\frac{1}{\beta U_0}\frac{3\pi}{8\sqrt{2}}\left(\frac{m}{\gamma} + \frac{c_2 K\tau_V^2}{\gamma}\right) + 4\sqrt{2\frac{m}{K}} \\ &+ \frac{\sqrt{2}\pi\gamma}{K}\frac{1}{1 + 3c_1 K\tau_V/(16\beta U_0\gamma)} + \frac{\sqrt{2}\pi\gamma}{K}\left(1 + \frac{4c_3\tau_V^2 K^2}{\gamma^2}\right)^{1/2}\Bigg].\end{aligned} \tag{4.29}$$

In Fig.4.3, we compare Eq. (4.29) for various values of τ_m/τ_D as a function of the rescaled memory time τ/τ_D with the simulation data for two different values of the numerical constant c_3. We observe that we need a small value of $c_3 \simeq 0.01$ in order to obtain an accurate agreement with the simulation

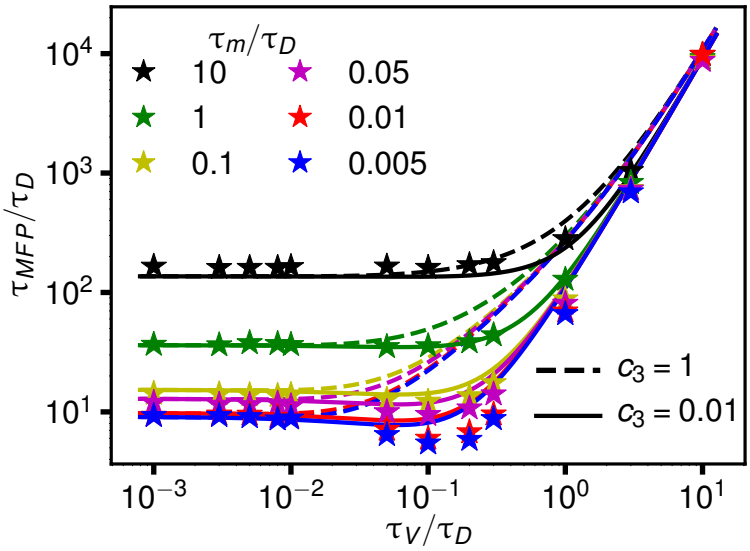

Figure 4.3: MFPT in the equilibrium non-Markovian case for fixed $\beta U_0 = 3$ and various values of τ_m/τ_D as a function of memory time τ_V/τ_D. Simulation results (symbols) are compared with Eq. (4.29) with $c_1 = 64/3$ and $c_2 = 2/3$.

data. It transpires that we can neglect this constant and actually set $c_3 = 0$; for this reason, we must replace the effective term only in the inertial term ($\propto m/\gamma$) because it is the dominant term compared with the high-friction and crossover terms respectively ($\propto \gamma/K$).

The value of the other two constants c_1 and c_2, which take into account the deviation from parabolic potential, is obtained by fitting the simulation data in Fig.4.4 for fixed barrier height $\beta U_0 = 3$ and several different rescaled masses τ_m/τ_D (symbols), the same data as in Fig.4.3. The Eq. (4.30) accurately describes the data for general mass/friction ratios and rescaled memory times τ_V/τ_D, when $c_1 = 64/3$ and $c_2 = 2/3$. For $c_1 = 1$ and $c_2 = 1$ is recovered from the exact harmonic model.

$$\tau_{MFP} = e^{\beta U_0}\left[\frac{1}{\beta U_0}\frac{3\pi}{8\sqrt{2}}\left(\frac{m}{\gamma}+\frac{c_2 K\tau_V^2}{\gamma}\right)\right.$$
$$\left.+\frac{2\sqrt{2}\pi\gamma}{K}\frac{1}{1+3c_1 K\tau_V/(32\beta U_0\gamma)}+4\sqrt{2\frac{m}{K}}\right], \tag{4.30}$$

an expression equivalent to a previous heuristic formula [18, 88].

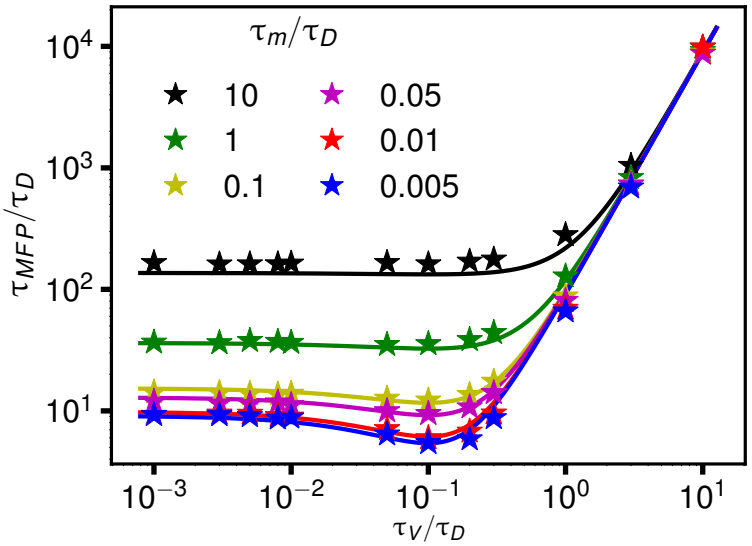

Figure 4.4: MFPT in the equilibrium non-Markovian case for fixed $\beta U_0 = 3$ and various values of τ_m/τ_D as a function of memory time τ_V/τ_D. Simulation results (symbols) are compared with Eq. (4.30) with $c_1 = 64/3$ and $c_2 = 2/3$.

4.5 Joint position-velocity distribution

The non-equilibrium case is the final step. Thus, we release the condition $\tau_V = \tau_R$. The only effective term (4.13), which depends on τ_R is the inverse of effective temperature Eq. (4.13c) and inserting in the relation the pole expressions in the limit of low and high friction, we obtain

$$\frac{\beta^L_{\text{eff}}}{\beta} = \frac{\tau_R^2 + m/K - c_1\tau_V\gamma^L_{\text{eff}}/K}{\tau_V^2 + m/K - c_1\tau_V\gamma^L_{\text{eff}}/K} \tag{4.31}$$

$$\frac{\beta^H_{\text{eff}}}{\beta} = \frac{\tau_R^2 - (\gamma^H_{\text{eff}}/K)^2}{\tau_V^2 - (\gamma^H_{\text{eff}}/K)^2}. \tag{4.32}$$

In the limits $\tau_m/\tau_V < 1$, $\tau_m/\tau_R < 1$, $\gamma/(K\tau_V) > 1$, $\gamma/(K\tau_R) > 1$, which applies to the systems considered numerically, as we will demonstrate below, we can write

$$\beta_{\text{NEQ}}/\beta = \tau_R^2/\tau_V^2 \approx \beta^L_{\text{eff}}/\beta \approx \beta^H_{\text{eff}}/\beta. \tag{4.33}$$

The new temperature for a system in a state of non-equilibrium is proportional to the square ratio τ_R/τ_V. Subsequently, we must concentrate on the overdamped case, as most of the systems we model with the GLE fall within this regime, and we choose $\tau_m/\tau_D = 0.1$.

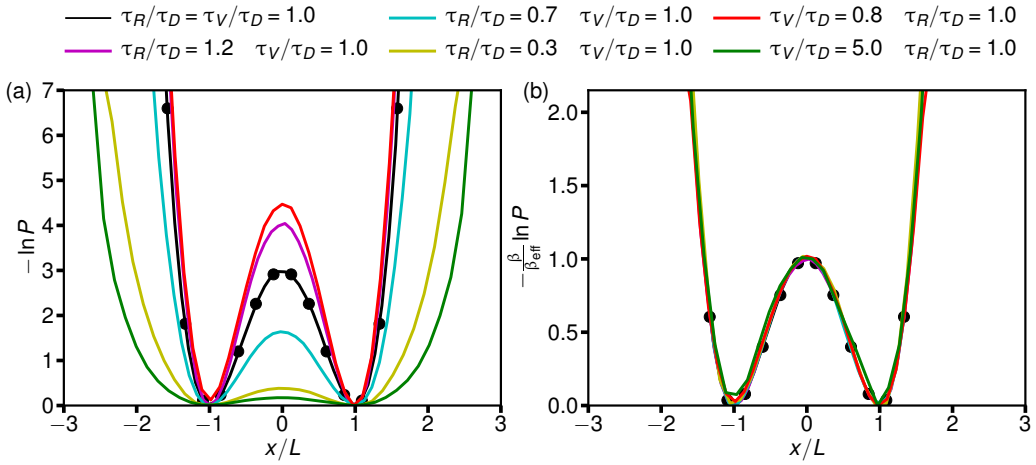

Figure 4.5: a) Logarithmic position distributions for $\tau_m/\tau_D = 0.1$, $\beta U_0 = 3$ and various τ_R/τ_D and τ_V/τ_D. b) Logarithmic position distributions rescaled by the fitted factor β/β_{eff}.

We can test our mapping with the joint position-velocity distribution.The distribution with the effective parameters is given by

$$P(x,v) \propto e^{-\beta_{\text{eff}}U(x)-\beta_{\text{eff}}v^2 m_{\text{eff}}/2}. \tag{4.34}$$

In Fig.4.5 we show on the left the logarithmic positional distribution $-\ln P(x)$ and on the right the rescaled distribution $-\ln P(x)\beta/\beta_{\text{eff}}$ for various values of τ_V/τ_D and τ_R/τ_D. The simulation data are shifted to agree for $x = \pm L$. In both plots, the equilibrium case $\tau_R = \tau_V$ is represented by the black line, with the black spheres indicating the expected result $-\ln P(x) = \beta U(x)$; we, therefore, observe perfect agreement between the simulation data and the expected result. The other colored lines represent the non-equilibrium simulation data.

In Fig.4.5b), all distributions begin to overlap when they are rescaled with the fitted prefactor β/β_{eff}. In Fig.4.6, we consider the same plot as in Fig.4.5, except for the velocity distribution. On the left, we depict the logarithmic velocity distribution $-\ln P(v)$ for various values of τ_V/τ_D and τ_R/τ_D. The data are shifted to agree for $v = 0$. Also, in this case, the colored lines show the non-equilibrium simulation data, the black line the equilibrium case, and the black spheres the Maxwell-Boltzmann distribution $-\ln P(v) = \beta m v^2/2$. Thus, the rescaled prefactor in b) is β/β_{eff}, and furthermore, the rescaled simulation data with the fitted parameter are superimposed.

In Fig.4.7, we plot the rescaled parameters, with red stars, as a function of τ_R/τ_D in a) and c) and τ_V/τ_D in b) and d). In all of the plots, we observe

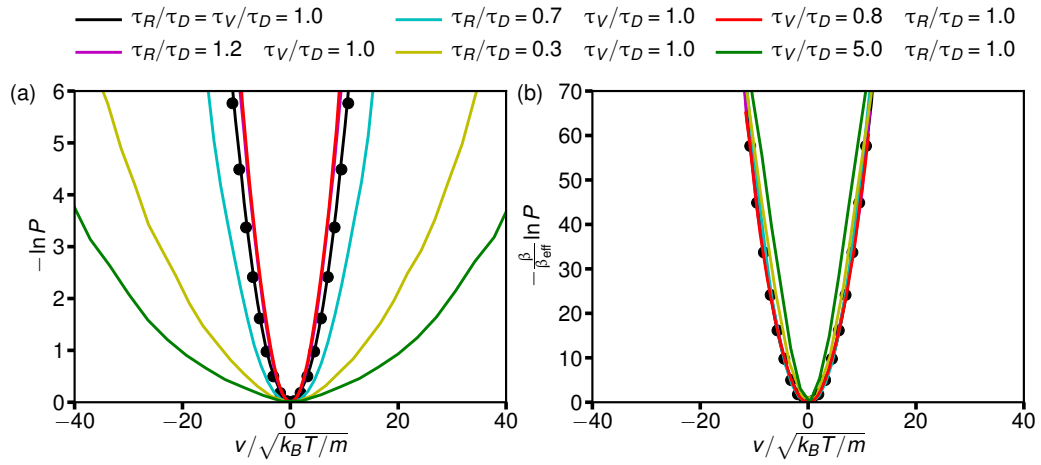

Figure 4.6: a) Logarithmic velocity distributions for $\tau_m/\tau_D = 0.1$, $\beta U_0 = 3$ and various τ_R/τ_D and τ_V/τ_D. b) Logarithmic velocity distributions rescaled by the fitted factor β/β_{eff}.

an agreement between the data and the effective parameter written above in the Eqs. (4.31) dashed red line, (4.32) blue line, and (4.33) black dots. By studying the position and velocity distribution, we can verify that an effective temperature (ratio of memory and random relaxation times) accurately describes the non-equilibrium case.

4.6 MFPT formula far from equilibrium

After verifying the joint position-velocity distribution, we insert β_{NEQ} instead of β in Eq. (4.30), we achieve a formula for the MFPT, that is valid also for the non-equilibrium case

$$\tau_{\text{MFP}} = e^{\beta_{\text{NEQ}} U_0} \left[\frac{1}{\beta_{\text{NEQ}} U_0} \frac{3\pi}{8\sqrt{2}} \left(\frac{m}{\gamma} + \frac{2K\tau_V^2}{3\gamma} \right) + \frac{2\sqrt{2}\pi\gamma}{K} \frac{1}{1 + 2K\tau_V/(\beta_{\text{NEQ}} U_0 \gamma)} + 4\sqrt{2\frac{m}{K}} \right]. \tag{4.35}$$

We compare Eq. (4.35) with the simulation data, in Fig.4.8. In this figure, we plot the rescaled MFPT as a function of τ_R/τ_V for three values of τ_V/τ_D. Note that we recover the equilibrium case by setting $\tau_R/\tau_V = 1$. The data are quite well described by Eq. (4.35), which is an equation deduced using a non-equilibrium, non-Markovian harmonic oscillator model applied to the

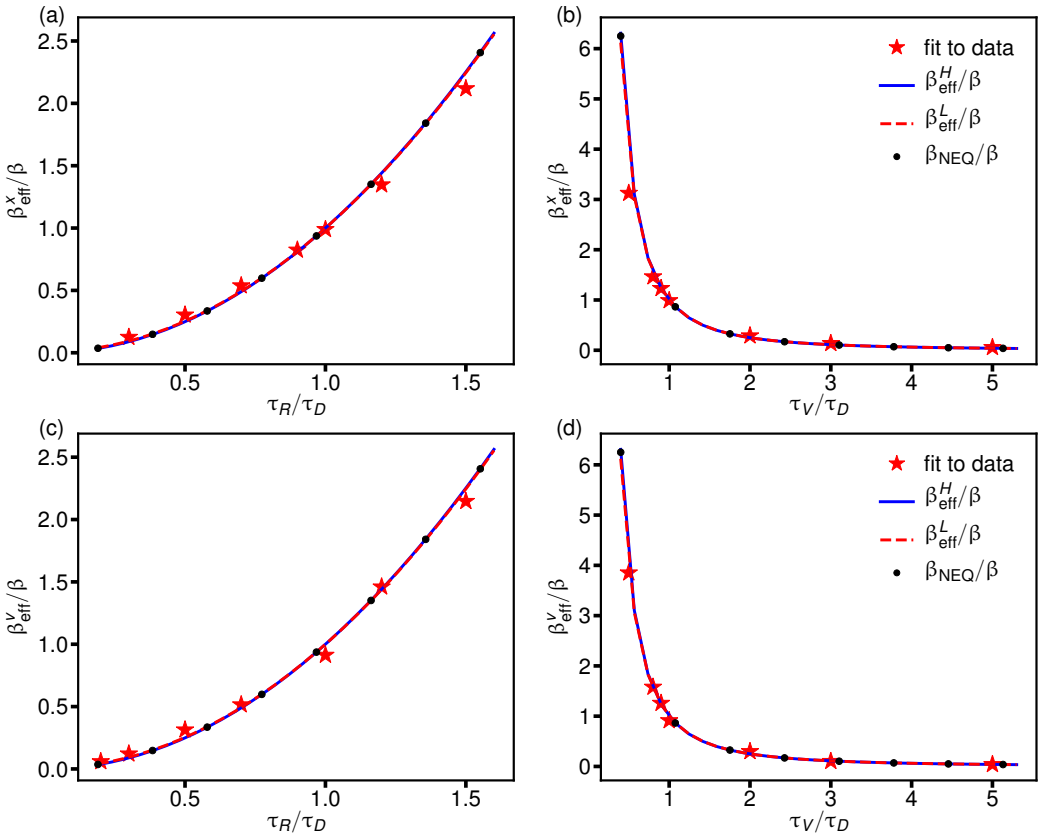

Figure 4.7: a), b), c) and d), $\beta_{\rm eff}/\beta$ from the fit (symbols) are compared with the predictions of the effective parameters in Eqs. (4.31) blue line, (4.32) red dashed line, (4.33) black dots. The fitting factors in a) and b) come from the position distribution in Fig.4.5, respectively on the left for various τ_R/τ_D and on the right for τ_V/τ_D. In c) and d), the velocity distribution rescaled factors are shown (Fig.4.6).

barrier-crossing dynamics in a double-well potential. The pronounced feature that we can see in the figure is the monotonic increase of the MFPT with τ_R/τ_V.

4.7 Conclusion

In conclusion, we insert the effective friction, mass, and temperature (derived by solving the non-equilibrium, non-Markovian harmonic oscillator) in the heuristic formula for the barrier crossing dynamics of a Markovian single massive particle and obtain an equation for the non-equilibrium non-Markovian

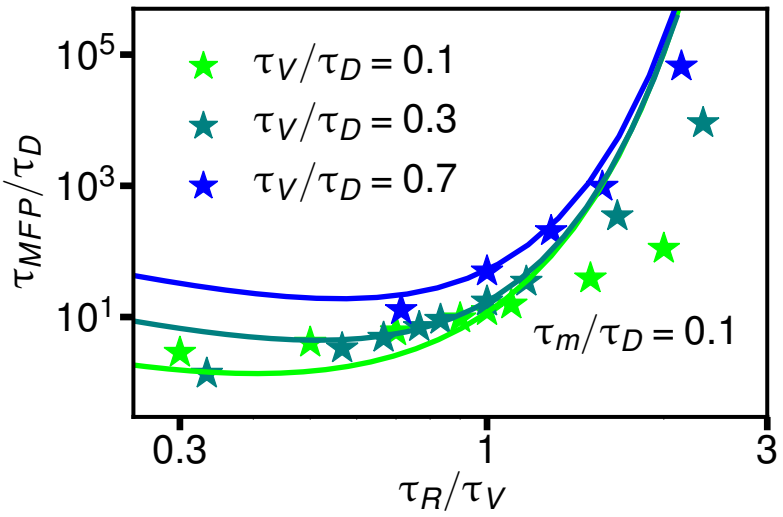

Figure 4.8: Non-equilibrium MFPT as a function of τ_R/τ_V for various values of τ_V/τ_D for fixed $\beta U_0 = 3$ and $\tau_m/\tau_D = 0.1$. The lines show the predictions from Eq. (4.35), and the stars denote simulation data.

barrier-crossing dynamics. The final expression (4.30) at the equilibrium is equivalent to a previously suggested heuristic formula [18,88]. We have thus demonstrated how the new non-equilibrium formula is asymmetrically influenced by the random correlation time τ_R and the memory friction time τ_V. The barrier crossing time increases monotonically as τ_R/τ_V increases. Apart from the memory and inertial effects that modify the exponential prefactor in the MFPT, the Arrhenius factor changes in non-equilibrium, which dramatically changes the MFPT. This result could be significant for *in vivo* non-equilibrium protein folding because in recent experiments, a delay of the folding has been measured for the folding speed of a nascent polypeptide during translation [74]. Our results, therefore, depend on the functional form of the memory kernel, which we adopt to be exponential in this thesis. Additionally, we have proved that the derived effective temperature accurately describes the position and velocity joint-probability for a non-linear barrier-crossing system far from equilibrium.

Chapter 5

Asymmetric double-well potential

5.1 Introduction

Starting with Arrhenius' early works [54, 78, 100], the escape rate over a potential barrier sparked universal interest in the physics and chemistry communities. Kramers developed a Markovian theory for the transition rate [25], introducing the interaction between the particle and the heat bath. Additionally, Kramers calculated explicit formulae for the high and low friction limit escape rate. The regime between the two limits (high and low friction), the Kramers turnover, was considered by Mel'nikov and Meshkov (MM) [27]. Another essential step was the introduction of the generalized Langevin equation by Zwanzig [10]. Using the Mori-Zwanzig projection [8,9], the dimension of the system can be reduced since with the projection, we concentrate only on some relevant observables, but this produces non-Markovian effects [31,38,101]. Grote and Hynes (GH) [26] derived a self-consistent equation for the mean first passage time (MFPT) in the limit of short memory time and medium to high friction regime. A solution for the turnover problem in the presence of short and long memory was given by Pollak, Grabert, and Hänggi (PGH) [57]. Many of the studies above considered a parabolic well approximation of the potential $U(x) = -\frac{1}{2}Kx^2$ [102].

However, in many biological and chemical events, the relaxation in the potential well is also considered to be essential. Hence, a double-well potential is more realistic for chemical reactions and protein folding [48–55]. Most previous theoretical studies consider symmetric double well potentials. However, in many simulation and experimental systems, we find that free energy potential profiles are typically asymmetric. For example, in Fig.5.1 we show the free energy profiles for four different proteins as a function of the fraction of native contacts, i.e. coordinate Q. It is evaluated in connectivity space

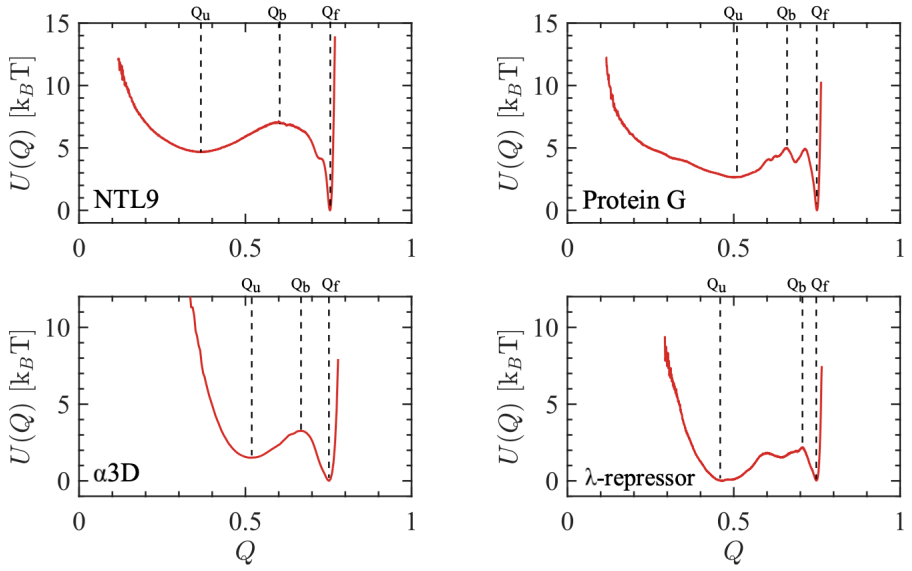

Figure 5.1: Free energy profiles for the fraction of native contacts reaction coordinate Q evaluated for four fast-folding proteins. The unfolded Q_u, barrier Q_b, and folded Q_f reaction coordinate values are indicated for each protein. Free energy profiles are calculated from $U(Q) = -k_B T \log[p(Q)]$ where $p(Q)$ is the probability density for a given reaction coordinate value. The parameters that define these proteins are the free-energy barriers $U_f = U(Q_b) - U(Q_f)$, $U_u = U(Q_b) - U(Q_u)$ and the separation between the barrier and minima, $L_f = Q_b - Q_f$ and $L_u = Q_u - Q_b$. Respectively we find for NTL9: $\beta U_f = 6.7$, $\beta U_u = 2.3$, $L_f = 0.23$, $L_u = 0.16$ for Protein G: $\beta U_f = 4.5$, $\beta U_u = 2.3$, $L_f = 0.16$, $L_u = 0.10$, for $\alpha 3D$: $\beta U_f = 3.2$, $\beta U_u = 1.7$, $L_f = 0.14$, $L_u = 0.09$ and for λ-repressor: $\beta U_f = 2.1$, $\beta U_u = 2.1$, $L_f = 0.24$, $L_u = 0.047$, as reported in [46].

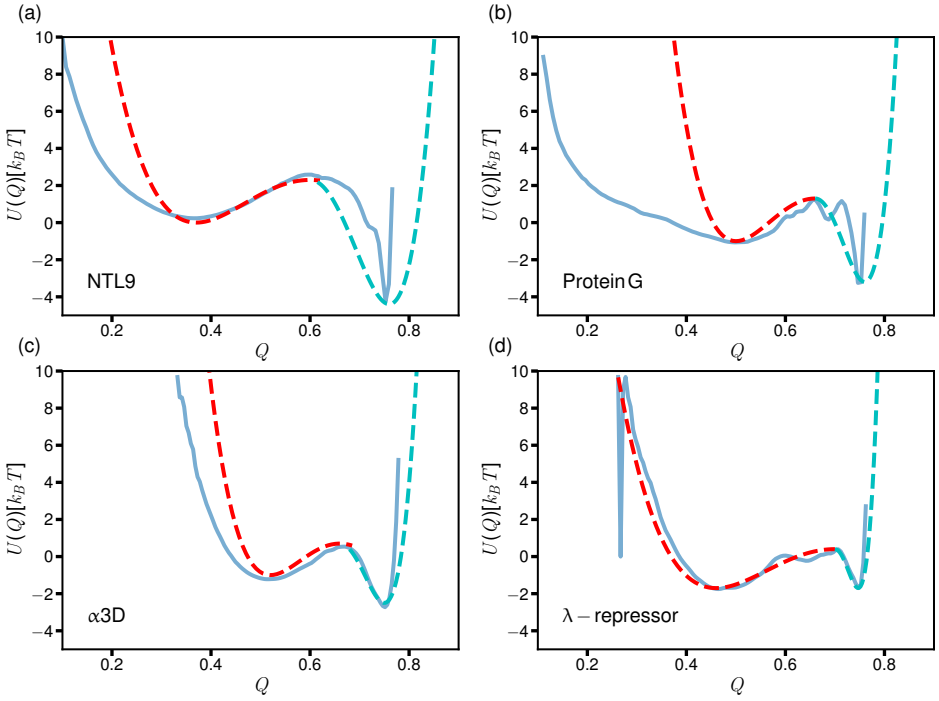

Figure 5.2: Free energy profiles for the fraction of native contacts reaction coordinate Q. Free energy profiles are calculated from $U(Q) = -k_BT\log[p(Q)]$ where $p(Q)$ is the probability density for a given reaction coordinate value. The dashed lines denote the analytical potential that describes the free-energy profile around the folded an unfolded states.

and is, for this reason, dimensionless. In the folded state, it is close to Q = 1. In the unfolded state, it is closer to Q = 0. The research group of David E. Shaw provided the data, and this was originally published by Lindorff-Larsen et al. [103]. The figure demonstrates that the reaction coordinate free energy landscape could be approximated by a double-well potential but not by a symmetric one.

In Fig.5.2, we fit the free-energy profile to provide analytical expressions for these profiles,

a)

$$U(x) = \begin{cases} 2.3\left[\left(\frac{x}{0.23}\right)^2 - 0.6\right]^2 & \text{if } x < 0 \\ 6.7\left[\left(\frac{x}{0.16}\right)^2 - 0.6\right]^2 - 4.4 & \text{if } x > 0, \end{cases} \tag{5.1}$$

b)

$$U(x) = \begin{cases} 2.3\left[\left(\frac{x}{0.16}\right)^2 - 0.66\right]^2 & \text{if } x < 0 \\ 4.5\left[\left(\frac{x}{0.1}\right)^2 - 0.66\right]^2 - 2.2 & \text{if } x > 0, \end{cases} \tag{5.2}$$

c)

$$U(x) = \begin{cases} 1.7\left[\left(\frac{x}{0.14}\right)^2 - 0.66\right]^2 & \text{if } x < 0 \\ 3.2\left[\left(\frac{x}{0.09}\right)^2 - 0.66\right]^2 - 1.5 & \text{if } x > 0, \end{cases} \tag{5.3}$$

d)

$$U(x) = \begin{cases} 2.1\left[\left(\frac{x}{0.24}\right)^2 - 0.7\right]^2 & \text{if } x < 0 \\ 2.1\left[\left(\frac{x}{0.047}\right)^2 - 0.7\right]^2 & \text{if } x > 0. \end{cases} \tag{5.4}$$

In this chapter, we investigate the effects of asymmetric double-well potential [104, 105] on the MFPT, i.e., the mean of the time taken to reach a target state from an initial point, also recrossing the initial point. We develop another formula for a non-Markovian system with a massive particle. We know that the time to reach the top of the barrier starting from one well is half of the time to go from well to well for a diffusive Markovian system. In the next section, we present a model to study our formula for MFPTs in an asymmetric double-well potential. We use the results of chapter 4 to develop the new formula.

5.2 Setup

As was shown previously [46, 85], the folding of short homopeptide chains and fast-folding proteins follows non-Markovian dynamics, and the best prediction of the folding time is given by a generalized Langevin equation (GLE) with multi-exponential memory. As an approximation, we consider the GLE with linear friction [8, 10, 106, 107]

$$m\ddot{x}(t) = -\int_{t_0}^{t} \Gamma(t-t')\dot{x}(t')dt' - \nabla U(x(t)) + F_R(t), \tag{5.5}$$

where m is the mass of the reaction coordinate, $\Gamma(t)$ the memory kernel, t_0 some initial time and, $F_R(t)$ denotes the random force characterized by the general autocorrelation

$$\langle F_R(t)F_R(t')\rangle = \beta^{-1}\Gamma(t-t'), \tag{5.6}$$

where $\beta = 1/k_B T$ is the inverse thermal energy. As a memory kernel, we choose a single exponential

$$\Gamma(t) = \frac{\gamma}{\tau} e^{-\frac{|t|}{\tau}}, \tag{5.7}$$

where τ is the decay time scale of the memory effects.

To represent the experimental system, we select an asymmetric double-well potential

$$U(x) = \begin{cases} U_L \left[\left(\frac{x}{L_L} \right)^2 - 1 \right]^2 & \text{if } x < 0 \\ U_R \left[\left(\frac{x}{L_R} \right)^2 - 1 \right]^2 + (U_L - U_R) & \text{if } x > 0, \end{cases} \tag{5.8}$$

where $(L_L + L_R)$ is the separation between the two minima, and U_L and U_R are the barrier heights, as shown in Fig.5.3a). Note that the second derivative is discontinuous at the top of the barrier, but this is not problematic when we only consider MFPTs to the top of a barrier.

In order to rescale the system, we must first introduce two essential time scales. They are the diffusion time τ_D and inertial time τ_m, respectively:

$$\begin{aligned} \tau_D &= \beta L_L^2 \gamma, \\ \tau_m &= \frac{m}{\gamma}. \end{aligned} \tag{5.9}$$

To illustrate the influence of our choice of parameters on the system dynamics, we depict in Fig.5.3 the trajectories of a particle for various memory times, barrier heights, and potential widths. In Fig.5.3b), we fix the memory time and the potential widths L_L and L_R, and we vary the barrier height. Subsequently, we observe that the green trajectory, where the right barrier height is lower (symmetric case), spends more time in the right well than the yellow trajectory. Considering the same time frame, between 200 and 400 t/τ_D, in Figures c), we vary the width of the potential, and the red trajectory shows a shorter MFPT than the yellow trajectory. In Figure d), we plot only one trajectory with $L_R/L_L = 0.5$, $\beta U_R = 5$, and memory time $\tau/\tau_D = 1$. Considering a longer memory time with respect to Figures b) and c), we need a longer time frame to observe a relevant number of crossing. From Fig.5.3, it is clear that these variables (barrier height, length scale, and memory time) influence the dynamics of the particle.

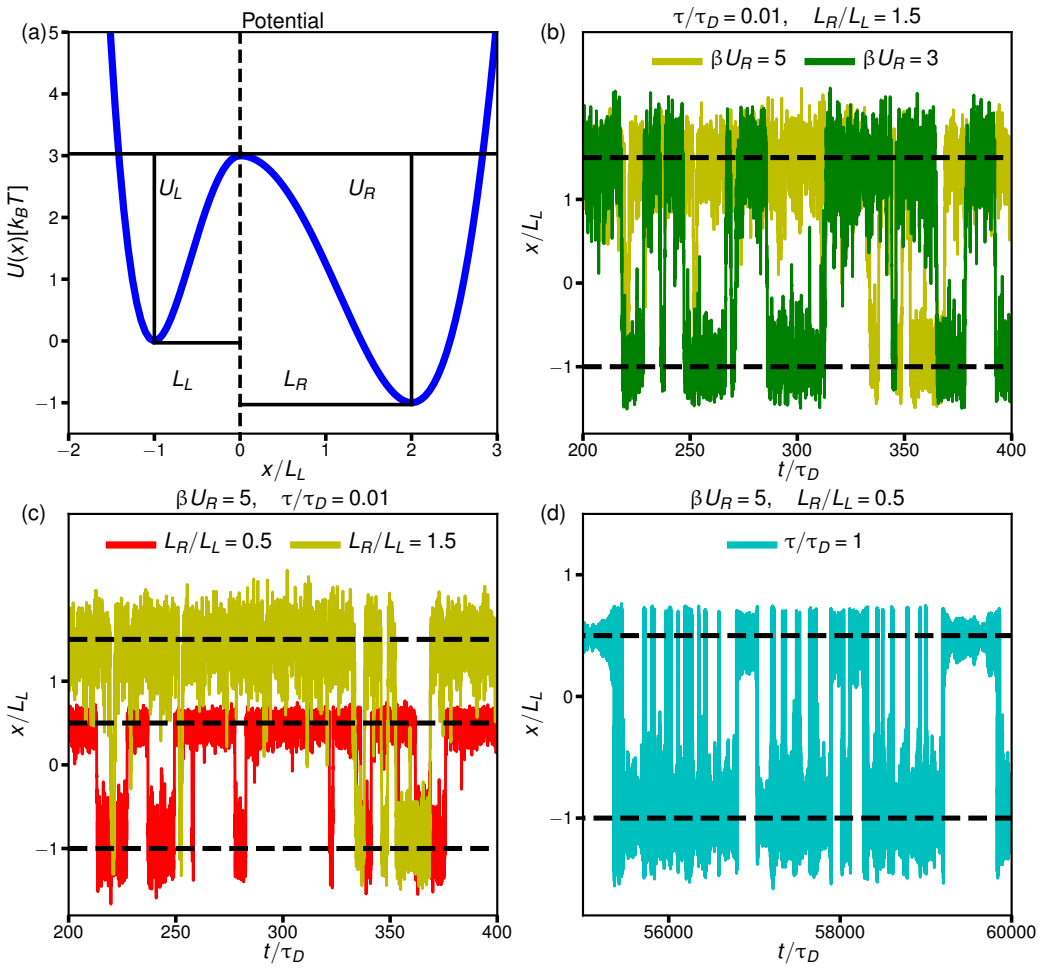

Figure 5.3: In a) the potential is depicted as in Eq. (5.8). In b), c), and d) trajectories of various systems with different parameters are shown, the same color trajectories show systems with the same parameters. All the trajectories have $\beta U_L = 3$ and $\tau_m/\tau_D = 0.01$. In b), memory time is fixed to $\tau/\tau_D = 0.01$ and $L_R/L_L = 1.5$, and for the yellow line $\beta U_R = 5$ and for the dark-green $\beta U_R = 3$. In c) $\beta U_R = 5$ and the same memory time as in b) $\tau/\tau_D = 0.01$, but with two different L_R/L_L. In d) the right potential height as in c) $\beta U = 5$, but only for $L_R/L_L = 0.5$ and with $\tau/\tau_D = 1$.

5.3 Formula comparison

In chapter 3 and chapter 4, we proposed two formulae to calculate the MFPT as a function of the particle mass, the friction coefficient, memory time, and the symmetric potential [18, 19, 88, 108]. In this section, we explain the difference, and propose another choice.

From chapter 3, if we rewrite the MFPT for a single exponential memory kernel as a function of mass, friction, and potential curvature ($\beta U_0/\tau_D = K/(8\gamma)$), we obtain

$$\begin{aligned}\tau_{\mathrm{MFP}} = e^{\beta U_0}\Bigg[&\frac{1}{\beta U_0}\left(\frac{m}{\gamma}+\frac{K\tau^2}{2\gamma}\right)\\ &+\frac{2\sqrt{2}\pi\gamma}{K}\frac{1}{1+5K\tau/\gamma}+4\sqrt{2\frac{m}{K}}\Bigg].\end{aligned} \tag{5.10}$$

In chapter 4 for the equilibrium case, we use the following formula

$$\begin{aligned}\tau_{\mathrm{MFP}} = e^{\beta U_0}\Bigg[&\frac{1}{\beta U_0}\frac{3\pi}{8\sqrt{2}}\left(\frac{m}{\gamma}+\frac{2K\tau^2}{3\gamma}\right)\\ &+\frac{2\sqrt{2}\pi\gamma}{K}\frac{1}{1+2K\tau/(\beta U_0\gamma)}+4\sqrt{2\frac{m}{K}}\Bigg].\end{aligned} \tag{5.11}$$

And in this chapter, we introduce the new expression,

$$\begin{aligned}\tau_{\mathrm{MFP}} = e^{\beta U_0}\Bigg[&\frac{1}{\beta U_0}\frac{3\pi}{8\sqrt{2}}\left(\frac{m}{\gamma}+\frac{2K\tau^2}{3\gamma}\right)\\ &+\frac{2\sqrt{2}\pi\gamma}{K}\frac{1}{1+K\beta U_0\tau/(4\gamma)}+4\sqrt{2\frac{m}{K}}\Bigg].\end{aligned} \tag{5.12}$$

Comparing the three formulae, we can conclude that the main difference is the speed-up term. The other difference is the constants used in front of the first two terms, but in front of the inertial term in Eqs. (5.11) and (5.12), coming from the Kramers limit, we have $3\pi/(8\sqrt{2}) \simeq 0.833 \approx 1$ the constant in the Eq. (5.10). In front of the memory slow-down term in the last two equations, there is $\pi/(4\sqrt{2}) \approx 0.5$ as in the formula in chapter 3. So, we can conclude that the three equations are the same, except for the speed-up term. With regards to the speed-up term, the $\beta U_0/4$ in the denominator in the Eq. (5.12) becomes $\beta U_0/4 \to 5$ in Eq. (5.10) and $\beta U_0/4 \to 2/\beta U_0$ in

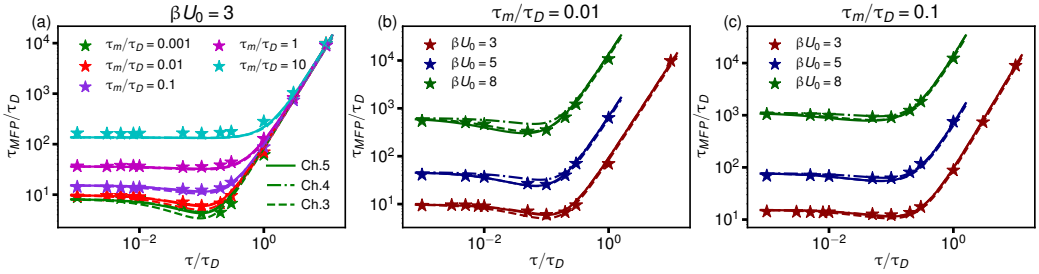

Figure 5.4: In a) MFPT is shown as a function of rescaled τ/τ_D for a symmetric double-well potential with $\beta U_0 = 3$ for various values of τ_m/τ_D. Comparison of simulation results (stars), Eq. (5.12) (continuous lines), Eq. (5.10) (dashed lines) and Eq. (5.11) (dash-dotted lines). In b) and c) MFPT respectively for $\tau_m/\tau_D = 0.01$ and $\tau_m/\tau_D = 0.1$ for three different values of the barrier height is shown.

Eq. (5.11). This variation is significant when we consider a system with a small mass, as it is relevant for protein folding.

In Fig.5.4, we plot the rescaled MFPT for various inertial times in a) and three different barrier heights in b) and c) and we compare the three Eqs. (5.10) dashed line, (5.11) dashed-dotted line, and (5.12) continuous line. The main differences between the three formulae are visible for small values of the inertial time at the minimum of the MFPT in Fig.5.4a) and for high barrier weights in Fig.5.4b),c). As we can see from Fig.5.4, the equation that best describes the data is Eq. (5.12). Equation (5.10) does not adequately describe the data at the minimum for small mass, and Eq. (5.11) does not fit the data for a high value of potential height.

In any case, the differences between the formulae are rather small. And in the preceding chapters, we concentrated on the weight potential $\beta U_0 = 3$; for this reason, the results in the chapter 3 and chapter 4 remain valid.

In Fig.5.5, we repropose Fig.5.4, but showing only Eq. (5.12). The equation describes the simulation data considering various values of τ_m/τ_D in a) and different potential heights in b) and c). In this chapter as in the previous one from the simulation we consider the mean of all-to-first passage time. As mentioned in section 5.1, Grote-Hynes (GH) developed a theory for the MFPT in the limit of short memory time and medium-to-high friction; in fact, for short memory time, GH describes the MFPT, but in the limit $\tau \to \infty$, τ_{MFP} decreases and, in particular, goes to zero as $m \to 0$, as shown in the chapter 2. On the other hand, Eq. (5.12) shows a finite value at the minimum. In fact, assuming $10\beta U_0 \tau/\tau_D \gg 1$ and $m \to 0$, Eq. (5.12) becomes

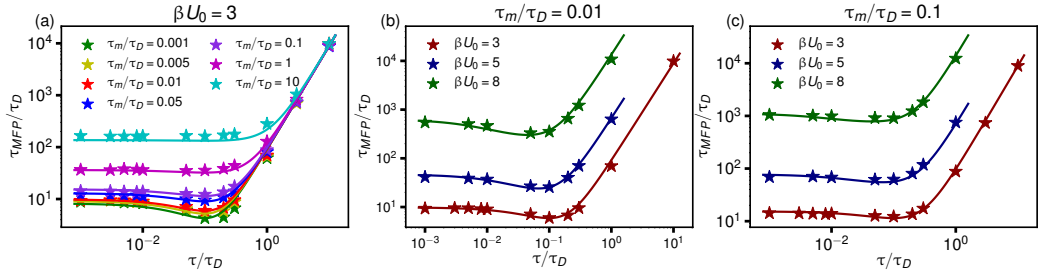

Figure 5.5: In a) MFPT as a function of rescaled τ/τ_D for a symmetric double-well potential with $\beta U_0 = 3$ for various values of τ_m/τ_D is depicted. Comparison of simulation results (stars) and Eq. (5.12) (lines). In b) and c) MFPT respectively for $\tau_m/\tau_D = 0.01$ and $\tau_m/\tau_D = 0.1$ for three different values of the barrier heights ($\beta U_0 = \{3, 5, 8\}$) is shown.

$$\tau_{MFP} = e^{\beta U_0} \left[\frac{1}{\beta U_0} \frac{3\pi}{8\sqrt{2}} \frac{2K\tau^2}{3\gamma} + \frac{2\sqrt{2}\pi\gamma}{K} \frac{1}{K\beta U_0 \tau/(4\gamma)} \right]. \tag{5.13}$$

The memory time, for which we have the minimum $\left(\frac{\partial \tau_{MFP}}{\partial \tau} = 0\right)$, is given by

$$\tau^* = \frac{\sqrt[3]{32}\gamma}{K}, \tag{5.14}$$

it is finite and goes to zero as $U_0 \to \infty$. The value of the mean first passage time at the minimum is

$$\tau_{MFP} = \frac{e^{\beta U_0}}{\beta U_0} \frac{\pi\gamma}{K} \left[(\sqrt[3]{4})^2 + \frac{4\sqrt{2}}{\sqrt[3]{4}} \right]. \tag{5.15}$$

5.4 Mean-first passage time from well to top

Before studying the asymmetric case, we must first investigate the role of memory and inertial time in the symmetric case. This section does not consider the MFPT from well to well. Rather, we consider the mean first passage time to the top of the barrier from either the left well τ^L_{MFP} or the right well τ^R_{MFP}. In other words, we consider the time necessary for a massive particle to go from one of the two minima to the top of the barrier. By doing so, we can decouple the dynamics in the two wells. The only coupling contribution is due to recrossing. Still, these events are rare and do

not significantly contribute to the mean. As we know from previous studies and analysis [23, 109], when we consider an overdamped Markovian system ($\tau = 0$ and $m = 0$), also taking into account high barriers, the time to reach the top is half that of the time to go from one well to the other,

$$\tau^L_{MFP} = \tau^R_{MFP} = \tau_{MFP}/2, \tag{5.16}$$

where τ^L_{MFP} and τ^R_{MFP} are the mean first passage time to reach the top, starting from the left and from the right well, respectively. In order to test the relation (5.16) for inertial non-Markovian systems, in Fig.5.6a) we plot the rescaled MFPT as a function of the rescaled memory time for two values of the inertial time ($\tau_m/\tau_D = 0.01$ and $\tau_m/\tau_D = 0.1$). The red and black lines show Eq. (5.12), while the circles denote the simulation data for τ_{MFP}. The triangles depict the simulation data for the rescaled τ^R_{MFP}. We only show τ^R_{MFP}, because we are considering the symmetric case, therefore $\tau^R_{MFP} = \tau^L_{MFP}$. As we anticipated from Eq. (5.16) for small values of the memory time, there is more discrepancy between the time taken to reach the top and the time taken to go from one to the other well, in particular, for the system with a smaller mass. This aspect can be better investigated in Fig.5.6b), where we plot the ratio between τ^R_{MFP} and τ_{MFP} for the two inertial memory times. For small inertial times and memory times, we record a value closer to 0.5 than when we consider higher inertial time, we are taking into consideration a massive non-Markovian system. Both curves increase along with the memory time, both approaching a value of 1. This necessitates a new formula for the well-to-the-barrier-top case.

5.5 Asymmetric potential with different barrier-height and potential length

To design a formula for τ^L_{MFP} and τ^R_{MFP}, we must first understand the origin of the different terms in Eq. (5.12). Equation (5.12) was derived by summing the low and high friction limits of the MFPT for a non-Markovian system plus an intermediate term (chapter 4) [108].

When we calculate the mean first passage time from one of the two wells to the barrier top (and not from well to well), the only term influenced by this change is the high friction term. As suggested by Fig.5.6b), the black line is close to 0.5. This can therefore be taken into account if we assume that $\tau^L_{MFP} = \tau^R_{MFP} = \tau_{MFP}/2$ when $m = 0$ and $\tau = 0$. For this reason, we insert one half in front of the high friction term proportional to γ/K in Eq. (5.12), and we must therefore consider that, in the asymmetric case, the

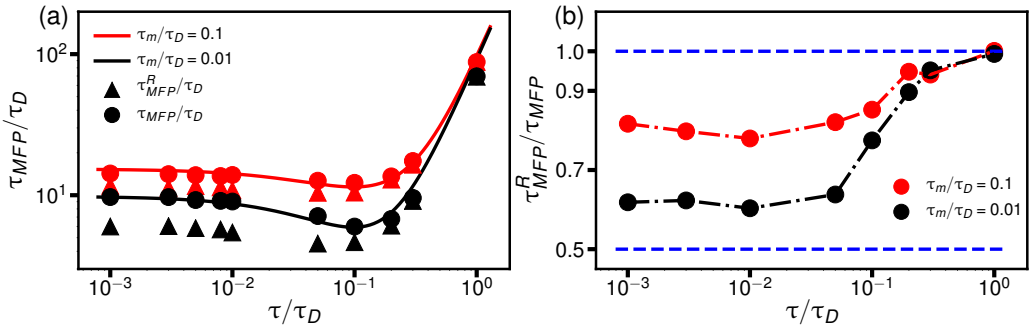

Figure 5.6: a) MFPT as a function of rescaled τ/τ_D for a symmetric double-well potential with $\beta U_0 = 3$. Comparison of simulation results to go from the left to the right well (black circles) and Eq. (5.12) (lines) for two values of the inertial memory time (red for $\tau_m/\tau_D = 0.1$ and black for $\tau_m/\tau_D = 0.01$). The triangles show the simulation data for the time to reach the barrier top starting from the right well τ^R_{MFP}. b) The ratio τ^R_{MFP}/τ_{MFP} as a function of rescaled memory time. The dashed lines show the two limits. On the top ($\tau^R_{MFP}/\tau_{MFP} = 1$), the plateau value that the two curves reach for $\tau/\tau_D \to \infty$. On the bottom, $\tau^R_{MFP}/\tau_{MFP} = 0.5$ the limit for $\tau/\tau_D = 0$ and $\tau_m/\tau_D = 0$ and $\beta U_0 \gg 1$.

height and length of the potential are different in the left and right parts. Therefore, we must substitute $U_0 \to U_{L,R}$ and $K \to K_{L,R} = 8U_{L,R}/L^2_{L,R}$.

From Eq. (5.12), we arrive at the formula

$$\tau^{L,R}_{MFP} = e^{\beta U_{L,R}} \left[\frac{1}{\beta U_{L,R}} \frac{3\pi}{8\sqrt{2}} \left(\frac{m}{\gamma} + \frac{2K_{L,R}\tau^2}{3\gamma} \right) + \frac{\sqrt{2}\pi\gamma}{K_{L,R}} \frac{1}{1 + \beta U_{L,R} K_{L,R}\tau/(4\gamma)} + 4\sqrt{2\frac{m}{K_{L,R}}} \right]. \tag{5.17}$$

Initially, we must take into consideration a symmetric potential as in Fig.5.3a), where the widths of the two wells are identical ($L_L = L_R$), and $\beta U_L = 3$ is fixed and only the right barrier height βU_R varies. Figure 5.7 shows the rescaled $\tau^{L,R}_{MFP}$ as a function of the rescaled memory time for two different values of τ_m/τ_D, respectively, $\tau_m/\tau_D = 0.001$ on the left and $\tau_m/\tau_D = 1$ on the right. In both plots, we are thus able to observe an agreement between Eq. (5.17) (lines) and the simulation data (symbols), so we are thus able to conclude that the formula is indeed applicable for various values of mass, memory time, and potential barrier height. On the grey lines, many markers are overlapping as they represent the data for τ^L_{MFP}/τ_D, obtained

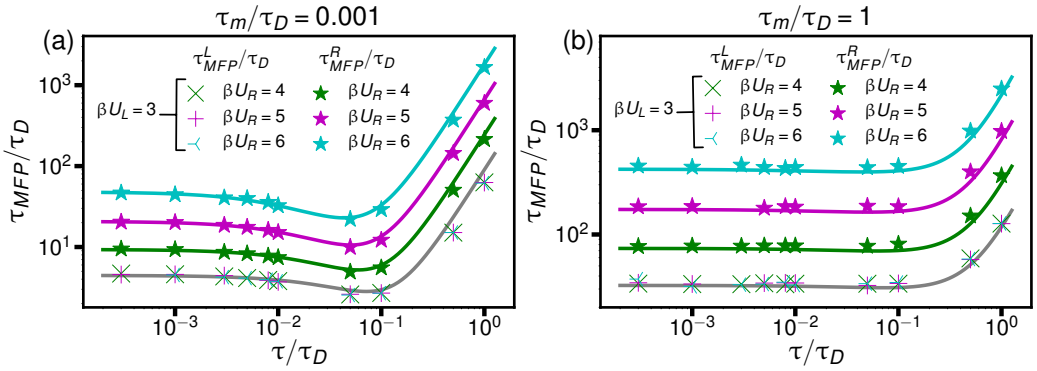

Figure 5.7: Well-to-top MFPT as a function of rescaled τ/τ_D for asymmetric double-well potential with equal distance between the two minima $L_L = L_R$. The potential has fixed-left height barrier $\beta U_L = 3$, and τ^R_{MFP}/τ_D is shown by the color lines for the three different potentials $\beta U_R = 4$ (green), $\beta U_R = 5$ (magenta) and $\beta U_R = 6$ (light blue). The lines show Eq. (5.17) in a) for $\tau_m/\tau_D = 0.001$ and in b) $\tau_m/\tau_D = 1$. The grey line depicts τ^L_{MFP}/τ_D with the simulation data overlapping for different barrier heights on the right-hand side.

by varying the barrier heights on the right well when the left well is fixed. Therefore, we can conclude that the dynamics in one well are independent of the other well. As we have already stated, the only coupling would come from recrossing events, which are rather be uncommon.

In the previous part, we studied the case with two different barrier heights on the left and on the right while maintaining an equal distance between the two minima $L_L = L_R$. In Fig.5.3a), we consider different lengths between the two minima and the top. In particular, we fix the barrier heights, changing only the distance between the top and the right-hand minimum L_R/L_L. In Fig.5.8 we plot $\tau^{L,R}_{MFP}/\tau_D$ for $\beta U_L = 3$ and $\beta U_R = 5$ as a function of the memory time when $\tau_m/\tau_D = 0.01$ and various values of L_R/L_L. For every value of L_R/L_L corresponding a color, we observe a good agreement between the stars (simulation data) and the lines (Eq. (5.17)). The grey line depicts τ^L_{MFP}/τ_D, and the yellow marks overlap because the particle motion in the left well is independent of the right well. The dependence of the lengths scale in the Eq. (5.17) is only in the function $K(L, U)$. In other words, if Eq. (5.17) does not explicitly depend on one of the two wells, it comes back to Eq. (5.12), except for the factor 1/2. We thus conclude that Eq. (5.17) accurately describes the simulation data for various values of inertial time, asymmetric barrier-height, and length scale.

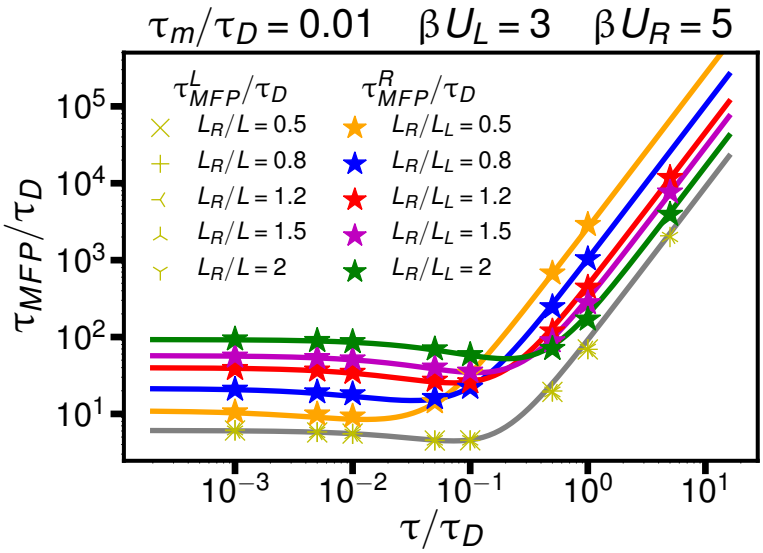

Figure 5.8: Well-to-top MFPT as a function of rescaled τ/τ_D for $\tau_m/\tau_D = 0.01$ for an asymmetric double-well potential, where the barrier heights are fixed (on the left $\beta U_L = 3$ and the right $\beta U_R = 5$) and various potential lengths on the right. The grey line depicts τ^L_{MFP}/τ_D with overlapping yellow marks that express the simulation data for different potential lengths on the right-hand side. The colored lines show τ^R_{MFP}/τ_D for the different potentials. The lines represent Eq. (5.17), while the stars and yellow marks are the simulation data.

5.6 Non-equilibrium system

We subsequently investigate the case when the system is not in equilibrium. For this, we consider a GLE where the fluctuation-dissipation theorem (FDT) is violated [96–98],

$$m\ddot{x}(t) = -\int_{t_0}^{t} \Gamma_V(t-t')\dot{x}(t')dt' - \nabla U(x(t)) + F_R(t), \tag{5.18}$$

$$\langle F_R(t)F_R(t')\rangle = \beta^{-1}\Gamma_R(t-t'), \tag{5.19}$$

as introduced in chapter 4. We consider both functions as exponentials with the explicit form

$$\begin{aligned} \Gamma_V(|t|) &= \frac{\gamma}{\tau_V} e^{-\frac{|t|}{\tau_V}}, \\ \Gamma_R(t) &= \frac{\gamma}{\tau_R} e^{-\frac{|t|}{\tau_R}}, \end{aligned} \tag{5.20}$$

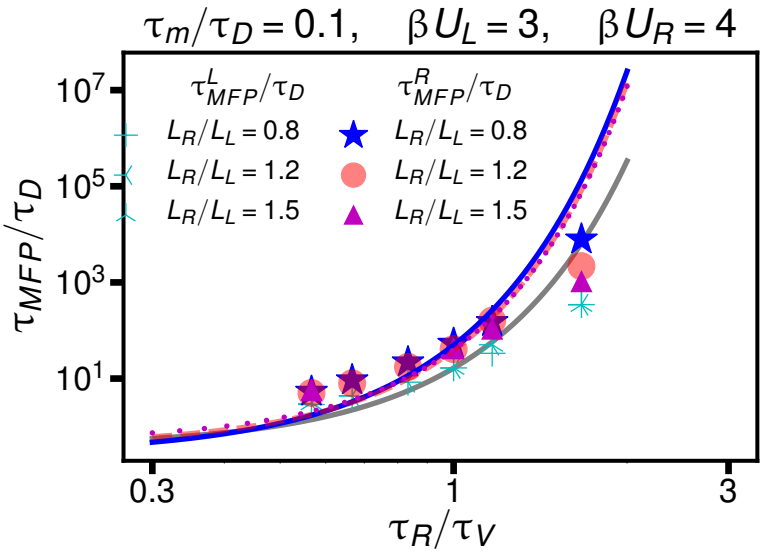

Figure 5.9: Non-equilibrium well-to-top MFPT as a function of the ratio τ_R/τ_V, for various potential lengths in the right well, the weight potential on the left is $\beta U_L = 3$, on the right $\beta U_R = 4$ and $\tau_m/\tau_D = 0.1$. The grey line depicts τ^L_{MFP}/τ_D, while the other colored lines show τ^R_{MFP}/τ_D for the various potential lengths. The lines exhibit the Eq. (5.21) and the markers the simulation data.

where the friction coefficients are the same but have different memory times. The system is in equilibrium when the two memory times are the same ($\tau_V = \tau_R$). For the non-equilibrium case, Eq. (5.17) can be adapted by including an effective temperature, as shown in the chapter 4, leading to

$$\begin{aligned}\tau^{L,R}_{MFP} = \\ e^{\beta_{NEQ}U_{L,R}} \Bigg[\frac{1}{\beta_{NEQ}U_{L,R}} \frac{3\pi}{8\sqrt{2}} \left(\frac{m}{\gamma} + \frac{2K_{L,R}\tau_V^2}{3\gamma} \right) \\ + \frac{\sqrt{2}\pi\gamma}{K_{L,R}} \frac{1}{1 + \beta_{NEQ}U_{L,R}K_{L,R}\tau_V/(4\gamma)} \\ + 4\sqrt{2\frac{m}{K_{L,R}}} \Bigg],\end{aligned} \tag{5.21}$$

where $\beta_{NEQ}/\beta = \tau_R^2/\tau_V^2$, as shown previously [108]. Figure 5.9 shows that the MFPT increases with τ_R/τ_V. We plot the rescaled MFPT as a function of the ratio of the two memory times, showing with the lines the formula (5.21) and with the markers the simulation data. The non-equilibrium effective temper-

ature β_{NEQ} in the exponential in Eq. (5.21) is the main contributing factor concerning the variation of the potential length scale. Therefore the three colored lines are mostly overlapping. In conclusion, Eq. (5.21) qualitatively describes the simulation data for a system out of equilibrium [108].

5.7 Conclusion

Having studied the mean first passage times from a well to the barrier top, we reach the following conclusion: for an asymmetric double-well potential, the time necessary for a particle to travel from one of the two minima to the top barrier in a non-Markovian system is independent of the dynamics in the other well. For this reason, we must study the problem separately and find an equation that allows time to reach the top from the left or right-hand side. From the literature, [18, 108], we understand how to modify Eq. (5.12) to arrive at the Eq. (5.17). Using the simulation data, we show that Eq. (5.17) accurately describes the τ^L_{MFP} and τ^R_{MFP} for various values of barrier-height, potential length, and inertial time. In the last part, we investigate the case of a system far from a state of equilibrium, observing the qualitative agreement between the data and the Eq. (5.21).

Chapter 6

Barrier-crossing transition path times for non-Markovian systems

6.1 Introduction

Many biological transitions, particularly protein-folding, can be modeled as diffusion of a reaction coordinate in a one-dimensional, free-energy landscape. In the last decade, various experiments have been conducted to measure the transition path times in nucleic acids and protein folding [54, 110–118]. The measurement of the transition path time was found to be a challenge, as it represents only a small fraction of the stochastic trajectories, as illustrated in Fig.6.1. The barrier potential for proteins is typically higher than the characteristic thermal energy k_BT; for this reason, the particle spends most of its time close to the two minima of the double well potential. These new measurements brought about a push to investigate this process, taking a theoretical and computational approach [119,120]. Many of these studies considered Markovian models, but computational simulation and experimental studies suggested that the protein-folding dynamics is subdiffusive [46, 85, 121, 122]. This implies that memory effects must be included in the theory, and in recent years, new studies centering around non-Markovian models have been developed [84, 95, 122–124]. The importance of non-Markovianity, i.e., memory effects, is also shown in Fig.6.1; in fact, in Fig.6.1 a) and b) we plot the trajectories for two different memory times, observing a different value for the first passage time, as these are more than ten times longer than the corresponding transition path times in c) and d). We also notice the opposite effect of memory time on the first passage time and the transition path time. Longer memory time induces a shorter transition path time, as shown in c) and d), but a longer first passage time, as observed in a) and b).

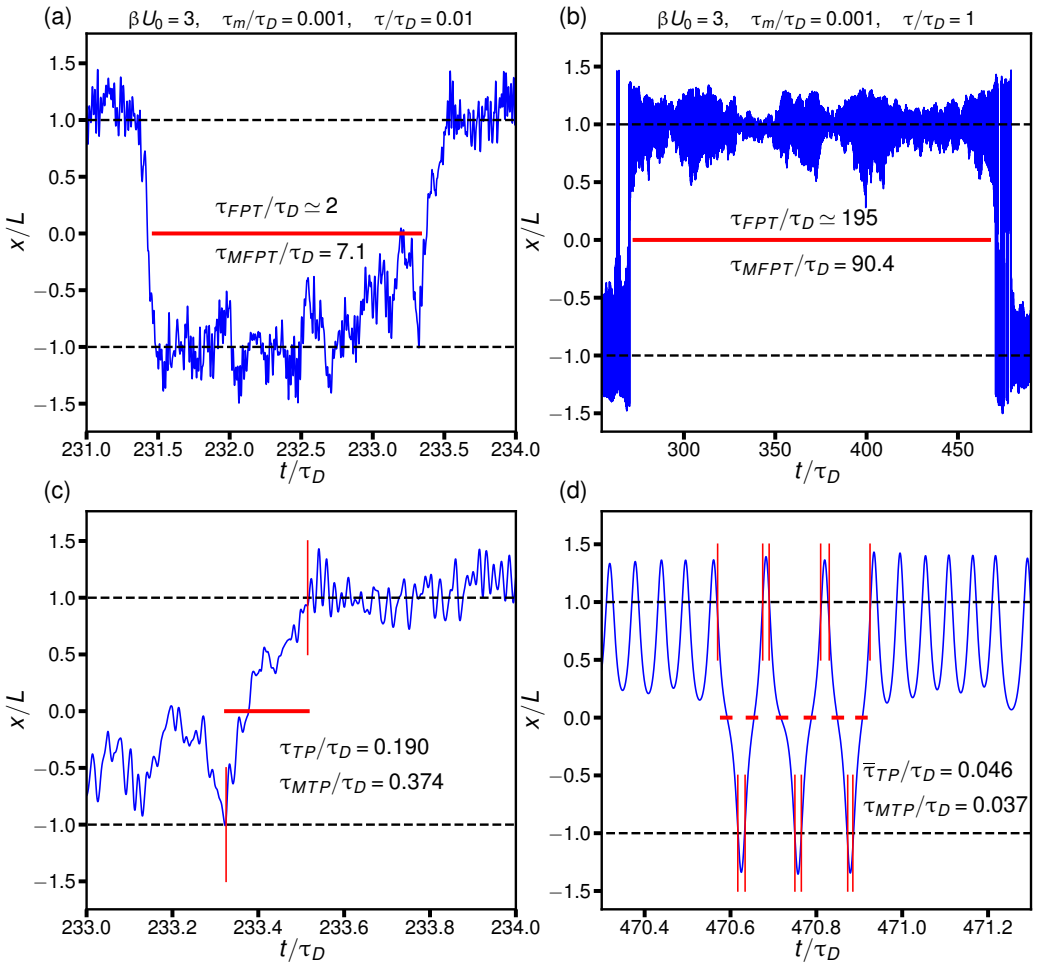

Figure 6.1: Trajectory for a non-Markovian system, where the potential height $\beta U_0 = 3$, $\tau_m/\tau_D = 0.001$ and respectively in a) and c) $\tau/\tau_D = 0.001$ and in b) and d) $\tau/\tau_D = 1$. The dashed black lines show the two potential minima. In a) and b), the horizontal red lines show the first passage time, and in c) and d), the transition path time. In a) $\tau_{FPT}/\tau_D \simeq 2$ and $\tau_{MFPT}/\tau_D = 7.1$, in b) $\tau_{FPT}/\tau_D \simeq 195$ and $\tau_{MFPT}/\tau_D = 90.4$, the values of the mean first passage time (MFPT) come from the formula in (5.12). The vertical red lines highlight the last and the first time the particle crossed a minimum before and after passing the barrier. In c) $\tau_{TP}/\tau_D = 0.190$ and in d) $\overline{\tau}_{TP}/\tau_D = 0.046$ is the average on the six transition path times in the figure. Using the Eq. (6.27) respectively, we obtain $\tau_{MTP}/\tau_D = 0.374$ in c) and $\tau_{MTP}/\tau_D = 0.037$ in d). The averages are of the same order of magnitude as the values found in this case.

6.2 Setup

In order to investigate the transition path time in 1D while considering memory effects, we will derive a heuristic formula that we will compare with simulation data. With τ_{MTP} we denote the average of the transition path time [125–129], in other words, the time necessary to go from one minimum to the other without recrossing the initial minima, as depicted in Fig.6.1 c) and d).

We begin by writing out the generalized Langevin equation (GLE)

$$m\ddot{x}(t) = -\int_{t_0}^{t} \Gamma(t-t')\dot{x}(t')dt' - \nabla U(x(t)) + F_R(t), \tag{6.1}$$

where m is the particle mass, $\Gamma(t)$ the memory kernel, t_0 a value of initial time and $\nabla U(x(t))$ is the derivative of a double-well potential

$$U(x) = U_0 \left[\left(\frac{x}{L} \right)^2 - 1 \right]^2. \tag{6.2}$$

$F_R(t)$ denotes the random force characterized by its first two moments

$$\begin{aligned} \langle F_R(t) \rangle &= 0 \\ \langle F_R(t) F_R(t') \rangle &= \beta^{-1} \Gamma(t-t'), \end{aligned} \tag{6.3}$$

where $\beta = 1/k_B T$. As a memory kernel, we choose a single exponential

$$\Gamma(t) = \frac{\gamma}{\tau} e^{-\frac{|t|}{\tau}}, \tag{6.4}$$

where τ is the memory time, and γ is the friction coefficient. We define diffusion and inertial time, respectively, as

$$\begin{aligned} \tau_D &= \beta L^2 \gamma, \\ \tau_m &= \frac{m}{\gamma}. \end{aligned} \tag{6.5}$$

The diffusion time τ_D is the time it would take the particle to diffuse by L in the overdamped limit and in absence of a potential. The inertial time τ_m characterizes the time scale of the viscous dissipation of particle momentum.

Previously, it was discovered that, for a Markovian system with finite mass in the large barrier limit, the mean transition path time is [126]

$$\tau_{MTP} = \frac{1}{\lambda_+(\gamma, m)} \left(log(\beta U_0) + A(\gamma, m) \right), \tag{6.6}$$

where

$$\lambda_+(\gamma, m) = \frac{-\gamma + \sqrt{\Delta}}{2m}, \tag{6.7}$$

$$A(\gamma, m) = \log\left(\frac{4\sqrt{\Delta}}{\gamma + \sqrt{\Delta}} e^C\right), \tag{6.8}$$

with $\Delta = \gamma^2 + 8m\beta U_0$ and $C = 0.577$ is the Euler-Mascheroni constant. The result was obtained by calculating the transition path distribution, thus approximating a parabolic barrier.

6.2.1 Transition path time in overdamped case

In the overdamped case $\Delta = \gamma^2 + 8m\beta U_0 \simeq \gamma^2$, if we insert this value into Eq. (6.8), we obtain

$$A = \log\left(\frac{4\sqrt{\Delta}}{\gamma + \sqrt{\Delta}} e^C\right) = \log\left(\frac{4\gamma}{2\gamma} e^C\right) = \log\left(2e^C\right), \tag{6.9}$$

and λ_+ becomes

$$\begin{aligned} \lambda_+ &= \frac{-\gamma + \sqrt{\gamma^2(1 + 8m\beta U_0/\gamma^2)}}{2m} \\ &= \frac{\gamma(-1 + 1 + 4m\beta U_0/\gamma^2)}{2m} = 2\beta U_0/\gamma. \end{aligned} \tag{6.10}$$

Inserting these two values in the Eq. (6.6), we arrive at

$$\tau^{\gamma}_{MTP} = \frac{\gamma}{2\beta U_0} \log(2e^C \beta U_0). \tag{6.11}$$

6.2.2 Transition path time in inertial case

The other limit (inertial case), for $\gamma \to 0$, is described by [127]

$$\tau^{m}_{MTP} = \int_{U_0}^{\infty} dE \frac{\beta e^{-\beta E}}{e^{-\beta U_0}} \int_{-L}^{L} dx \sqrt{\frac{m/2}{E - U(x)}}. \tag{6.12}$$

The expression in (6.12), is equivalent to the integral,

$$\tau_{MTP} = \int_0^{\infty} dt \; p_{TP}(t) \; \tau_{TP}, \tag{6.13}$$

where the transition path time can be described as a function of the total energy given by

$$\tau_{TP}(E) = \int_{-L}^{L} \frac{dx\sqrt{m/2}}{\sqrt{E - U(x)}}. \tag{6.14}$$

At equilibrium, the distribution of transit time is given by

$$p_{TP}(t) = \frac{\int_{U_0}^{\infty} dE\ e^{-\beta E}\delta\left(t - \tau_{TP}(E)\right)}{\int_{U_0}^{\infty} dE\ e^{-\beta E}}. \tag{6.15}$$

For a parabolic barrier, the distribution can be rewritten as

$$\begin{aligned} p_{TP}(t) =& \sqrt{\frac{2\beta U_0}{m}}\beta U_0 \frac{\cosh\left(\sqrt{\frac{2\beta U_0}{m}}t/2\right)}{\sinh^3\left(\sqrt{\frac{2\beta U_0}{m}}t/2\right)} \times \\ & \exp\left[-\frac{\beta U_0}{\sinh^2\left(\sqrt{\frac{2\beta U_0}{m}}t/2\right)}\right], \end{aligned} \tag{6.16}$$

in the limit of high barrier $\beta U_0 \gg 1$, it becomes

$$\begin{aligned} p_{TP}(t) \approx& 4\sqrt{\frac{2\beta U_0}{m}}\beta U_0 \times \\ & \exp\left[-\sqrt{\frac{2\beta U_0}{m}}t - 4\beta U_0 e^{-\sqrt{\frac{2\beta U_0}{m}}t}\right]. \end{aligned} \tag{6.17}$$

The maximum of the distribution is achieved for $t = \sqrt{\frac{m}{2\beta U_0}}\ln(4\beta U_0)$ and the corresponding mean transition path time is Eq. (6.18).

In conclusion, if we approximate the double-well potential of a parabolic barrier with potential $U(x) = -U_0(x/L)^2$, and within the limits of the high barrier $\beta U_0 \gg 1$, we reach the asymptotic expression [119, 126],

$$\tau^m_{MTP} \simeq \sqrt{\frac{m}{2\beta U_0}}\log(4e^C\beta U_0). \tag{6.18}$$

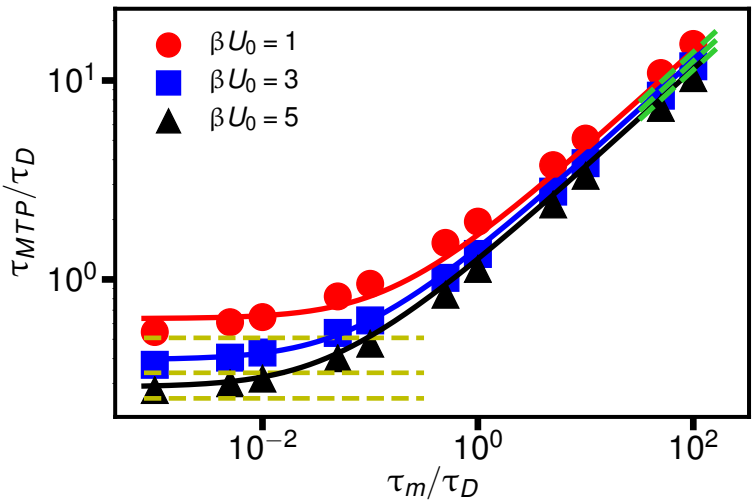

Figure 6.2: Transition path time as a function of the inertial time for various values of the potential height in a Markovian system ($\tau = 0$). Different markers denote the simulation data, and the lines show Eq. (6.6). The dashed yellow horizontal lines and the green lines show the overdamped case (Eq. (6.11)) and the limit for $\gamma \to 0$ respectively Eq. (6.18).

6.2.3 Transition path time for Markovian case

In Fig.6.2, we present the transition path time as a function of inertial time for various values of the potential height U_0 and in the absence of memory effects, i.e., for $\tau = 0$. The colored lines show that Eq. (6.6) aligns perfectly with the simulation data plotted with different markers. Eq. (6.6) was derived in the large barrier limit, although we observe that it can also be used to describe the case when $\beta U_0 = 1$. The dashed yellow horizontal lines denote the overdamped limit ($m \to 0$) Eq. (6.11) [125, 126, 130]. The expression (6.18), inertial case, is shown as the dashed green lines. In Fig.6.2, we reproduce the τ_{MTP} and its asymptotic behaviors.

6.3 Transition path time for non-Markovian system

To consider the effect of memory on τ_{MTP}, we must first present analytical results for the positional autocorrelation function $C(t) = \langle x(t)x(0)\rangle$ [18, 108], as previously shown in chapter 4. Therefore, we must employ a harmonic approximation of Eq. (6.1) and use $U_{\text{har}}(x) = Kx^2/2$, where K is the second derivative of the double-well potential at the minima, $K = U''(L) = 8U_0/L^2$.

Fourier transforming Eq. (6.1) for $t_0 \to -\infty$ and solving for $\tilde{x}(\omega)$, we obtain

$$\tilde{x}(\omega) = \frac{\tilde{F}_R(\omega)}{K - m\omega^2 + i\omega\tilde{\Gamma}^+(\omega)} \equiv \tilde{\chi}(\omega)\tilde{F}_R(\omega), \tag{6.19}$$

which defines the response function $\tilde{\chi}(\omega)$. The half-sided Fourier transform $\tilde{\Gamma}^+(\omega)$ of $\Gamma(t)$ is given by

$$\tilde{\Gamma}^+ = \int_0^\infty dt e^{-i\omega t}\Gamma(t) = \frac{\gamma}{1 + i\omega\tau}, \tag{6.20}$$

while the Fourier transform of the symmetric random force correlation $\Gamma(t)$ is

$$\tilde{\Gamma}(\omega) = \tilde{\Gamma}^+(\omega) + \tilde{\Gamma}^+(-\omega) = \frac{2\gamma}{1 + \omega^2\tau^2}. \tag{6.21}$$

The Fourier transform of $C(t)$ is given by $\tilde{C}(\omega) = \beta^{-1}\tilde{\Gamma}(\omega)\tilde{\chi}(\omega)\tilde{\chi}(-\omega)$ and reads (as in the chapter 4)

$$\tilde{C}(\omega) = \frac{2\gamma\beta^{-1}(1 + \omega^2\tau^2)^{-1}}{\left(K - \omega^2\left[m - \frac{\tau\gamma}{1+\tau^2\omega^2}\right]\right)^2 + \frac{\omega^2\gamma^2}{(1+\omega^2\tau^2)^2}}. \tag{6.22}$$

This can be rewritten in a form that corresponds to the standard result for the memory-less harmonic oscillator (i.e., $\tau = 0$)

$$\tilde{C}(\omega) = \frac{2\gamma_{\text{eff}}\beta^{-1}}{(K - m_{\text{eff}}\omega^2)^2 + \omega^2\gamma_{\text{eff}}^2}, \tag{6.23}$$

where we have introduced effective frequency-dependent friction, mass, and temperature

$$\gamma_{\text{eff}} = \frac{\gamma}{1 + \tau^2\omega^2}, \tag{6.24a}$$

$$m_{\text{eff}} = m - c_1\tau\gamma_{\text{eff}}. \tag{6.24b}$$

We have, therefore introduced a numerical constant that, in the harmonic case, assumes the value $c_1 = 1$, which will be used as a fit parameter for non-harmonic corrections. Note that the potential curvature K is not renormalized. In the low and high friction limits, we find the following poles $\omega_L^2 = K/m_{\text{eff}}$ for $Km_{\text{eff}} > \gamma_{\text{eff}}^2$ and $\omega_H^2 = -K^2/\gamma_{\text{eff}}^2$ for $Km_{\text{eff}} < \gamma_{\text{eff}}^2$ (see chapter 4). From these characteristic frequencies, we obtain from Eq. (6.24a) the effective friction in the low friction limit (see chapter 4)

$$\gamma_{\text{eff}}^L = \frac{\gamma}{1 + c_2\tau^2 K/m}, \tag{6.25}$$

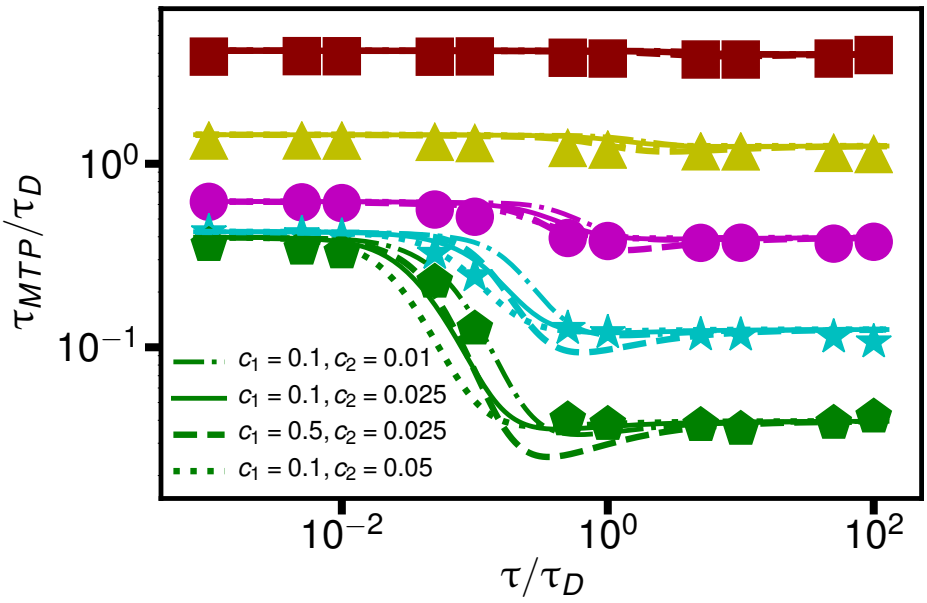

Figure 6.3: Transition path time as a function of memory time for various values of inertial memory time ($\tau_m/\tau_D = 0.001$ green, $\tau_m/\tau_D = 0.01$ blue, $\tau_m/\tau_D = 0.1$ magenta, $\tau_m/\tau_D = 1$ yellow and $\tau_m/\tau_D = 10$ red) and fixed height potential $\beta U_0 = 3$. Different markers plot the simulation data. The lines show Eq. (6.27) for different values of the constants c_1 and c_2, as explained in the legend.

where we introduced another numerical constant, c_2. As for the high friction limit, we have already demonstrated in [108] that

$$\gamma^H_{\text{eff}} \simeq \gamma. \tag{6.26}$$

Returning to the problem of the transition path time τ_{MTP}, we must apply the effective parameters at the low friction limit to consider the memory time's effect on the dynamics. For this reason, we will insert the effective parameters (6.25) and (6.26) into Eq. (6.6) thus arriving at the expression

$$\tau_{MTP} = \frac{1}{\lambda_+(\gamma^L_{\text{eff}}, m^L_{\text{eff}})} \left(log(\beta U_0) + A(\gamma^L_{\text{eff}}, m^L_{\text{eff}}) \right). \tag{6.27}$$

In Fig.6.3, we plot the transition path time as a function of the rescaled memory time for various values of inertial time and fixed potential weight $\beta U_0 = 3$. We show results for different values of the two constants c_1 and c_2 and observe that the values $c_1 = 0.1$ $c_2 = 0.025$ give a better agreement with the simulation data. The dash-dotted line with the values $c_1 = 0.1$, $c_2 = 0.01$

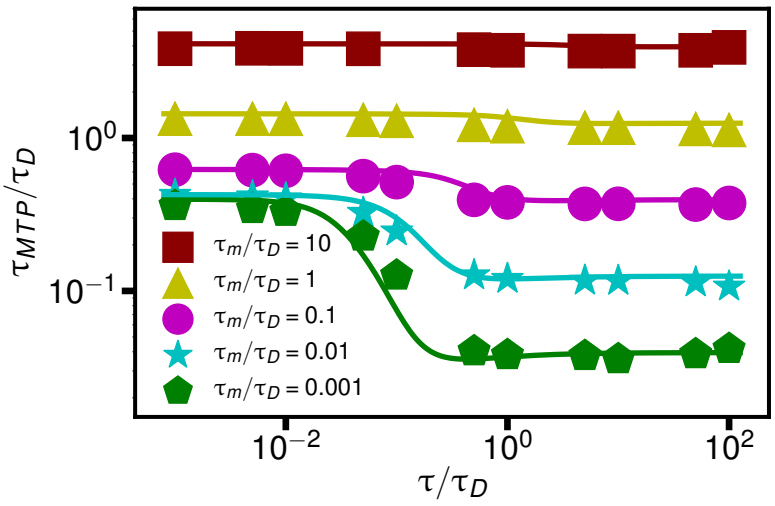

Figure 6.4: Transition path time as a function of memory time for various values of inertial memory time (τ_m/τ_D) and fixed potential height $\beta U_0 = 3$ [131]. Different markers plot the simulation data, and the lines demonstrate Eq. (6.27) with $c_1 = 0.1$ and $c_2 = 0.025$.

better describes the simulation data for the lower mass but is inaccurate for the higher mass data ($\tau_m/\tau_D = 0.01$ and $\tau_m/\tau_D = 0.1$).

In Fig.6.4, we have the same plot as in Fig.6.3, where the Eq. (6.27), depicted as colored lines, aligns well with the simulation data. In Ref. [95], the authors derived the same quantity (τ_{MTP}) as in Eq. (6.27), but in the overdamped case and with a power-law memory kernel, using the same procedure as in [126]. They discovered that the transition path time in the non-Markovian case is always less than in the Markovian case, and it decreases as the memory time value increases. For intermediate memory times, we can reach the same conclusion as is observed in Fig.6.4, particularly for small values of mass, the closer scenario to the overdamped case. We are thus able to explain the decrease in the transition path time, observing that the effective friction coefficient Eq. (6.25) decreases with the increase of the memory time. The reason for this decrease is the insertion of this new effective friction into Eq. (6.11). This behavior is also observed in the mean first passage time for intermediate memory time, but for higher values of memory time, it increases due to $\tau_{MFP} \sim \tau^2/\tau_D$ see Eq. (5.12). In the mean transition path time, no term is found to increase with the memory time.

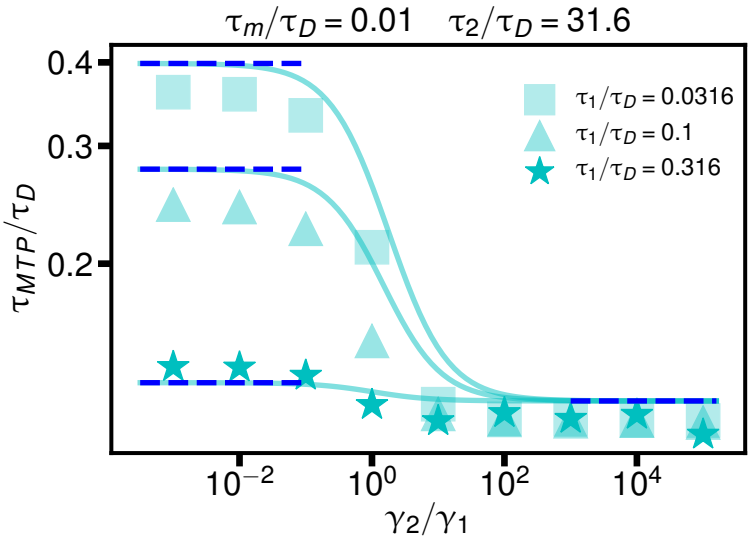

Figure 6.5: Transition path time as a function of the ratio between the two friction coefficients. For a fixed value of $\tau_m/\tau_D = 0.01$, $\tau_2/\tau_D = 31.6$ and height potential $\beta U_0 = 3$ for various values of τ_1/τ_D. Different markers are therefore used to plot the simulation data, and the lines demonstrate Eq. (6.29). The blue dashed lines denote the singular exponential formula (6.27) respectively on the left and the right for τ_1/τ_D and τ_2/τ_D.

6.4 Transition path time for bi-exponential memory kernel

In the following section, we will study the case of a double exponential memory kernel; instead of Eq. (6.4) in the GLE, we will consider the following kernel,

$$\Gamma(t) = \frac{\gamma_1}{\tau_1} e^{-\frac{|t|}{\tau_1}} + \frac{\gamma_2}{\tau_2} e^{-\frac{|t|}{\tau_2}}, \tag{6.28}$$

and we thus define $\gamma = \int_0^\infty \Gamma(t)dt = \gamma_1 + \gamma_2$ as the total friction coefficient. To obtain a transition path time formula for a double exponential GLE, we sum the single-exponential formula Eq. (6.27) with their weights

$$\begin{aligned} \tau_{MTP} = &\frac{\gamma_1}{\gamma} \frac{1}{\lambda_+(\gamma^1_{\text{eff}}, m^1_{\text{eff}})} \left(log(\beta U_0) + A(\gamma^1_{\text{eff}}, m^1_{\text{eff}})\right) + \\ &\frac{\gamma_2}{\gamma} \frac{1}{\lambda_+(\gamma^2_{\text{eff}}, m^2_{\text{eff}})} \left(log(\beta U_0) + A(\gamma^2_{\text{eff}}, m^2_{\text{eff}})\right), \end{aligned} \tag{6.29}$$

where the superscript defines which effective friction coefficient is to be considered. If we draw a parallel with the formula for the MFPT [19, 88], the MFPT has an overdamped term and an energy-diffusion term. The overdamped term is additive for the multi-exponential memory kernel, but the energy-diffusion term is inversely addictive. For the mean transition path time, the energy-diffusion contribution gives a constant contribution, and the overdamped term induces the speed-up behavior; for this reason, we can assume the additivity for the multi-exponential memory kernel.

In Fig.6.5 we compare Eq. (6.29) with the data for a fixed inertial time $\tau_m/\tau_D = 0.01$ and $\tau_2/\tau_D = 31.6$ for various values of τ_1/τ_D and potential $\beta U_0 = 3$. We selected a small inertial time because, for higher values, the transition path time is almost constant for every value of memory time. The agreement between the data and the formula in Fig.6.5 is clear, in particular for $\tau_1/\tau_D = 0.0316$ and $\tau_1/\tau_D = 0.316$, where in both of the cases we are on the plateau (Fig.6.4). For the intermediate value of τ_1/τ_D, there is a discrepancy between the data and the formula, though this value is in the inflection area in Fig.6.4. Additionally, in the inflection zone, we observe slight deviations from Eq. (6.27), and in Fig.6.5, the y-scale is smaller.

6.5 Conclusion

In conclusion, starting from a GLE, we derive a heuristic formula for the transition path time, using a previous derivation Eq. (6.6) and inserting the effective mass and friction coefficient derived in [108]. The heuristic formula (6.27) corresponds perfectly with the simulation data, therefore demonstrating that the Markovian case represents the maximum of the transition path time. The transition path time exhibits a constant behavior for both small and large memory times, with a decrease for the intermediate values more evident for smaller values of inertial time. In the final section, we study the case of a double exponential memory kernel, observing that Eq. (6.29) accurately describes the simulation data.

Chapter 7

Summary and Outlook

During the course of this thesis, several open questions have been put forth, particularly concerning the effects of memory time on barrier crossing in various biological soft-matter system dynamics. In particular, we have investigated different aspects of the barrier crossing in non-Markovian model systems, considering single and multi-exponential memory, in and far from equilibrium. Besides using a system in a double-well potential, we have taken into account a more generic potential compared to the symmetric double-well, which mimics barrier crossing in biological systems more realistically. In the last chapter, we studied another important system characteristic: the transition path time and the ways in which it is modified by the memory time.

In chapter 3 we set out to investigate the mean first passage time for non-Markovian dynamics, where the memory kernel is a sum of single-exponential functions, which exhibit different memory times and friction coefficients. In particular, we considered the cases featuring double and triple exponential memory kernel. We were thus able to derive a formula to predict the MFPT over many orders of magnitude for the mass, friction coefficient, and memory time. We compared the analytical prediction with results from Langevin simulations. We discovered that the multi-exponential memory kernel could be reduced to an effective single memory kernel, simplifying the description of the system. Each exponential is described by the scaling variable γ_i/τ_i^2; the exponential with short memory time or higher amplitude is most relevant with regards to the other. Using the formula for the MFPT, we established a scaling diagram in which we recognize a Markovian inertial regime, a memory slowdown regine, and two intermediate memory regimes, which include regimes of slow-down and speed-up. In the intermediate memory speed-up regime, the memory times reduce the barrier crossing time, compared to the

Markovian case. This formula is a useful tool for understanding the relevance of memory effects in many systems or estimating memory times from MFPT measured in experiments or MD simulations. Future investigations of the barrier-crossing process may involve, for example, a more complex memory kernel expressed as a sum of exponential memories and instantaneous frictional forces [46, 85, 132].

In chapter 4 we considered a system far from a state of equilibrium, thus violating the fluctuation-dissipation theorem. The inequality between the single exponential function that defines the memory kernel and the single exponential function in the random force autocorrelation is obtained by considering two different relaxation times. When the two times are equal, equilibrium is reached. We find three effective parameters: mass, friction, and temperature by conducting an asymptotic analysis of the propagator for the generalized Langevin equation. Extending the standard result for the memory-less harmonic oscillator in equilibrium, we can obtain the effective mass and friction for the non-Markovian case; the effective temperature becomes relevant when the system is far from a state of equilibrium. The effective mass and friction corroborate the formula for the mean first passage time similarly to the formula that we considered in the chapter 3. The effective temperature is proportional to the square of the memory and random relaxation times ratio. By rescaling the joint position-velocity distribution with the effective temperature, the distributions of our nonlinear barrier-crossing system achieve an agreement, meaning that the effective temperature accurately describes the system when it is far from a state of equilibrium. Starting from the Kramers limits for the MFPT (and inserting the effective parameters), we obtain a formula that describes qualitatively the simulation data for a barrier-crossing system far from a state of equilibrium. In particular, we notice that the MFPT increases dramatically when the ratio between the random and the memory time is greater than 1. This is primarily because the effective temperature modifies the Arrhenius factor. In the equilibrium case, where the memory time only modifies the constant in front of the Arrhenius exponential, the state of non-equilibrium brings about a number of changes. In this thesis, we took the first step in understanding non-equilibrium systems; further study could also take into consideration a memory function given by the sum of a single exponential decay and instantaneous frictional forces.

Another step in generalizing our model of barrier crossing we made in chapter 5, where we considered barrier crossing with a single exponential memory kernel. In contrast to previous studies [18, 78, 88, 102], where a

symmetric double-well potential was taken into consideration as in chapter 3, we considered an asymmetric double-well potential. In that chapter, we presented another version of the heuristic formula, similar to chapter 3 and chapter 4, but with a variation in the speed-up term, more accurately describing barrier crossing in asymmetric potentials. Considering varying potential widths and barrier heights in the left and right well, we analyzed the mean time taken to reach the peak, starting from one of the two wells, not the time taken to reach one well from the other. In overdamped Markovian systems, the time taken to reach the barrier is half that of the time taken to arrive at the other well. In this formula, we inserted one half in front of the over-damped Markovian term, thus obtaining a formula that describes the simulation data for a wide range of asymmetrical potentials, both in equilibrium and non-equilibrium. Simulating the particle's dynamic, we understand that the dynamics in the two wells are independent of one another because the recrossing is the only coupled contribution. However, it occurs only rarely, and its contribution is not significant. Therefore, we can construct a heuristic formula with the characteristics of only one well. In this chapter, we contributed to creating a formula that better determines the MFPT for the given system. In fact, in multiple experiments (or in MD simulation), the free-energy profile obtained for chemical reactions or protein folding [48–55] can be approximated by a double-well potential, but not to a symmetric one. A future step could be to consider a more complicated potential that more accurately describes these processes or even include multiple minima.

In chapter 6, we investigate another important property of soft matter systems: the mean transition path time. The transition path time is only a fraction of the first passage time, as it represents the required time for a particle to reach a certain point without recrossing the starting point. We generalized a formula for the transition path time for a particle crossing a parabolic barrier in the Markovian case, which was derived in previous work [126], for the non-Markovian case. For this we substitute the mass and the friction coefficient by the effective parameters derived in chapter 4 to include the effects of the memory time. The new formula accurately describes the data that we have obtained, simulating the generalized Langevin equation for a single exponential memory function in a double-well potential. We were subsequently able to observe that the maximum value of MTPT is reached for the Markovian case, as was also found in a previous work [95], but for an overdamped system with a power-law memory kernel. The MTPT decreases for intermediate values of memory time, particularly for low values of the inertial time, and is constant for both high and low values of the mem-

ory time. Furthermore, we discovered that we obtain a good description of simulation data by taking the sum of the contributions of each memory time (we made a simulation for bi-exponential memory). Also, in this section, as in chapter 3 and chapter 4, the obvious next step would be the generalization of the memory function.

In conclusion, in this thesis, we were able to tackle barrier crossing in different important applications, which will be relevant for experiments and future work on realistic biological systems.

Bibliography

[1] Robert Brown. Xxvii. a brief account of microscopical observations made in the months of june, july and august 1827, on the particles contained in the pollen of plants; and on the general existence of active molecules in organic and inorganic bodies. *The Philosophical Magazine*, 4(21):161–173, 1828.

[2] Eugene F. Fama. Random walks in stock market prices. *Financial Analysts Journal*, 21(5):55–59, 1965.

[3] M. E. Nor S. N. A. M. Razali R. M. Salleh A. Khamis, M. A. A. Sukor. Modeling and Forecasting Volatility of Financial Data using Geometric Brownian Motion. 4, 2017.

[4] Daniel Hodyss, Justin G. McLay, Jon Moskaitis, and Efren A. Serra. Inducing tropical cyclones to undergo brownian motion: A comparison between itô and stratonovich in a numerical weather prediction model. *Monthly Weather Review*, 142(5):1982 – 1996, 2014.

[5] A. Einstein. Über die von der molekularkinetischen theorie der wärme geforderte bewegung von in ruhenden flüssigkeiten suspendierten teilchen. *Annalen der Physik*, 322(8):549–560, 1905.

[6] M. von Smoluchowski. Zur kinetischen theorie der brownschen molekularbewegung und der suspensionen. *Annalen der Physik*, 326(14):756–780, 1906.

[7] P. Langevin. Sur la théorie de mouvement brownien. *C.R. Acad. Sci. Paris*, 146:530–533, 1908.

[8] Hazime Mori. Transport, Collective Motion, and Brownian Motion*). *Progress of Theoretical Physics*, 33(3):423–455, 03 1965.

[9] Robert Zwanzig. Memory effects in irreversible thermodynamics. *Phys. Rev.*, 124:983–992, Nov 1961.

[10] Robert Zwanzig. Nonlinear generalized langevin equations. *Journal of Statistical Physics*, 9(3):215–220, 1973.

[11] Oliver F. Lange and Helmut Grubmüller. Collective Langevin dynamics of conformational motions in proteins. *The Journal of Chemical Physics*, 124(21):214903, 06 2006.

[12] H. K. Shin, C. Kim, P. Talkner, and E. K. Lee. Brownian motion from molecular dynamics. *Chemical Physics*, 375(2-3):316–326, October 2010.

[13] Steven S. Plotkin and Peter G. Wolynes. Non-markovian configurational diffusion and reaction coordinates for protein folding. *Physical Review Letters*, 80(22):5015–5018, jun 1998.

[14] Cihan Ayaz, Laura Scalfi, Benjamin A. Dalton, and Roland R. Netz. Generalized langevin equation with a nonlinear potential of mean force and nonlinear memory friction from a hybrid projection scheme. *Phys. Rev. E*, 105:054138, May 2022.

[15] Tapan K. Chaudhuri and Subhankar Paul. Protein-misfolding diseases and chaperone-based therapeutic approaches. *The FEBS Journal*, 273(7):1331–1349, 2006.

[16] Christopher M. Dobson. Protein folding and misfolding. *Nature*, 426(6968):884–890, 2003.

[17] Huafeng Xu. Non-equilibrium protein folding and activation by atp-driven chaperones. *Biomolecules*, 12(6), 2022.

[18] Julian Kappler, Jan O. Daldrop, Florian N. Brünig, Moritz D. Boehle, and Roland R. Netz. Memory-induced acceleration and slowdown of barrier crossing. *The Journal of Chemical Physics*, 148(1):014903, 01 2018.

[19] Julian Kappler, Victor B. Hinrichsen, and Roland R. Netz. Non-markovian barrier crossing with two-time-scale memory is dominated by the faster memory component. *The European Physical Journal E*, 42(9):119, 2019.

[20] Robert Brown and John J. (John Joseph) Bennett. *The miscellaneous botanical works of Robert Brown*, volume 1. London, Published for the Ray society by R. Hardwicke, 1866-68, 1866. https://www.biodiversitylibrary.org/bibliography/21295.

[21] Ludwig Boltzmann. Ueber die natur der gasmoleküle. *Annalen der Physik*, 236(1):175–176, 1877.

[22] Hermann Grabert. *Projection Operator Techniques in Nonequilibrium Statistical Mechanics*. Springer Berlin, Heidelberg, 2013.

[23] Robert Zwanzig. *Nonequilibrium statistical mechanics*. Oxford university press, 2001.

[24] Alexandre J. Chorin, Ole H. Hald, and Raz Kupferman. Optimal prediction and the mori–zwanzig representation of irreversible processes. *Proceedings of the National Academy of Sciences*, 97(7):2968–2973, 2000.

[25] H.A. Kramers. Brownian motion in a field of force and the diffusion model of chemical reactions. *Physica*, 7(4):284–304, 1940.

[26] Richard F. Grote and James T. Hynes. The stable states picture of chemical reactions. II. Rate constants for condensed and gas phase reaction models. *The Journal of Chemical Physics*, 73(6):2715–2732, 07 1980.

[27] VI Mel'nikov and SV Meshkov. Theory of activated rate processes: Exact solution of the kramers problem. *The Journal of chemical physics*, 85(2):1018–1027, 1986.

[28] Philip McCord Morse; Herman Feshbach. *Methods of Theoretical Physics Vol.1*. McGrawHill, New York, 1953.

[29] Jing-Dong Bao, Rong-Wu Li, and Wei Wu. Numerical simulations of generalized langevin equations with deeply asymptotic parameters. *Journal of Computational Physics*, 197(1):241–252, 2004.

[30] A Tocino and Ramón Ardanuy. Runge–kutta methods for numerical solution of stochastic differential equations. *Journal of Computational and Applied Mathematics*, 138(2):219–241, 2002.

[31] David de Sancho, Anshul Sirur, and Robert B. Best. Molecular origins of internal friction effects on protein-folding rates (article). *Nature Communications*, 5(1):4307, 2014.

[32] Robert O Rosenberg, Bruce J Berne, and David Chandler. Isomerization dynamics in liquids by molecular dynamics. *Chemical Physics Letters*, 75(1):162–168, 1980.

[33] José M. Sancho, Aldo H. Romero, and Katja Lindenberg. The Kramers problem in the energy-diffusion limited regime. *The Journal of Chemical Physics*, 109(22):9888–9900, 12 1998.

[34] Daniel M Zuckerman and Thomas B Woolf. Transition events in butane simulations: Similarities across models. *The Journal of Chemical Physics*, 116(6):2586–2591, 2002.

[35] Zhen Li, Xin Bian, Xiantao Li, and George Em Karniadakis. Incorporation of memory effects in coarse-grained modeling via the Mori-Zwanzig formalism. *The Journal of Chemical Physics*, 143(24):243128, 11 2015.

[36] R. Rey and E. Guardia. Dynamical aspects of the sodium(1+)-chloride ion pair association in water. *The Journal of Physical Chemistry*, 96(11):4712–4718, 1992.

[37] Ryan Gotchy Mullen, Joan-Emma Shea, and Baron Peters. Transmission coefficients, committors, and solvent coordinates in ion-pair dissociation. *Journal of Chemical Theory and Computation*, 10(2):659–667, 2014. PMID: 26580043.

[38] Steven S Plotkin and Peter G Wolynes. Non-markovian configurational diffusion and reaction coordinates for protein folding. *Physical review letters*, 80(22):5015, 1998.

[39] Atanu Das and Dmitrii E Makarov. Dynamics of disordered proteins under confinement: Memory effects and internal friction. *The Journal of Physical Chemistry B*, 122(39):9049–9060, 2018.

[40] Bernhard G. Mitterwallner, Christoph Schreiber, Jan O. Daldrop, Joachim O. Rädler, and Roland R. Netz. Non-markovian data-driven modeling of single-cell motility. *Phys. Rev. E*, 101:032408, Mar 2020.

[41] Bartosz Kowalik, Jan O. Daldrop, Julian Kappler, Julius C. F. Schulz, Alexander Schlaich, and Roland R. Netz. Memory-kernel extraction for different molecular solutes in solvents of varying viscosity in confinement. *Phys. Rev. E*, 100:012126, Jul 2019.

[42] Gerhard Jung, Martin Hanke, and Friederike Schmid. Generalized langevin dynamics: construction and numerical integration of non-markovian particle-based models. *Soft matter*, 14(46):9368–9382, 2018.

[43] Dominika Lesnicki, Rodolphe Vuilleumier, Antoine Carof, and Benjamin Rotenberg. Molecular hydrodynamics from memory kernels. *Phys. Rev. Lett.*, 116:147804, Apr 2016.

[44] Jan O. Daldrop, Bartosz G. Kowalik, and Roland R. Netz. External potential modifies friction of molecular solutes in water. *Phys. Rev. X*, 7:041065, Dec 2017.

[45] Igor S. Tolokh, George W. N. White, Saul Goldman, and C. G. Gray. Prediction of ion channel transport from grote—hynes and kramers theories. *Molecular Physics*, 100(14):2351–2359, 2002.

[46] Benjamin A. Dalton, Cihan Ayaz, Henrik Kiefer, Anton Klimek, Lucas Tepper, and Roland R. Netz. Fast protein folding is governed by memory-dependent friction. *Proceedings of the National Academy of Sciences*, 120(31):e2220068120, 2023.

[47] Alexander Berezhkovskii and Attila Szabo. One-dimensional reaction coordinates for diffusive activated rate processes in many dimensions. *The Journal of chemical physics*, 122(1), 2005.

[48] Joseph D. Bryngelson, José Nelson Onuchic, Nicholas D. Socci, and Peter G. Wolynes. Funnels, pathways, and the energy landscape of protein folding: A synthesis. *Proteins: Structure, Function, and Bioinformatics*, 21(3):167–195, 1995.

[49] Joseph D. Bryngelson and Peter G. Wolynes. Intermediates and barrier crossing in a random energy model (with applications to protein folding). *The Journal of Physical Chemistry*, 93(19):6902–6915, 1989.

[50] Olga K. Dudko, Gerhard Hummer, and Attila Szabo. Intrinsic rates and activation free energies from single-molecule pulling experiments. *Phys. Rev. Lett.*, 96:108101, Mar 2006.

[51] N. D. Socci, J. N. Onuchic, and P. G. Wolynes. Diffusive dynamics of the reaction coordinate for protein folding funnels. *The Journal of Chemical Physics*, 104(15):5860–5868, 04 1996.

[52] David Chandler. Roles of classical dynamics and quantum dynamics on activated processes occurring in liquids. *Journal of Statistical Physics*, 42:49–67, 1986.

[53] Bruce J. Berne, Michal Borkovec, and John E. Straub. Classical and modern methods in reaction rate theory. *The Journal of Physical Chemistry*, 92(13):3711–3725, 1988.

[54] Peter Hänggi, Peter Talkner, and Michal Borkovec. Reaction-rate theory: fifty years after kramers. *Rev. Mod. Phys.*, 62:251–341, Apr 1990.

[55] Robert B. Best and Gerhard Hummer. Diffusive model of protein folding dynamics with kramers turnover in rate. *Phys. Rev. Lett.*, 96:228104, Jun 2006.

[56] Julian Schmidt, Alex Meistrenko, Hendrik van Hees, Zhe Xu, and Carsten Greiner. Simulation of stationary gaussian noise with regard to the langevin equation with memory effect. *Physical Review E*, 91(3):032125, 2015.

[57] Eli Pollak, Hermann Grabert, and Peter Hänggi. Theory of activated rate processes for arbitrary frequency dependent friction: Solution of the turnover problem. *The Journal of Chemical Physics*, 91(7):4073–4087, 10 1989.

[58] Gerhard Jung, Martin Hanke, and Friederike Schmid. Iterative reconstruction of memory kernels. *Journal of Chemical Theory and Computation*, 13(6):2481–2488, 2017. PMID: 28505440.

[59] John E. Straub, Michal Borkovec, and Bruce J. Berne. Molecular dynamics study of an isomerizing diatomic in a Lennard-Jones fluid. *The Journal of Chemical Physics*, 89(8):4833–4847, 10 1988.

[60] Peter Talkner and Hans-Benjamin Braun. Transition rates of a non-Markovian Brownian particle in a double well potential. *The Journal of Chemical Physics*, 88(12):7537–7549, 06 1988.

[61] Sriram Ramaswamy. The mechanics and statistics of active matter. *Annual Review of Condensed Matter Physics*, 1(1):323–345, 2010.

[62] J Dzubiella, GP Hoffmann, and H Löwen. Lane formation in colloidal mixtures driven by an external field. *Physical Review E*, 65(2):021402, 2002.

[63] Clemens Bechinger, Roberto Di Leonardo, Hartmut Löwen, Charles Reichhardt, Giorgio Volpe, and Giovanni Volpe. Active particles in complex and crowded environments. *Reviews of modern physics*, 88(4):045006, 2016.

[64] Félix Ginot, Isaac Theurkauff, Demian Levis, Christophe Ybert, Lydéric Bocquet, Ludovic Berthier, and Cécile Cottin-Bizonne. Nonequilibrium equation of state in suspensions of active colloids. *Phys. Rev. X*, 5:011004, Jan 2015.

[65] Hans Vandebroek and Carlo Vanderzande. The effect of active fluctuations on the dynamics of particles, motors and dna-hairpins. *Soft matter*, 13(11):2181–2191, 2017.

[66] Andrew GT Pyo, Noel Q Hoffer, Krishna Neupane, and Michael T Woodside. Transition-path properties for folding reactions in the limit of small barriers. *The Journal of chemical physics*, 149(11), 2018.

[67] Étienne Fodor and M Cristina Marchetti. The statistical physics of active matter: From self-catalytic colloids to living cells. *Physica A: Statistical Mechanics and its Applications*, 504:106–120, 2018.

[68] Pierre Bohec, François Gallet, Christian Maes, Soghra Safaverdi, Paolo Visco, and Frédéric Van Wijland. Probing active forces via a fluctuation-dissipation relation: Application to living cells. *Europhysics Letters*, 102(5):50005, 2013.

[69] Suman Kumar Banik, Jyotipratim Ray Chaudhuri, and Deb Shankar Ray. The generalized kramers theory for nonequilibrium open one-dimensional systems. *The Journal of Chemical Physics*, 112(19):8330–8337, 2000.

[70] Binny J Cherayil. Particle dynamics in viscoelastic media: Effects of non-thermal white noise on barrier crossing rates. *The Journal of Chemical Physics*, 155(24), 2021.

[71] Erik Van Nimwegen and James P Crutchfield. Metastable evolutionary dynamics: crossing fitness barriers or escaping via neutral paths? *Bulletin of mathematical biology*, 62(5):799–848, 2000.

[72] Adriana Rico, Pavel KindlmAnn, and Frantisek Sedlacek. Barrier effects of roads on movements of small mammals. *FOLIA ZOOLOGICA-PRAHA-*, 56(1):1, 2007.

[73] David B Brückner, Alexandra Fink, Joachim O Rädler, and Chase P Broedersz. Disentangling the behavioural variability of confined cell migration. *Journal of The Royal Society Interface*, 17(163):20190689, 2020.

[74] Lisa M Alexander, Daniel H Goldman, Liang M Wee, and Carlos Bustamante. Non-equilibrium dynamics of a nascent polypeptide during translation suppress its misfolding. *Nature communications*, 10(1):2709, 2019.

[75] Till Stensitzki, Yang Yang, Valeri Kozich, Ashour A Ahmed, Florian Kössl, Oliver Kühn, and Karsten Heyne. Acceleration of a ground-state reaction by selective femtosecond-infrared-laser-pulse excitation. *Nature Chemistry*, 10(2):126–131, 2018.

[76] Krishna Neupane, Ajay P Manuel, and Michael T Woodside. Protein folding trajectories can be described quantitatively by one-dimensional diffusion over measured energy landscapes. *Nature Physics*, 12(7):700–703, 2016.

[77] Srabanti Chaudhury, Debarati Chatterjee, and Binny J Cherayil. The dynamics of single enzyme reactions: A reconsideration of kramers' model for colored noise processes. *The Journal of chemical physics*, 129(7), 2008.

[78] S Arrhenius. On the reaction rate of the inversion of non-refined sugar upon souring. *Z. Phys. Chem*, 4(226):135501, 1889.

[79] Scott H Northrup and James T Hynes. Reactive dynamics for diffusive barrier crossing. *The Journal of Chemical Physics*, 69(12):5246–5260, 1978.

[80] Victor Barcilon, Duanpin Chen, Robert S Eisenberg, and Mark A Ratner. Barrier crossing with concentration boundary conditions in biological channels and chemical reactions. *The Journal of chemical physics*, 98(2):1193–1212, 1993.

[81] Hoi Sung Chung and William A Eaton. Single-molecule fluorescence probes dynamics of barrier crossing. *Nature*, 502(7473):685–688, 2013.

[82] Hoi Sung Chung, Stefano Piana-Agostinetti, David E Shaw, and William A Eaton. Structural origin of slow diffusion in protein folding. *Science*, 349(6255):1504–1510, 2015.

[83] Jan O Daldrop, Julian Kappler, Florian N Brünig, and Roland R Netz. Butane dihedral angle dynamics in water is dominated by internal friction. *Proceedings of the National Academy of Sciences*, 115(20):5169–5174, 2018.

[84] Divya Singh, Kinjal Mondal, and Srabanti Chaudhury. Effect of memory and inertial contribution on transition-time distributions: Theory and simulations. *The Journal of Physical Chemistry B*, 125(17):4536–4545, 2021. PMID: 33900087.

[85] Cihan Ayaz, Lucas Tepper, Florian N. Brünig, Julian Kappler, Jan O. Daldrop, and Roland R. Netz. Non-markovian modeling of protein folding. *Proceedings of the National Academy of Sciences*, 118(31):e2023856118, 2021.

[86] Brandon R Ferrer, Juan Ruben Gomez-Solano, and Alejandro V Arzola. Fluid viscoelasticity triggers fast transitions of a brownian particle in a double well optical potential. *Physical Review Letters*, 126(10):108001, 2021.

[87] Benny Carmeli and Abraham Nitzan. Non-markoffian theory of activated rate processes. *Physical Review Letters*, 49(7):423, 1982.

[88] Laura Lavacchi, Julian Kappler, and Roland R Netz. Barrier crossing in the presence of multi-exponential memory functions with unequal friction amplitudes and memory times. *Europhysics Letters*, 131(4):40004, 2020.

[89] Jacques Prost, J-F Joanny, and Juan MR Parrondo. Generalized fluctuation-dissipation theorem for steady-state systems. *Physical review letters*, 103(9):090601, 2009.

[90] L Dinis, Pascal Martin, J Barral, J Prost, and JF Joanny. Fluctuation-response theorem for the active noisy oscillator of the hair-cell bundle. *Physical review letters*, 109(16):160602, 2012.

[91] Lucian Willareth, Igor M Sokolov, Yael Roichman, and Benjamin Lindner. Generalized fluctuation-dissipation theorem as a test of the markovianity of a system. *Europhysics Letters*, 118(2):20001, 2017.

[92] Roland R Netz. Approach to equilibrium and nonequilibrium stationary distributions of interacting many-particle systems that are coupled to different heat baths. *Physical Review E*, 101(2):022120, 2020.

[93] Hugues Meyer, Philipp Pelagejcev, and Tanja Schilling. Non-markovian out-of-equilibrium dynamics: A general numerical procedure to construct time-dependent memory kernels for coarse-grained observables. *Europhysics Letters*, 128(4):40001, jan 2020.

[94] Roland R. Netz. Fluctuation-dissipation relation and stationary distribution of an exactly solvable many-particle model for active biomatter far from equilibrium. *The Journal of Chemical Physics*, 148(18):185101, 2018.

[95] E. Carlon, H. Orland, T. Sakaue, and C. Vanderzande. Effect of memory and active forces on transition path time distributions. *The Journal of Physical Chemistry B*, 122(49):11186–11194, 2018. PMID: 30102039.

[96] Marco Baiesi and Christian Maes. An update on the nonequilibrium linear response. *New Journal of Physics*, 15(1):013004, 2013.

[97] Christian Maes, Soghra Safaverdi, Paolo Visco, and Frédéric Van Wijland. Fluctuation-response relations for nonequilibrium diffusions with memory. *Physical Review E*, 87(2):022125, 2013.

[98] A Puglisi, A Sarracino, and A Vulpiani. Temperature in and out of equilibrium: A review of concepts, tools and attempts. *Physics Reports*, 709:1–60, 2017.

[99] Yu. P. Kalmykov, W. T. Coffey, and S. V. Titov. Thermally activated escape rate for a Brownian particle in a double-well potential for all values of the dissipation. *The Journal of Chemical Physics*, 124(2):024107, 01 2006.

[100] V.I. Mel'nikov. The kramers problem: Fifty years of development. *Physics Reports*, 209(1):1–71, 1991.

[101] Alexander M. Berezhkovskii and Dmitrii E. Makarov. Single-molecule test for markovianity of the dynamics along a reaction coordinate. *The Journal of Physical Chemistry Letters*, 9(9):2190–2195, 2018. PMID: 29642698.

[102] Eli Pollak and Peter Talkner. Activated rate processes: Finite-barrier expansion for the rate in the spatial-diffusion limit. *Phys. Rev. E*, 47:922–933, Feb 1993.

[103] Kresten Lindorff-Larsen, Stefano Piana, Ron O. Dror, and David E. Shaw. How fast-folding proteins fold. *Science*, 334(6055):517–520, 2011.

[104] Benjamin Schüller, Alex Meistrenko, Hendrik van Hees, Zhe Xu, and Carsten Greiner. Kramers' escape rate problem within a non-markovian description. *Annals of Physics*, 412:168045, 2020.

[105] Gregor Diezemann. Nonlinear response theory for markov processes. iv. the asymmetric double-well potential model revisited. *Physical review. E*, 106 6-1:064122, 2022.

[106] N.G. Van Kampen. Elimination of fast variables. *Physics Reports*, 124(2):69–160, 1985.

[107] Hannes Risken. *The Fokker-Planck Equation*. Springer Berlin, Heidelberg, 1996.

[108] Laura Lavacchi, J. O. Daldrop, and Roland R. Netz. Non-arrhenius barrier crossing dynamics of non-equilibrium non-markovian systems. *Europhysics Letters*, 139(5):51001, aug 2022.

[109] Crispin Gardiner. *Stochastic Methods*. Springer Berlin, Heidelberg, 2004.

[110] Hoi Sung Chung, John M. Louis, and William A. Eaton. Experimental determination of upper bound for transition path times in protein folding from single-molecule photon-by-photon trajectories. *Proceedings of the National Academy of Sciences*, 106(29):11837–11844, 2009.

[111] Krishna Neupane, Dustin B. Ritchie, Hao Yu, Daniel A. N. Foster, Feng Wang, and Michael T. Woodside. Transition path times for nucleic acid folding determined from energy-landscape analysis of single-molecule trajectories. *Phys. Rev. Lett.*, 109:068102, Aug 2012.

[112] Hoi Sung Chung, Kevin McHale, John M. Louis, and William A. Eaton. Single-molecule fluorescence experiments determine protein folding transition path times. *Science*, 335(6071):981–984, 2012.

[113] Katherine Truex, Hoi Sung Chung, John M. Louis, and William A. Eaton. Testing landscape theory for biomolecular processes with single molecule fluorescence spectroscopy. *Phys. Rev. Lett.*, 115:018101, Jul 2015.

[114] Krishna Neupane, Daniel A. N. Foster, Derek R. Dee, Hao Yu, Feng Wang, and Michael T. Woodside. Direct observation of transition paths during the folding of proteins and nucleic acids. *Science*, 352(6282):239–242, 2016.

[115] Krishna Neupane, Feng Wang, and Michael T. Woodside. Direct measurement of sequence-dependent transition path times and conformational diffusion in dna duplex formation. *Proceedings of the National Academy of Sciences*, 114(6):1329–1334, 2017.

[116] Noel Q. Hoffer, Krishna Neupane, Andrew G. T. Pyo, and Michael T. Woodside. Measuring the average shape of transition paths during the folding of a single biological molecule. *Proceedings of the National Academy of Sciences*, 116(17):8125–8130, 2019.

[117] Noel Q Hoffer and Michael T Woodside. Probing microscopic conformational dynamics in folding reactions by measuring transition paths. *Current Opinion in Chemical Biology*, 53:68–74, 2019. Mechanistic Biology • Chemical Biophysics.

[118] Jae-Yeol Kim and Hoi Sung Chung. Disordered proteins follow diverse transition paths as they fold and bind to a partner. *Science*, 368(6496):1253–1257, 2020.

[119] Srabanti Chaudhury and Dmitrii E. Makarov. A harmonic transition state approximation for the duration of reactive events in complex molecular rearrangements. *The Journal of Chemical Physics*, 133(3):034118, 07 2010.

[120] Rohit Satija, Alexander M. Berezhkovskii, and Dmitrii E. Makarov. Broad distributions of transition-path times are fingerprints of multidimensionality of the underlying free energy landscapes. *Proceedings of the National Academy of Sciences*, 117(44):27116–27123, 2020.

[121] Sergei V. Krivov. Is protein folding sub-diffusive? *PLOS Computational Biology*, 6(9):1–7, 09 2010.

[122] Rohit Satija, Atanu Das, and Dmitrii E. Makarov. Transition path times reveal memory effects and anomalous diffusion in the dynamics of protein folding. *The Journal of Chemical Physics*, 147(15):152707, 07 2017.

[123] Eli Pollak. Transition path time distribution and the transition path free energy barrier. *Phys. Chem. Chem. Phys.*, 18:28872–28882, 2016.

[124] Rohit Satija and Dmitrii E. Makarov. Generalized langevin equation as a model for barrier crossing dynamics in biomolecular folding. *The Journal of Physical Chemistry B*, 123(4):802–810, 2019.

[125] Won Kyu Kim and Roland R. Netz. The mean shape of transition and first-passage paths. *The Journal of Chemical Physics*, 143(22):224108, 12 2015.

[126] M. Laleman, E. Carlon, and H. Orland. Transition path time distributions. *The Journal of Chemical Physics*, 147(21):214103, 12 2017.

[127] Jan O. Daldrop, Won Kyu Kim, and Roland R. Netz. Transition paths are hot. *Europhysics Letters*, 113(1):18004, jan 2016.

[128] Gerhard Hummer. From transition paths to transition states and rate coefficients. *The Journal of Chemical Physics*, 120(2):516–523, 12 2003.

[129] Florian N. Brünig, Manuel Rammler, Ellen M. Adams, Martina Havenith, and Roland R. Netz. *Nature Communications*, 13(1):4210, 2022.

[130] Pilar Cossio, Gerhard Hummer, and Attila Szabo. Transition paths in single-molecule force spectroscopy. *The Journal of Chemical Physics*, 148(12):123309, 12 2017.

[131] Rajesh Dutta and Eli Pollak. Microscopic origin of diffusive dynamics in the context of transition path time distributions for protein folding and unfolding. *Phys. Chem. Chem. Phys.*, 24:25373–25382, 2022.

[132] Florian Brünig, Roland Netz, and Julian Kappler. Barrier-crossing times for different non-markovian friction in well and barrier: A numerical study. *Physical Review E*, 106, 10 2022.

Acknowledgements

I would like to express my gratitude to my supervisor, Dr. Roland Netz, for the opportunity to write this thesis. In our discussion, he supported me and offered deep insight into the study. My gratitude goes to Dr. Julian Kappler and Dr. Jan Daldrop for their collaborations in my articles and for always being available to answer my questions and the helpful discussion.

I would like to express my sincere gratitude to my ex-officemates, Dr. Otto Schulian and Dr. Philip Loche. In particular, Philip, who, at the beginning of my Ph.D., tried to answer all my questions about the work, but also about the bureaucracy and practical aspects of my life and made in the office at atmosphere as at home.

The assistance provided by Annette Schumann-Weld and Henrike Giebl was greatly appreciated. I wish to extend my special thanks to my ex-colleagues Bernhard Mitterwallner, Dr. Amanuel Wolden-Kida, Dr. Chian Ayaz, and my current colleagues Dr. Laura Scalfi, Dr. Anil Sahoo, Dr. Benjamin Dalton, Dr. Hossein Batebi, Dr. Florian Brünig, Amir Abbasi, Maximilian Becker, Shane Carlson, Benjamin Hery, Henrik Kiefer, Anton Klimek, Louis Lehmann, Lucas Tepper and in particular to Sina Zendehroud for the interesting scientific discussion, but also for the time spent out of the office.

I would also like to thank my close friends here in Berlin, Dr. Maryam Sadeghi, Dr. Moslem Mishmastnehi, Lisa Farulli, and Andrea Margherita Valsecchi Grillmaister, with whom we shared our experiences and suffering to finish our Ph.D.

I am deeply grateful to my father, who always helped and supported my decision. My heartfelt thanks to my boyfriend Francesco for his unwavering support and belief in me in these long years of my research. Last, but not least, gratitude goes to my child Lorenzo; this first year of life gave me even more energy to finish and write this thesis.